Univerzita Karlova v Praze

Přírodovědecká fakulta

Studijní program: Biochemie

Studijní obor: Biochemie

Bc. Jitka Šlegerová

Konjugáty biomolekul s nanodiamanty: příprava a aplikace

Biomolecule conjugates with nanodiamonds: preparation and application

Diplomová práce

Vedoucí práce: Doc. RNDr. Jan Konvalinka CSc.

Konzultant: Petr Cígler, PhD.

Praha 2013

Prohlašuji, že jsem závěrečnou práci zpracovala samostatně a že jsem uvedla všechny použité informační zdroje a literaturu. Tato práce ani její podstatná část nebyla předložena k získání jiného nebo stejného akademického titulu.

V Praze, 13.5.2013

Podpis: Jitka Šlegerová

Děkuji svému vedoucímu práce Doc. RNDr. Janu Konvalinkovi CSc. za odborné vedení mé práce a konzultantovi Mgr. Petru Cíglerovi, PhD. za všestrannou pomoc při vypracování této práce.
Dále děkuji Ivanu Řehořovi za jeho pomoc, mnoho rad a čas, který mi věnoval, a Evě Muchové za rady při vypracování diplomové práce.
Jsem ráda, že jsem mohla vypracovávat diplomovou práci na Ústavu organické chemie a biochemie, a tímto děkuji celému kolektivu laboratoře za vytvoření příjemné atmosféry pro práci.

ČESKÝ ABSTRAKT

Fluorescenční nanodiamanty jsou perspektivním materiálem pro tvorbu fluorescenčních značek využitelných v biologických systémech pro zobrazování. Jejich fluorescence nepodléhá fotodestrukci a nedochází k jejímu blikání. Nanodiamanty emitují fluorescenci v červené oblasti vlnových délek, a tudíž oddělitelnou od vlastní fluorescence buněk. Pro použití nanodiamantů jako fluorescenčních značek je třeba zlepšit jejich chování v živých systémech. Zejména je třeba zajistit aglomerační stálost částic v biologických médiích, zabránit jejich nespecifické interakci s proteiny a umožnit kovalentní modifikaci dalšími molekulami. Proto byly na nanodiamantových částicích vytvořeny obaly z hydrofilních polymerů a následně modifikovány transferinem nebo inhibitorem glutamátkarboxypeptidasy II. Tyto molekuly se vážou na specifické receptory na povrchu rakovinných buněk a umožňují efektivní internalizaci částic do buněk. Konjugáty byly úspěšně připraveny a v případě konjugátu inhibitoru glutamátkarboxypeptidasy II s nanodiamantem byla navíc ověřena schopnost vazby na příslušný receptor. Nicméně vliv transferinu nebo inhibitoru glutamátkarboxypeptidasy II na internalizaci nebyl dostatečně prokázán kvůli nespecifické interakci nanodiamantů s buněčnou membránou. Také použitá optimalizace polymerních obalů nepomohla překonat tento problém. Snížení afinity částic k buněčným membránám bude cílem dalšího výzkumu.

(in English)

ENGLISH ABSTRACT

Fluorescent nanodiamonds are a perspective material for the preparation of fluorescent labels for bioimaging due to their stable fluorescence. Contrary to other compounds, nanodiamonds do not photobleach or photoblink. Furthermore, nanodiamonds emit fluorescence in the red part of the spectrum which is well separated from auto-fluorescence. However, before the employment of nanodiamonds as fluorescent labels in biological systems, several properties have to be improved. Primarily, their colloidal stability in biological media has to be ensured. Preventing of non-specific interactions of nanodiamonds with proteins is next crucial step. Finally, it is necessary to enable their high-yield further modifications with various molecules. Hydrophilic polymer coating surrounding a nanodiamond particle was introduced as a successful modification. Coated nanodiamonds were subsequently modified with transferrin or the inhibitor of glutamate carboxypeptidase II. These molecules bind specifically to receptors on cell membranes and enable cellular internalization. Nanodiamond conjugates were successfully prepared and the ability of binding to respective receptors was verified for the nanodiamond conjugate with the inhibitor of glutamate carboxypeptidase II. However, the effect of transferrin or the inhibitor of glutamate carboxypeptidase II on cellular internalization has not been sufficiently demonstrated due to non-specific binding of the particles to cellular membranes. The optimization of polymerization did not solve this problem. Decreasing the affinity of particles to cell membranes will be the aim of the future research.

CONTENTS

1. LIST OF ABBREVIATIONS

2-PMPA	2-(phosphonomethyl)pentanedioic acid
2-MPPA	2-(3-mercaptopropyl)pentanedioic acid
A_{488}	Alexa-fluor 488
A_{488}-N_3	Alexa-fluor 488 modified with azide group
AAA	Aminoacid analysis
aTf	Apotransferrin
AzpAAm	3-azidopropylacrylamide
BSA	Bovine serum albumin
CuAAC	Copper-catalyzed azide-alkyne cycloaddition reaction
DCL	N-[N-[(S)-1,3-dicarboxypropyl]carbamoyl]-(S)-lysin
det	Detergent
DLS	Dynamic light scattering
DMSO	Dimethyl sulfoxide
EDC	1-Ethyl-3-[3-dimethylaminopropyl]carbodiimide
EDTA	Ethylenediaminetetraacetic acid
EPR effect	Enhanced permeability and retention effect
FBS	Fetal bovine serum
Fl	Fluorescein
Fl-N_3	Fluorescein modified with azide group
GCP II	Glutamate carboxypeptidase II
GPI 5232	2-(hydroxypentafluorophenylmethylphosphinoylmethyl)pentanedioic acid
HEPES	4-(2-hydroxyethyl)-1-piperazineethanesulfonic acid
H-MEMd	Minimum Essential Medium with HEPES
HPMA	N-(2-hydroxypropyl)methacrylamide
HSA	Human serum albumin
HT-29	Adherent human colon carcinoma cell line
hTf	Holotransferrin
I	Fluorescence intensity
I_{max}	Maximal fluorescence intensity

K562	Non-adherent human myelogenous leukemia cell line
LNCaP cells	Lymph node carcinoma of the prostate cells
NAA	N-acetyl-L-aspartate
NAAG	N-acetyl-L-aspartyl-L-glutamate
NAALADase	N-acetylated-α-linked Acidic Dipeptidase
ND	Nanodiamond
NHS	N-Hydroxysuccinimide
(N-V) center	Nitrogen vacancy center
Opti-MEM	Improved Minimal Essential Medium
PBS	Phosphate buffered saline
PEG	Polyethylene glycol
PLGA-PEG	Poly(lactide-co-glycolide)-block-poly(ethylene glycol)
PrAAm	Propargylacrylamide
PSMA	Prostate-specific membrane antigen
PteGlu	Pteroyl-γ-L-glutamic acid
PteGlu2	Pteroyldi-γ-L-glutamic acid
QDs	Quantum dots
RB	Reaction buffer
RPMI medium	Roswell Park Memorial Institute medium
RT	Room temperature
SDS	Sodium dodecyl sulfate
SA10	Sodium acetate 10 mM
SPR	Surface plasmon resonance
THPTA	Tris(3-hydroxypropyltriazolylmethyl)amine
Tris	Trishydroxymethylaminomethane
Tf	Transferrin
TfR	Transferrin receptor
U373	Adherent human glioblastoma cell line

The nomenclature of all prepared samples is stated on Fig. 19, p. 46.

2. INTRODUCTION

2.1. FLUORESCENT LABELING

Labeling in cell biology can be generally described as a connection of a reporting molecule or a particle (label) to a place of interest. Any tissue, cell, cell compartment or molecule can serve as a place of interest. Isotope markers, colorimetric biosensors, electrochemical sensors, fluorescent labels and many others can be used as labels. [1] Moreover, labels can enable real-time imaging of processes in living cells (sensing) and work as a powerful tool for cell biologists. Fluorescent labeling is the most common labeling method. The ideal fluorescent label should meet the requirements such as chemical stability and solubility, convenient size, minimal interference, low toxicity and high brightness. Another important feature is the possibility to modify the label and to bind it efficiently and selectively to the place of interest. [1,2] There are different types of fluorescent labels. The most frequently used labels are fluorescent proteins, organic dyes and semiconductor nanocrystals. These labels are briefly described in the following paragraphs.

Green fluorescent proteins exhibit green fluorescence when exposed to light. Green fluorescent protein was the first fluorescent protein isolated from jellyfish *Aequorea victoria*. There are many derivatives of green fluorescent protein with modified spectral characteristics such as the shift in the excitation or emission spectra, intensity of fluorescence or photostability. The advantage of fluorescent proteins is that its gene can be introduced into the genome of an organism; it can be co-expressed with the protein of interest and respond to various biological events and signals. The disadvantage can be their large size and non-stable fluorescence intensity which suffers from photobleaching under continuous illumination. [3]

Organic dyes are nowadays the most widely used fluorescent labels. There are many types of organic dyes, for example, dyes based on oxygen, sulfur or nitrogen heterocycles, fluoresceins, rhodamines, bodipy fluorophores or cyanines. Small organic dyes usually do not interfere with biological function of the place of interest, contrary to fluorescent proteins or quantum dots (QDs) which can, for example, block the active site of an enzyme and reduce its function. Another benefit of organic dyes is the ease and high efficiency with which they undergo the labeling reaction. On the other hand, organic dyes

as well as fluorescent proteins suffer from photobleaching under continuous illumination. [2]

QDs are inorganic nanocrystal semiconductors (for example CdSe or ZnS). QDs have higher stability, lower photobleaching yield and higher brightness than organic dyes. QDs emit narrow fluorescence at the wavelength dependent on the size of the particle; this property can be considered both as a drawback and an advantage. [2] QDs have broad absorption spectrum in contrast to narrow spectra of organic dyes (Fig. 1). Organic dyes are usually excited with one specific and typical wavelength. QDs can be excited with any wavelength shorter than the wavelength of the fluorescence. Moreover, one wavelength can be used for different QDs. This fact enables to choose the wavelength which minimizes auto-fluorescence of biological samples. [2,4]

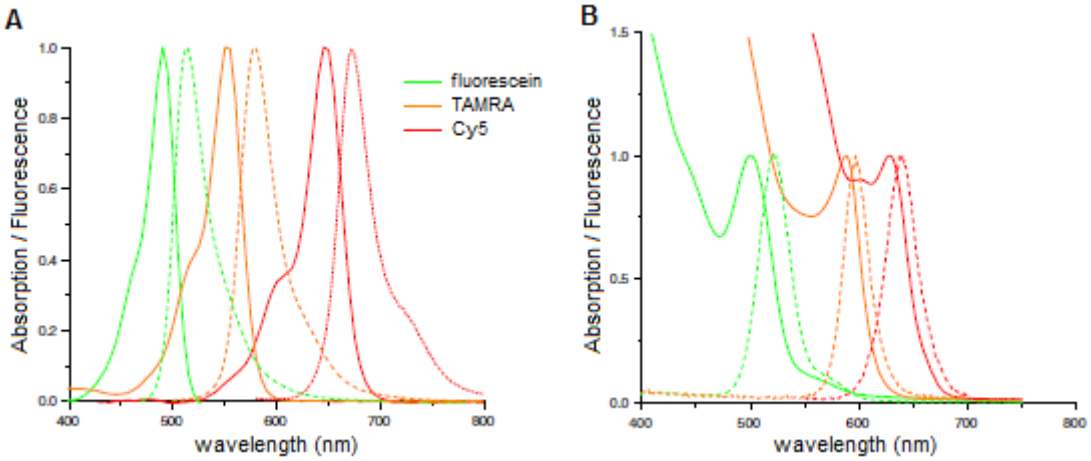

Fig. 1 **Absorption (solid curve) and fluorescence (dashed curve) spectra of organic dyes and QDs.** (A) Spectra of three typical organic dyes (fluorescein, carboxytetramethylrhodamine (TAMRA) and cyanine (Cy5)) in water. (B) Spectra of CdSe/ZnS QDs of different size in water. Adapted from Parak *et al.* [4]

Fluorescence of QDs differs from auto-fluorescence and fluorescence of organic dyes with long fluorescence lifetime. Fluorescence lifetime is the average time the fluorophore stays in its excited state before emitting a photon. QDs fluorescence lifetime is typically in few tens of nanoseconds range, contrary to auto-fluorescence and organic dyes with nanosecond lifetime. This distinction can be used in fluorescence lifetime imaging measurement. [2,4] Major drawbacks of QDs are cytotoxicity caused by the presence of toxic elements such as Cd or Te or intermittency of their fluorescence, so called photoblinking.

Photobleaching and photoblinking are light induced effects dependent on the irradiation intensity. [5] Photobleaching is irreversible photochemical destruction of a fluorophore. Fluorophore undergoes a light-induced chemical reaction to give a non-fluorescent molecule. Both fluorescent proteins and organic dyes photobleach. QDs are usually considered stable against photobleaching due to their inorganic structure. [4] However, their time-dependent degradation has been observed recently. [5] Photobleaching limits the time for which labels can be observed under microscope and makes, for example, single tracking of a molecule demanding. [2,4] On the other hand, it can be used in fluorescence recovery after photobleaching method which studies the diffusion and movement of labeled molecules. [1] Photoblinking is a process when a dye turns reversibly on and off its fluorescence under continuous illumination. Dark periods with no emission occur on the time scale of microseconds to seconds. [6] Photoblinking is typical for QDs, but organic dyes and fluorescent proteins are also not resistant to it. [2]

Fluorescent nanodiamonds (NDs) represent an alternative to previously described fluorescent labels. [7] NDs have advantages such as biocompatibility and low cytotoxicity which makes them suitable for *in vivo* experiments. Excellent optical properties with no photobleaching, no photoblinking and long fluorescence lifetime are also important characteristics. However, NDs have low brightness which is considered a major drawback. Above mentioned characteristics are described in more detail in this work.

2.2. NANODIAMONDS AND THEIR PROPERTIES

NDs belong to a vast group of carbon nanomaterials comprising for example graphene, carbon nanotubes, fullerenes or diamond nanofilms. Diamond structure formed by sp^3 hybridized carbon is unique and gives NDs its extraordinary properties such as exceptional hardness, high thermal conductivity and excellent resistance against corrosive chemicals. [8,9] These properties can be used for material engineering. [10] The long-term chemical stability of NDs, biocompatibility, low toxicity and exceptional optical properties are characteristics which enable wide range of use from bioapplications in biomedicine to for example quantum computing. In biomedicine, NDs have been used for fluorescent labeling and biosensing, cell targeting and internalization, drug delivery and controlled release and enzyme immobilization. [8,9,11]

2.2.1. Fluorescent properties of NDs

NDs fluorescence is caused by different types of point defects in its crystal lattice. The brightest point defects are so called nitrogen vacancy (N-V) centers. A nitrogen atom is present in the crystal lattice instead of a carbon atom as an impurity resulting from a production process. Vacancies are produced by irradiation with high-energy beam of particles. Annealing procedure at elevated temperatures is required to move them to proximity of a nitrogen atom to create the (N-V) center. There are two states of the (N-V) center inside the material: neutral $(N\text{-}V)^0$ and negatively charged $(N\text{-}V)^-$. Fluorescence of NDs undergoes neither photobleaching nor photoblinking (Fig. 2). [11–14]

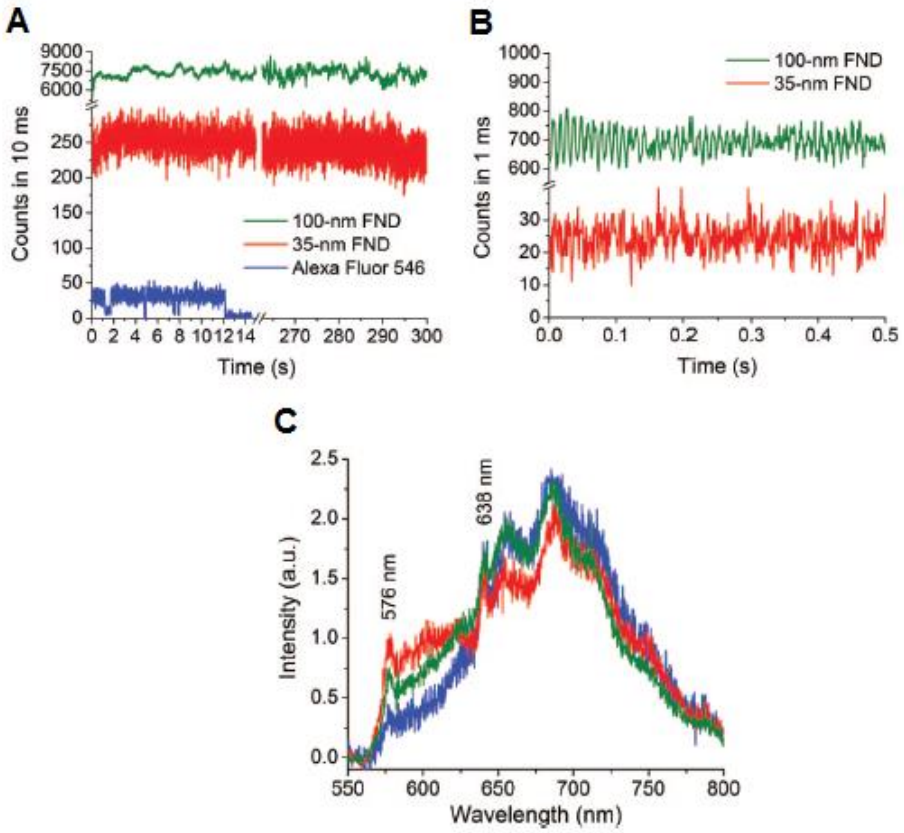

Fig. 2 **Fluorescent properties of NDs.** (A) Typical time traces of fluorescence under continuous excitation from 100-nm ND and 35-nm ND with no sign of photobleaching and from Alexa Fluor 546. (B) Time traces of same NDs showing no photoblinking behavior. Fluorescence intensity of 100-nm ND is higher than 35-nm ND. (C) Emission spectrum of ND with two characteristic peaks at 576 nm and 638 nm. Adapted from Fu *et al*. [12]

Irradiation of NDs at a specific wavelength results in fluorescence of the (N-V) centers. Usually, the wavelength 532 nm [13] or 560 nm [11,12,15] is used. NDs have a characteristic emission spectrum with the maximum around 700 nm and two characteristic peaks at

576 nm and 638 nm related to the electronic transitions of $(N\text{-}V)^0$ and $(N\text{-}V)^-$, respectively (Fig. 2, p. 6). Analogous to QDs, NDs exhibit a very long fluorescence lifetime, typically in few tens of nanoseconds scale. The intensity of fluorescence is size-dependent. Smaller NDs have lower number of the (N-V) centers than the bigger ones; their intensity of fluorescence is lower. The amount of the (N-V) centers in a particle is also dependent on the way of production and treatment. The number of the (N-V) centers is expected to be significantly increased in nearby future, this approach is currently under examination in our laboratory. [14]

It has been also shown recently [16] that NDs fluorescence is affected by chemical surroundings. Atoms and molecules which interact with the diamond surface change surface chemical potential and electric field. It leads to changes in the $(N\text{-}V)^-/(N\text{-}V)^0$ ratio what is reflected in shape of emission spectra. The change of fluorescence is observable with a classical confocal microscope. It means that NDs could be used not only as labels, but also as optical chemo-biosensors for monitoring of chemical processes or presence of specific molecules in biological environment. [16]

2.2.2. Production of NDs:

Characteristics of NDs depend on a way of their preparation. Several types of NDs are recognized. Detonation NDs are produced by detonation of explosive materials in presence of a non-oxidizing cooling medium. ND particles can be created also by plasma-assisted chemical vapor deposition or high-energy ball milling of high-pressure high-temperature NDs. [11,17] In our laboratory, the last type of NDs is used. The natural content of isolated substitutional nitrogen atoms impurities is their advantage. [11,14] In order to create the (N-V) centers and obtain fluorescent NDs, material is irradiated with high-energy particle beam in cyclotron and subsequently annealed in furnace at elevated temperatures. The surface of NDs is heterogenous after synthesis. Carboxyl or hydroxyl groups, ketones, anhydrides, lactones and other groups are present on the surface. The surface of NDs after synthesis also contains amorphous sp^2 carbons. [18] The sp^2 carbons can be removed by oxidation in air at elevated temperature for several hours. [14] The heterogenity of the surface can be reduced using treatment in oxidative acids. Surface with high fraction of carboxyles is produced by this process. Such pretreated NDs form stable colloidal solutions in water that are necessary for further applications. [14,18]

2.2.3. Biocompatibility, low toxicity, internalization and localization in cells

Biocompatibility and low toxicity are key properties for using NDs in biomedical applications. Biocompatibility refers to the ability of nanoparticles to perform its desired function without eliciting any undesirable local or systemic effects in the recipient. Nanoparticles toxicity is related to the ability of particles to adversely affect normal physiology or interrupt the normal structure of organs or tissues. [19] Nanoparticles are generally considered toxic because of their small size and possibility to internalize into cells and localize in critical organelles. [18,19] NDs stand out among other carbon nanoparticles due to previously mentioned qualities. NDs after post-synthetic modifications are reported as a biocompatible and low toxicity material. NDs do not induce inflammatory or cytotoxic responses such as generation of reactive oxygen species or cytokines and do not cause morphological alterations, viability changes or cell death in a wide variety of cell lines. [8,11,20–22] The morphology of cytoskeleton and nuclei is not altered after incubation with NDs, in contrast to incubation with positive control of human carcinogen sodium arsenite. [22] However, studies indicating NDs toxicity have appeared recently; the toxicity is referred as much lower than for the other carbon materials. [22] The long-term effect of NDs remains, similarly to other nanoparticles, unknown in both organism and cells. [18]

2.2.3.1. Cell internalization of NDs

NDs can spontaneously enter cultured cells. [8,12,24] Half-life of the uptake is dependent on a particle size. The smaller the size of NDs is the shorter it is the uptake half-life. [7] For the examination of NDs cellular uptake mechanism, cells were incubated under conditions of lower temperature and presence of sodium azide. The decrease of uptake under these conditions means that internalization depends on temperature and energy (sodium azide creates ATP-depleted environment) and implies active transport, endocytosis mechanism. Reduced uptake in the presence of sucrose, which is known to disrupt the formation of clathrin-coated vesicles, implies that a clathrin mediated pathway is employed. The clathrin mediated pathway is the most frequent process among different, in which ligand first binds to a cell surface receptor and then is internalized. Receptor-mediated endocytosis is facilitated thanks to proteins of the serum adsorbed onto the ND surface.

2.2.3.2. Cellular localization

Endosomes are vesicles involved in the transport of extracellular materials. Extracellular material is engulfed by a cell membrane and trapped in a newly created endosome during endocytosis. Endosomes can fuse with lysosomes. The content of a vesicle is degraded or can be recycled back to the plasma membrane. Some studies imply that some part of NDs is entrapped and localized in endosomes [7]. Smallest particles can be also observed in cytoplasm. It is not clear if these smallest NDs (approximately 5 nm) are directly internalized via passive transport across cellular membrane or are released from the endosomes. The fact that NDs do not stay inside the endosomes is a positive promise for application as a drug delivery. No NDs were observed in a nucleus in studied cases. [7,24]

2.2.4. Conjugation of biomolecules on the surface of NDs

NDs are stable and usually assumed to be easily modified. Two main connection modes are suitable for biomolecules attachment: non-covalent and covalent. Carboxyl groups on the surface of NDs are used for both types. Non-covalent connections are mediated mostly by adhesion, but important are also electrostatic interactions mediated through carboxyl groups. Non-covalent connections are experimentally easily created. The major disadvantage is non-specifity of the interaction; e.g. NDs can bind practically every protein in solution. Covalent grafting, on the other hand, brings much more specifity and strength in binding a molecule to the surface. This task is exacting and more time-consuming, though. [25] Amide bonds are the most frequently used connections of biomolecules amines to carboxyls on the surface. [26,27]

There are many reasons to connect molecules to the surface. Cellular targeting, internalization and drug delivery are some of them. Another reason can be enzyme immobilization. Disadvantages of enzymes, such as low long-lasting stability and difficulties in recovery and recycling, can be eliminated and improved by enzyme non-covalent [9] or covalent [27] immobilization on the surface. This immobilization increases stability, enables repeated use and easy separation from the reaction mixture and can also improve catalytic properties of an enzyme. [28] Maintaining the bioactivity of conjugated molecules is crucial. [11] Various molecules are used as spacers between a biomolecule and a ND to reduce steric constraints and retain the function of biomolecule. This is fundamental for enzymes with active sites sterically hindered near the surface. [29]

Spacers are also used for suppressing non-specific interactions [30] and suppressing proteins conformation change caused by strong biomolecule-particle interactions. [9,31]

2.2.5. Targeting of particles

A targeting molecule can be connected to the particle surface. The targeting molecule ensures accumulation of a conjugate in a region where targeted moiety is placed, for example, a cancer cell. Targeting of nanoparticles is recently widely used approach with many benefits. Targeting molecules can be bound on the surface in high concentration, therefore avidity to a targeted moiety is increased. [32] This is used in diagnostics; labels do not have to be directly attached to the targeted moiety, but can be attached to a targeting molecule that binds this targeted moiety via molecular recognition. [4] Targeting of cancer cells and internalization of a NDs modified with targeting biomolecules such as transferrin, folic acid or growth hormone has been described previously in literature. [33] NDs can serve not only as particles but, due to their fluorescence, also as labels.

Targeting using a targeting molecule is called active targeting. Another way how particles can get *in vivo* to cancer cells, more likely than to normal cells, is passive targeting, e.g. enhanced permeability and retention effect (EPR effect) (Fig. 3). EPR effect is based on a fact that newly formed tumor blood vessels have large gaps between endothelial cells and nanoparticles can get through these gaps from blood to tumor tissue. EPR effect influences nanoparticle distribution which is further affected by active targeting. [32,34]

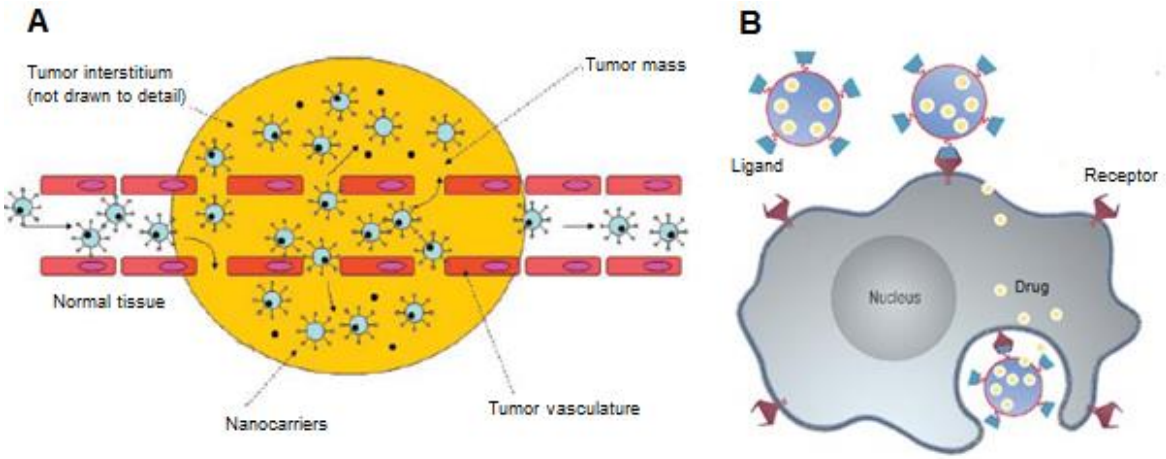

Fig. 3 **Schematic view represents different mechanisms by which nanoparticles can get to tumors.** (A) EPR effect. (B) Active cellular targeting following after EPR effect. Adapted from Prokop and Davidson [32] and Peer *et al*. [34]

2.2.6. Drug delivery

Modified particles capable of targeting can be furthermore used for targeted drug delivery (Fig. 3, p. 10). [32] During targeted drug delivery a drug is transported directly to diseased place where is released under control and has required medicinal effect. [35] Targeted therapy is specific and efficient, thus reducing toxic side effects and prevent normal cells death. [36] The drug molecule binds to a targeting molecule directly through a bond or indirectly if the drug molecule is associated with a carrier. Convenient carriers can carry a large amount of a drug and do not induce immune reaction; life of the drug in plasma is prolonged. The use of various types of carriers has been described earlier; molecules can be associated with liposomes, micelles, dendrimers, viruses or polymers. Chemotherapeutic drugs such as doxorubicin or cisplatin, toxic proteins such as ricin or diphtheria toxin, or nucleic acids can be used as the therapeutic molecule. [35–37] NDs have been used as drug carriers as well. Detonation NDs carrying doxorubicin hydrochloride are considered a convenient drug carrier for cancer therapy. Drug release is slow and sustained compared to a free drug. [38,39]

2.2.7. Novel surface architecture on the surface of NDs

Direct modifications of NDs, described briefly in paragraph 2.2.4, are sometimes problematic. One of the reasons is low accessibility and reactivity of functional groups present on the surface. To overcome this problem, it is convenient to transform the ND surface chemistry by coating ND by a thin layer of biocompatible, but reactive material. A possible way is to coat NDs surface with a silica shell. Silica is a well-defined and explored inorganic surface. Coating particles with silica has been described previously. [40] Silica layer allows high yield further modifications. [41] This procedure has been designed in our laboratory. Two different surface architectures are described in more detail in the following text. In both cases, surface architecture is designed from two covalently connected layers surrounding the ND particle, the layer of silica and the polymer layer.

2.2.7.1. Coating of NDs by silica and polyethylene glycol layer – ND-silica-PEG

ND-silica-PEG particles are coated with a solid silica shell bearing a flexible polyethylene glycol (PEG) layer. The silica layer is formed firstly by controlled hydrolysis of tetraethoxysilylesters followed by the growth of the amino-modified silica shell from the mixture of (3-aminopropyl)triethoxysilane and 1,2-bis(triethoxysilyl)ethane). 1,2-

bis(triethoxysilyl)ethane is used as a crosslinking agent which improves the shell´s resistance to hydrolysis. [42] The amino-modified silica shell enabling further direct functionalization is created as a result. In a subsequent reaction, the amino group reacts with the N-hydroxysuccinimidyl group at one end of the PEG chain (with the molecular weight of 5000 Da). The second end of heterobifunctional PEG is modified with the alkyne moiety. It enables the use of azide-alkyne cycloaddition catalyzed by copper (I) ions (CuAAC) for the attachment of various azide-modified molecules on the surface (Fig. 4). The attachment of ^{125}I-labeled RGDS peptide, fluorogenic probe coumarin and fluorescein on the surface was confirmed with different techniques. [43]

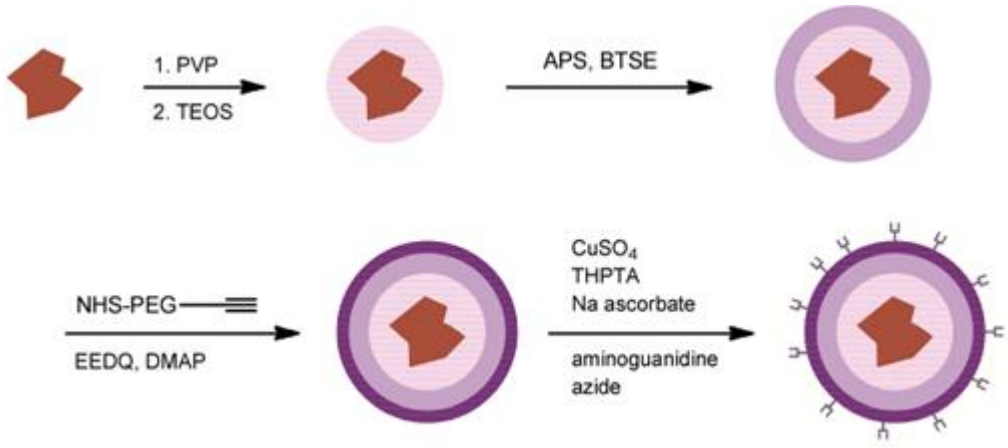

Fig. 4 **Schematic preparation of ND-silica-PEG particles.** ND is consecutively coated by silica shell (pink), thin aminopropyl-silica shell (violet), and PEG-alkyne layer (dark violet). Azide-modified moieties are attached using CuAAC on surface. TEOS – tetraethyl orthosilicate, PVP – polyvinypyrrolidone, APS- (3-aminopropyl)triethoxysilane, BTSE - 1,2-bis(triethoxysilyl)ethane), NHS-PEG-alkyne - α-succinimidyl ester-ω-propargylacetamido poly(ethylene glycol), EEDQ – 2-ethoxy-1-ethoxycarbonyl-1,2-dihydroquinoline, DMAP – 4-dimethylaminopyridine.

This surface architecture of ND-silica-PEG particles brings several advantages. Besides already mentioned improvement of the ND surface for high yield further modifications, the silica shell normalizes NDs irregular shape. Non-coated (naked) NDs are heterogeneous particles; they differ in size and have irregular shape. ND-silica-PEG coated particles are less polydisperse and have near-spherical shape (Fig. 5, p. 13). This geometry is generally considered biocompatible. [44] Moreover, the uptake of spherical particles in cells is higher in comparison to non-spherical particles. [44] The average diameter of ND-silica-PEG particles belongs to the optimal size range for nanoparticle biolabels (10-

100 nm). [32] Naked NDs are not stable in the environment with higher ionic strength, for example at buffers or cultivation media. PEG layer improves colloidal stability of particles, prevents particles from aggregation and therefore enables the use of NDs in biological applications. PEG layer is also expected to create a non-immunogenic surface and serves as a protection from opsonization. [45] This surface architecture does not change NDs fluorescence.

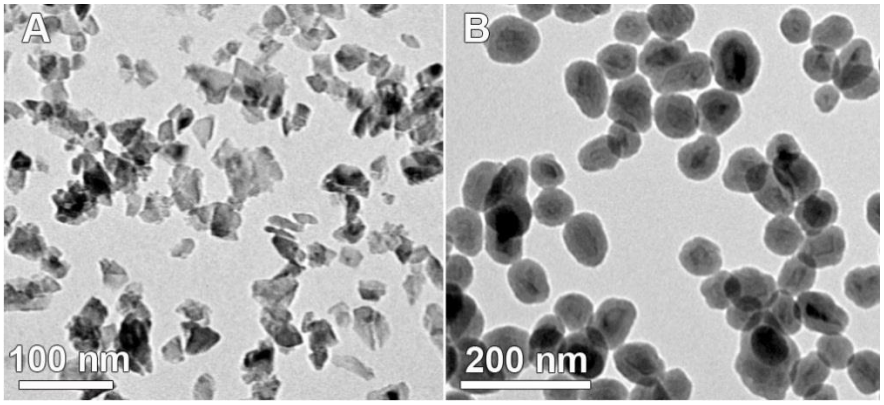

Fig. 5 **Transmission electron microscopy images of (A) non-coated and (B) ND-silica-PEG particles.**

2.2.7.2. Coating of NDs by ultrathin silica layer and acrylamide copolymer

The second possibility is to coat NDs with very thin layer of silica (< 1 nm) and subsequently with polymer N-(2-hydroxypropyl)methacrylamide (HPMA) to create ND-HPMA particles (Fig. 6). The silica layer is formed by the mixture of tetraethyl orthosilicate and 3-(trimethoxysilyl)propyl methacrylate. The silica layer is subsequently modified by radical polymerization with the mixture of HPMA and 3-azidopropylacrylamide (AzpAAm) or propargylacrylamide (PrAAm) (Fig. 7, p. 14).

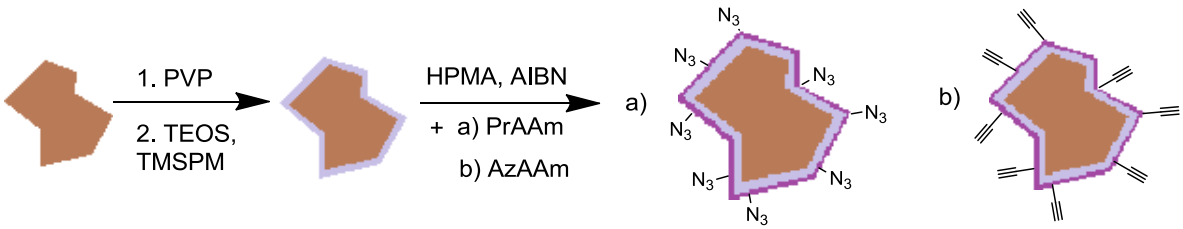

Fig. 6 **Schematic preparation of ND-HPMA particles.** ND is consecutively coated by silica shell (pink) and HPMA layer (violet). Polymer layer contain co-polymerized (a) PrAAm or (b) AzpAAm. PVP – polyvinylpyrrolidone, TEOS – tetraethyl orthosilicate, TMSPM - 3-(Trimethoxysilyl)propylmethacrylate, AIBN - azobis(isobutyronitrile).

The monomers form statistic copolymer chains starting from the surface. The used polymer determines the type of a prepared azide- or alkyne-modified ND. Modified NDs can react in CuAAC with alkyne- or azide-modified molecule, respectively. The ND surface is applicable to high yield further modifications. In contrary to ND-silica-PEG, ND-HPMA particles keep their irregular shape and are smaller than ND-silica-PEG.

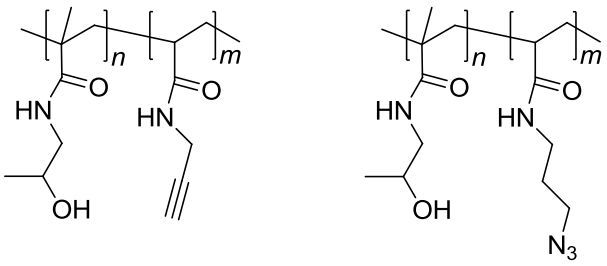

Fig. 7 **Structure of HPMA polymer with PrAAm or AzpAAm substitution.**

Analogous to ND-silica-PEG particles, polymer layer consisted of modified methacrylamide improves colloidal stability of particles and prevents particles from aggregation. It is beneficial for the use of the prepared particles in biological applications. This methacrylamide layer also creates a non-immunogenic surface and serves as a protection from opsonization. [46]

2.2.8. Chemical reactions used for covalent bioconjuations

Various types of connections are used for bioconjugations. Amide bond is in most cases used to connect a biomolecule to a surface. Carboxyl group on the surface of particles and amino group in a biomolecule participate in the formation of the amide bond. However, the bond is unspecific; biomolecules contain a large amount of amino groups and many of them can form the amide bond. The biomolecule is then immobile on the nanoparticle surface, yet it is crucial to preserve its structure, properties and function. It is convenient to know how the biomolecule is exposed to the surface and how to control the exposure. To ensure correct bonding, as little reacting groups as possible should be present in the biomolecule. For such purposes, the oxime ligation represents a convenient pathway; it is a reasonably efficient reaction at mild conditions and well defined way of attachment. [47] In this work, oxime ligation is used to connect an aldehyde (which is present in glycosylated Tf after cleavage of 1,2-diol of sialic acid [48]) to an aminooxy group (present on a short linkage molecule, 3-aminooxypropyl-1-azide).

CuAAC reaction, a reaction of azide- and alkyne- moieties, can be also used for bioconjugations. [49,50] This reaction is widely used for the connection of molecular entities of all sizes involving, for example, fluorescent dyes, peptides, proteins or polynucleotides. This reaction can be used for efficient grafting of larger units onto the surface of nanoparticles. [51] In this work, CuAAC is used to connect various organic dyes, transferrin and inhibitor of GCP II on the surface of coated NDs.

2.3. BIOMOLECULES AS AGENTS FOR TARGETING

Two biomolecules which could serve for targeting of cancer cells are used in experimental section of this diploma thesis. These selected targeting molecules, transferrin and an inhibitor of GCP II, will be described in more detail in the following paragraphs.

2.3.1. Transferrin and transferrin receptor

2.3.1.1. Transferrin

Transferrin (Tf) belongs to the family of Tf proteins, containing non-heme iron-binding glycoproteins. Other members of this family are, for example, ovotransferrin, lactoferrin and melanotransferrin. Tf can be found in the blood system and other mammalian fluids like cerebrospinal fluid, lymph, milk or others. [52] Tf controls levels of free iron and transport Fe^{3+} to various parts of a body. Iron is required as a cofactor for many proteins involved in metabolism, respiration, DNA synthesis, cell division and other processes. [53,54] Tf helps to control the metabolism of free toxic Fe^{2+} ions, which are harmful to DNA, cellular membranes or proteins (due to the formation of free toxic radicals via Fenton reaction). Tf is also important to prevent deposition of insoluble Fe^{3+} compounds and forming the aggregates or polymers. [53,54]

Tf is a glycoprotein with molecular weight 77 kDa [55] and pI around 5.6 - 5.8 [53], synthetized mainly in hepatocytes. Tf is composed of a single polypeptide chain containing 679 amino acids forming two different lobes. The lobes are called the C-lobe and the N-lobe and are separated by a short polypeptide strain (Fig. 8A, p. 16). Each lobe can bind one ferric ion. Both lobes are formed from two domains (N1, N2, C1, C2) [52,54,56]. The Fe^{3+} is in Tf hexa-coordinated with octahedral geometry. Four amino acids: two tyrosines, one aspartate (these amino acids are coordinated through the oxygen atom – phenolate or carboxylate) and one histidine (using nitrogen atom of imidazole)

participates in this interaction. The last two *cis*-positions are occupied by carbonate or (bi)carbonate anions anchored by an arginine residue (Fig. 8B, p. 16). [53,57] Four amino acids occur in different places in lobe´s tertiary structure; in both domains as well as in flexible hinge between the two domains. When Tf binds the iron ion, the full lobe undergoes a conformational change from "open" to "close" conformation and the whole protein structure is changed. This change of structure is pH-sensitive. [53,58]

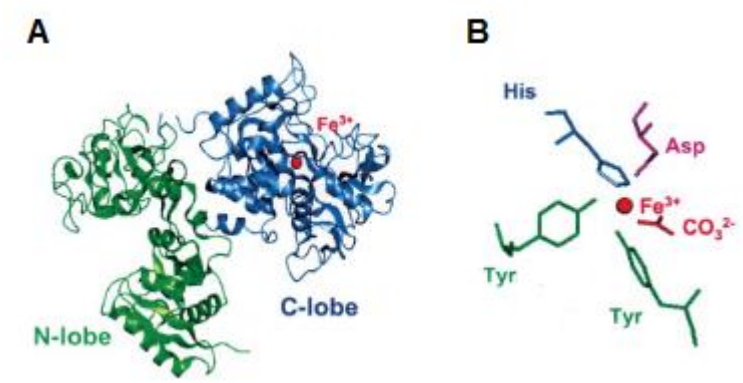

Fig. **8 Binding of the Fe^{3+} in the structure of Tf.** (A) X-ray crystal structure of Tf with one Fe^{3+} bound in the C-lobe. Full C-lobe is in "close" conformation, empty N-lobe in "open" conformation.
(B) The schematic figure of Tf residues which bind ferric ion. Adapted from Li and Qian. [53]

Tf has three different forms – apotransferrin (aTf) which binds no ferric ion, partially saturated Tf with one ferric ion and Tf with two full binding sites. The last one, which is called holotransferrin (hTf), interacts with the cell membrane receptor and become endocytosed. [53,54] The reason why receptor recognizes only hTf and not aTf is the different structure of these two proteins caused by Fe^{3+} binding. Tf can also bind other metal ions; yet the binding of the ferric ion is the most preferred. [54] aTf is achromatic. Binding of an ion to a specific site colors the protein differently. For example Tf with ferric ion (hTf) is orange, contrary to Cu^{2+}- or Co^{3+}-binding Tf which are yellow. [52]

2.3.1.2. Transferrin receptor

Transferrin receptor (TfR) is a homodimeric transmembrane glycoprotein with N-terminal part located in cytoplasm. Two subunits are connected with two disulfide bonds. [54] Each subunit has 760 amino acids, a molecular weight of approximately 90 kDa and consists of three regions (Fig. 9A, p. 17). [53] 67 amino acids long chain is in cytoplasm; 21 amino acids long chain forms the single-pass transmembrane region. The largest part of protein, 672

amino acids, belongs to the extracellular region. [54,55,59] The intracellular region has four potential phosphorylation sites, yet only one serine is used as a target of protein kinases. This phosphorylation is not required for the proper function of the receptor its function is unclear. On the other hand, glycosylation of three N-glycosylation sites (asparagine) and one O-glycosylation site (threonine) in extracellular region is necessary to guarantee the function (Fig. 9A). [54,59] There are also two palmitoylation sites in the intramembranous portion of TfR which help to anchor the receptor to the membrane. [60] The extracellular soluble region consists of three domains – the apical domain, the protease-like domain and the helical domain (Fig. 9B). [52,53] The protease-like domain is homologous to amino- or carboxy-peptidases, the most homologous protein is the protease domain of glutamate carboxypeptidase. This relationship is probably evolutionary because TfR has no protease activity. [52,56,60]

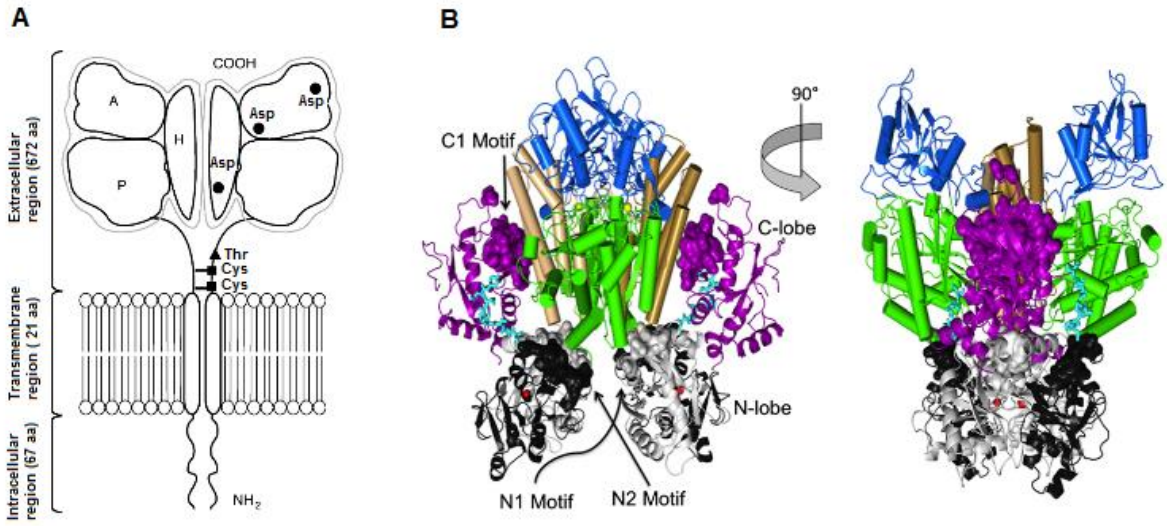

Fig. 9 **Structure of homodimeric TfR.** (A) Schematic structure of TfR with three different regions in both subunits – extracellular, transmembrane and intracellular. Subunits are connected by disulfide bridges at cysteins. Extracellular region consists of three domains – apical (A), helical (H) and protease-like (P). Three aspartates (Asp) and one threonine (Thr) are glycosylation sites. (B) Structure of Tf-TfR complex. The apical domain of TfR is blue, the protease-like domain is green and the helical domain is brown. C-lobe of Tf is purple, N1 domain of N-lobe is gray and N2 domain is black. Short polypeptide strain between lobes is cyan. N-lobe Tf bind with ferric ion (red). Adapted from Daniels *et al* [36] and Eckenroth *et al*. [57]

TfR is expressed in all cells with nuclei; it is thus found on almost all cells membranes. [53] No expression of TfR was found on pluripotent hematopoietic stem cells. Higher amount

of TfR is expressed in cells with a high rate of proliferation, such as the basal epidermis or the intestinal epithelium, or in cells which need higher amount of iron, for example, a maturating erythrocyte for heme synthesis. Cancer cells, primarily malignant cancer cells, also belong to the cells with a higher rate of proliferation and higher need of iron to growth. The number of TfR is even correlated with tumor stage and cancer progression. Fast dividing cancer cells probably need higher amounts of iron as a cofactor for enzymes involved in RNA polymeration, DNA synthesis and cell division. [54]

2.3.1.3. Mechanism of cellular iron uptake

Tf interacts with TfR in order to deliver the iron atom into a cell. TfR has a pH-dependent structure. hTf can bind to TfR in neutral or higher pH (in cytoplasm, it has 500-fold higher affinity for TfR than aTf [54,59]); aTf can bind in acidic environment. [53] Cell uptake is initiated by the contact of Tf with TfR. Studies have shown that for recognition and for binding, both part of Tf (C-lobe and N-lobe) are required. The N-lobe is probably sandwiched between the extracellular region of TfR and the cell membrane and is in contact with the helical and protease-like domain. The C-lobe touches the TfR´s helical domain at a single site. [54,57,61] After the successful interaction, both Tf and TfR are internalized in clathrin-coated pits by receptor-mediated endocytosis (Fig. 10).

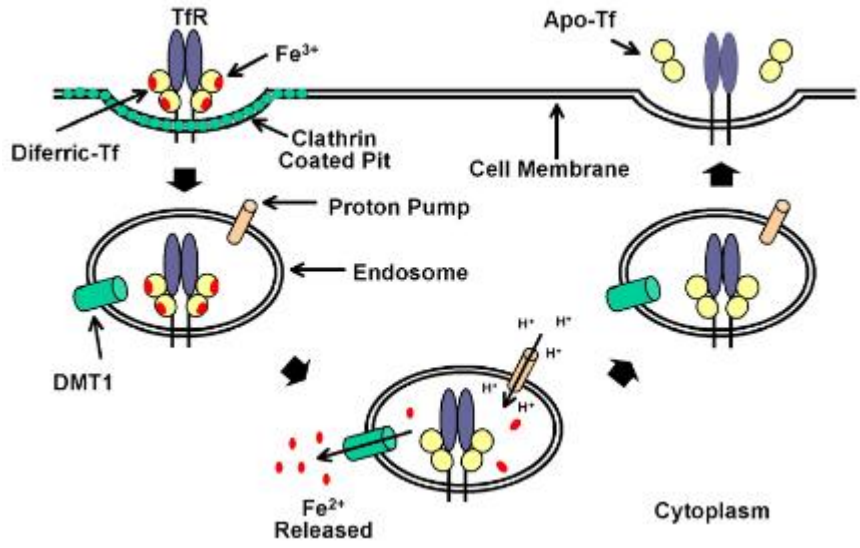

Fig. 10 **Cellular iron uptake by receptor mediated endocytosis.** To homodimeric TfR is bound differric Tf (hTf). Whole complex is internalized via clathrin-coated pits to an endosome. In the endosome pH is subsequently decrease by proton pumps, ferric ions are released, reduced to ferrous ions and transported by the divalent metal ion transporter 1 (DMT1) to cytoplasm. The complex of Tf-TfR is recycled back to the cell surface and Tf dissociates from the receptor. Adapted from Daniels *et al*. [37]

The complex is engulfed in the endosome; the endosomal pH is decreased by protons which are pumped inside by ATP synthase. The lumen of the endosome is acidified to pH 5.5, approximately. At this pH Tf changes structure and releases iron. Iron is reduced to ferrous ion and transported to cytoplasm by a divalent metal transporter. In the cytoplasm it can be used as a cofactor for proteins such as aconitase (with Fe-S cluster), cytochromes, hemoglobins, oxidases, peroxidases (with hemes) and others or it can be stored in the protein ferritin. [52,58] The complex of aTf and TfR escapes degradation and is removed from a cell by exocytosis. [52–54,56,59,60] On the cell membrane the complex dissociates. The whole cycle is usually completed within a few minutes. One Tf molecule participates in the cycle approximately 100-200 times. [60] Unlike other receptors, TfR is also significantly internalized into a cell without the interaction with the ligand. [54]

2.3.1.4. Targeting of cancer cells using Tf-TfR interaction

Several fold higher levels of TfR on cancer cells than on normal cells open up the possibility to use TfR for visualizing cancer cells by labels (diagnostics). The interaction between Tf and TfR can be also used for targeted cancer therapy. There are two different ways how to take advantage of the TfR for cancer therapy. The first approach is to block the receptor and make the iron uptake impossible, for example by specific antibodies. The influenced cell dies because no iron needed for growth and metabolism is available. The second approach is targeting of the TfR by a complex of Tf and a therapeutic molecule. This complex is endocytosed in a cell and can cause cell death. [36] Another feature applicable in therapy is the fact that Tf can bind other metal ions, Tf can deliver diagnostic radioisotopes ($^{67}Ga^{3+}$, $^{111}In^{3+}$) or therapeutical ions (Bi^{3+}, Ru^{3+}, Ti^{4+}). [35,52]

Different types of carriers are used for diagnostics or targeted therapy. Two carriers are described here in more detail. Liposomes are carriers which have been used for a long time and are well examined. NDs, as the second example, are particles were not described in the field of targeted therapy yet.

2.3.1.4.1. Targeting of TfR using Tf-liposome conjugate

Ishida *et al.* have shown that PEG coated liposomes with Tf can target Colon 26 cancer cells *in vitro* and even *in vivo* in mice. Liposomes with diameter 100-140 nm each bearing 25 Tf molecules were used. Tf was covalently linked by amidic coupling to the distal

terminal of PEG-COOH chain. Experiment confirmed that the surface of Tf-PEG-liposomes does not interact with macrophages; Tf-PEG-liposomes maintain in circulation longer than bare liposomes. [36,37] The binding ability and accumulation in tumor of Tf-PEG-liposomes was higher than for PEG-liposome particles. Internalization of these particles by a receptor-mediated endocytosis through clathrin-coated pits was furthermore confirmed by pre-incubation with Tf. Cells were incubated with free Tf in the pre-incubation experiment in order to saturate all TfR. The uptake of Tf-modified particles is subsequently limited. [62] The use of liposomes in cancer therapy was described, for example, by Iinuma *et al.* Tf-conjugated PEG liposomes were employed by the authors to deliver encapsulated cisplatin to human gastric cancer cells inoculated in mice. Therapeutic effect of cisplatin delivered in Tf-PEG-liposomes was proved by a significant increase of mice survival rate compared to free cisplatin, bare liposomes or PEG-liposomes. [45] Convenient properties of PEG coated liposomes were used in the research of the anticancer drug named Doxil ® (already approved for human use). Doxil® is doxorubicine encapsulated in a PEG coated liposome suitable for intravenous infusion.

2.3.1.4.2. Targeting of TfR using Tf-ND conjugate

Experiments similar to targeting cells with liposomes functionalized with Tf were carried out with ND particles (100-140 nm). [26,63,64] In all cases, naked carboxylated NDs were modified by the formation of an amide bond between ND and Tf. In the experiment, performed by Weng *et al*, HeLa cells were used. The HeLa cells overexpress TfR on the cell membrane. Carboxylated NDs and cells presaturated with free Tf were used as controls. Free Tf serves again as the confirmation of the internalization of these particles by a receptor-mediated endocytosis through clathrin-coated vesicles. Pictures from confocal microscope proved that ND-Tf conjugates were observed inside the cells, contrary to carboxylated NDs and ND-Tf conjugates in Tf-presaturated cells. The TfR mediated uptake of ND-Tf was confirmed by this experiment. [64]

2.3.2. Glutamate carboxypeptidase II and its inhibitors

2.3.2.1. Structure of Glutamate Carboxypeptidase II

Glutamate carboxypeptidase II (GCP II) is a homodimeric transmembrane glycoprotein. One subunit contains 750 aminoacids and has approximately 84 kDa after N-

deglycosylation (the whole subunit has a molecular weight of almost 100 kDa). GCP II is localized on an apical plasma membrane. [65,66] GCP II belongs to class II transmembrane proteins with short cytoplasmic amino-terminal region (19 amino acids) and short single transmembrane α-helix (25 amino acids). The rest of the protein is placed in the extracellular space. [65,67] GCP II has a structural similarity to TfR, however, sequence identity reaches only 28%. [65] The extracellular region is, similarly to TfR, composed of three domains (the protease, apical and C-terminal domain) (Fig. 11).

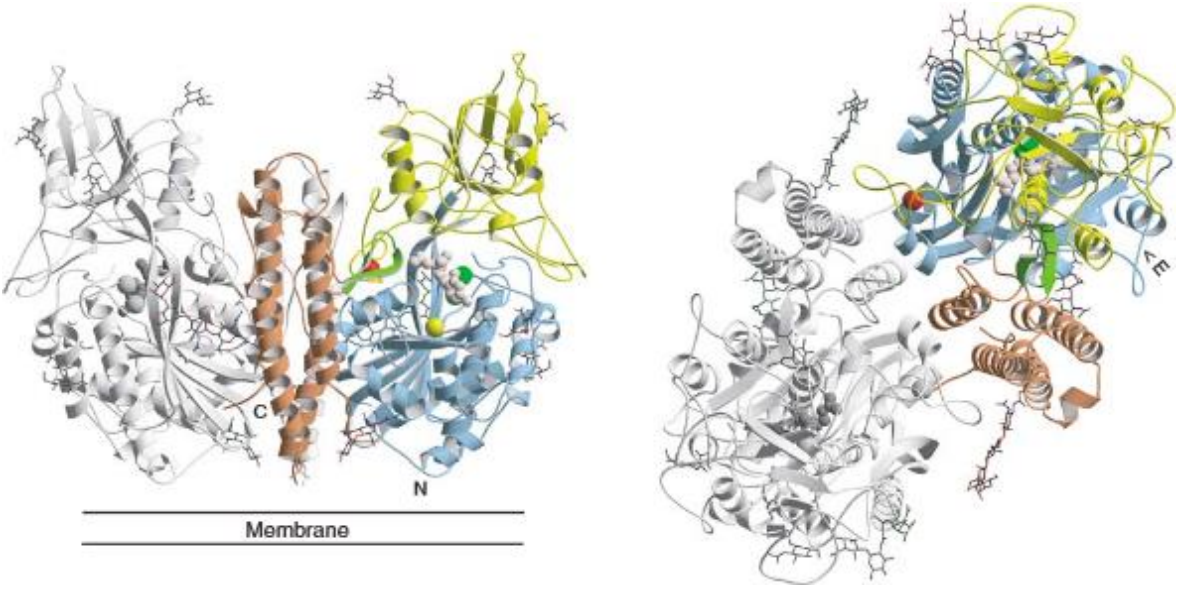

Fig. 11 **Structure of extracellular region of homodimeric GCP II.** One subunit of GCP II is shown in gray. Second subunit is divided to domains: C-terminal (brown), apical (yellow) and protease (blue). Ions are shown as spheres: the dinuclear zinc cluster at the active site (green), Ca^{2+} ion (red) and Cl^- ion (yellow). Inhibitor is shown as small beige balls. The „glutarate sensor" is shown in light green. The entrance to the catalytic site is marked in the right figure as „E". Adapted from Mesters *et al*. [65]

The protease domain contains α-helices as well as β-sheets. The apical domain is placed between two β-sheets of the protease domain and covers the active site of the enzyme. Both protease and apical domain create pockets for a substrate or inhibitor. S1 pocket prefers to bind a negatively charged residue on P1 position. S1´ pocket is responsible for recognition of P1´ amino acid of a substrate, which is in most cases glutamate for GCP II. S1´ pocket can also interact with other amino acids. [65] The C-terminal domain is composed of α-helices and helps protein to dimerize. GCP II, similarly to TfR, forms a homodimer. Saccharides contribute to homodimerization, apart from the C-terminal

domain. Up to ten N-glycosylation sites have been found; they increase solubility and stability of the protein and are required for proper folding and function. [65,66]

GCP II is a metalloprotease dependent on two Zn^{2+} ions with the assistance of two other ions: Cl^- and Ca^{2+} (Fig. 11, p. 21). Mechanism of its enzymatic activity is the same as for the other binuclear metalloproteases. The role of the chloride anion is to maintain the correct conformation of arginine residues in S1. Arginine residues place a substrate in a convenient position by interaction with its negatively charged residues. Ca^{2+} ion stabilizes a loop which is involved in dimerization. Two flexible segments are a part of the protein: the glutarate sensor (13 amino acids) and the entrance lid (8 amino acids). Substrate binding into the active site changes the conformation of the glutarate sensor which covers S1´ pocket. Subsequently, the entrance lid covers S1 pocket preventing other substrates to bind. The whole enzyme changes its conformation from "open" to "close" state after binding substrate in the active site. [65–67]

2.3.2.2. Different names and functions of Glutamate Carboxypeptidase II

GCP II had possessed many alternative names which were used for the protein before it was found that it is the same protein. The names of the protein were dependent on the reaction the enzyme catalyzes or on the place it can be found –prostate-specific membrane antigen (PSMA), folate hydrolase I and N-acetylated-α-linked acidic dipeptidase (NAALADase).

GCP II has enzymatic activity which is responsible for the cleavage of N-acetyl-L-aspartyl-L-glutamate (NAAG) to N-acetyl-L-aspartate (NAA) and glutamate (Fig. 12). [65,66,68,69]

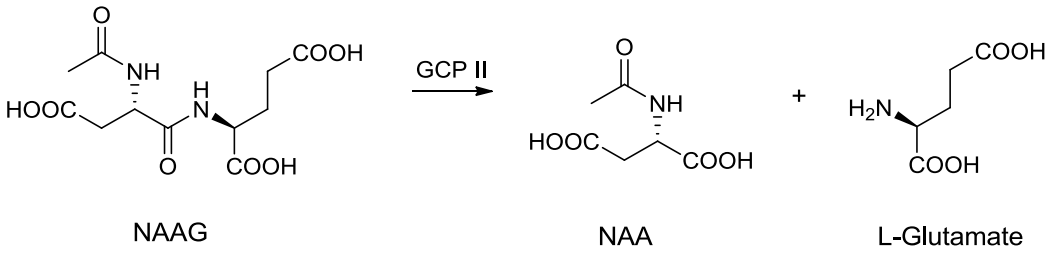

Fig. 12 **Cleavage of the peptide neurotransmitter N-acetyl-L-aspartyl-L-glutamate (NAAG) to N-acetyl-L-aspartate (NAA) and L-glutamate.**

Glutamate is an important excitatory neurotransmitter in central nervous system. Excitatory neurotransmitters activate receptors with excitatory effects (on the contrary to

inhibitory neurotransmitters like γ-aminobutyric acid which activate inhibitory receptors). Glutamate is at higher levels neurotoxic, it can cause necrosis of neurons in surrounding tissues. It has been found that excess of glutamate can lead to neurodegeneration in pathologies such a stroke, chronic pain, Parkinson´s disease, epilepsy and others. [65,68,70] The neuropathy might be decreased by the reduction of the glutamate concentration. Conventional therapies focus on blocking receptors of glutamate with small molecules. The second possibility is to prevent the production of glutamate. Since GCP II produces glutamate from NAAG, it is a convenient target for inhibition and yet for the treatment of neurological diseases. The inhibition of GCP II does not only reduce the amount of glutamate but also increases the level of NAAG, a neurotransmitter which is known for its neuroprotective effects. [65,68,71]

In the intestine, GCP II (as folate hydrolase I) participates in the cleavage of γ-linked glutamates from folyl-poly-γ-glutamate up to vitamin folic acid. This cleavage increases the intestinal uptake of folates. [65,66,68]

Physiological function of GCP II in prostate is not clear. No substrate for GCP II in prostate tissue has been identified; there is a possibility that its role in the prostate tissue is not enzymatic. Some authors suggest that GCP II might work as a receptor due to its similarity with TfR, but its ligand has not been described either. [66] Even though its physiological function remains unknown, the increase in expression in prostate cancer is evident. Higher levels of GCP II have been found in neovasculature in many types of solid tumors as well. [68,69,71] GCP II has been found in many classes of organisms. Only little expression of GCP II was found in animals in a prostate tissue and the distribution of GCP II expression varies a lot, it is evident that GCP II expression in tissues is species specific. This could be a problematic fact for the selection of an animal model for *in vivo* studies of GCP II-based therapy. [66]

2.3.2.3. GCP II inhibitors

There are two different categories of GCP II inhibitors. Analogues of NAAG (substrate for GCP II) are the first possibility, derivatives of glutamate (cleavage product of GCP II) are the second. NAAG analogues contain L-glutamic acid, non-hydrolysable isostere of a peptide bond and a group with affinity to zinc ions. Urea, in urea-based inhibitors,

imitates the planar peptide bond of NAAG; phosphonate containing groups simulate a tetrahedral transition state of an intermediate. Many inhibitors are symmetric compounds such as (S)-2-[3-(S)-(1,3-dicarboxypropyl)ureido]pentanedioic acid. (S)-2-[3-[(S)-1-carboxy-3-methylbutyl]ureido]pentanedioic acid is the most significant example of urea-based inhibitors. The molecule of 4,4'-phosphinicobis(butane-1,3-dicarboxylic acid) belongs for example among compounds with the central carbonyl group replaced with zinc-binding P(O)OH group (Fig. 13). [71]

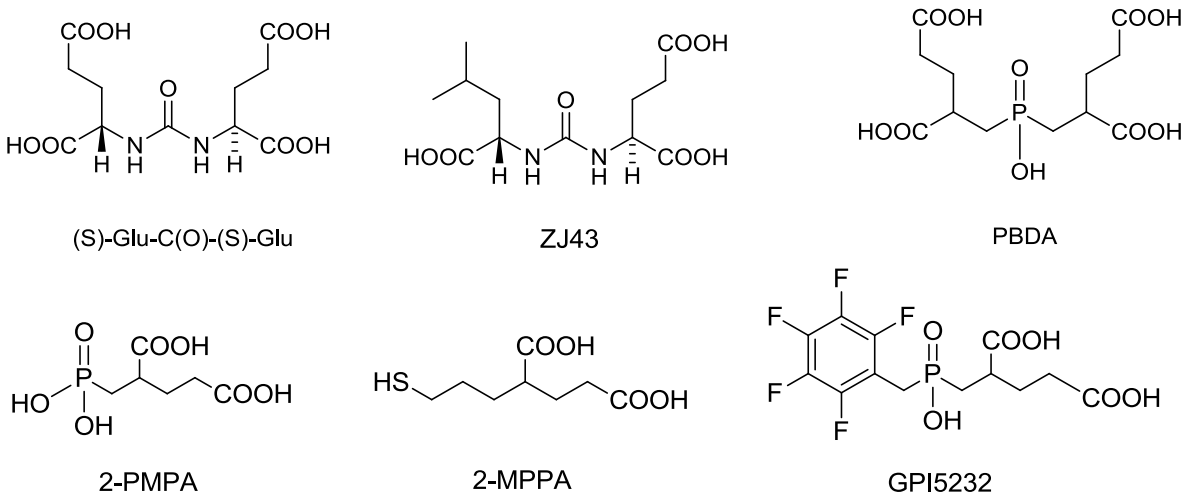

Fig. 13 **Inhibitors of GCP II (analogues of NAAG – first row, glutamate-based inhibitors – second row).** (S)-2-[3-(S)-(1,3-dicarboxypropyl)ureido]pentanedioic acid ((S)-Glu-C(O)-(S)-Glu), (S)-2-[3-[(S)-1-carboxy-3-methylbutyl]ureido]pentanedioic acid (ZJ43), 4,4'-phosphinicobis(butane-1,3-dicarboxylic acid) (PBDA), 2-(phosphonomethyl)pentanedioic acid (2-PMPA), 2-(3-mercaptopropyl)pentanedioic acid (2-MPPA), 2-(hydroxypentafluorophenyl methylphosphinoylmethyl) pentanedioic acid (GPI 5232). Both enantiomers of PBDA, 2-PMPA, 2-MPPA and GPI5232 are potent inhibitors (the racemic mixtures are used).

Glutamate-based inhibitors contain a glutamate scaffold and a zinc-binding group. The zinc-binding groups include phosphinate moieties [72] or thiol-based compounds. [70] The first analogue of glutamate 2-(phosphonomethyl)pentanedioic acid (2-PMPA) (Fig. 13) with high affinity and selectivity to enzyme GCP II was synthetized by Jackson *et al.* [72] This hydroxyphosphinyl derivative of glutamate is one of the most potent competitive GCP II inhibitors and has an very low inhibition constant; it is in picomolar range (Ki = 200 pM). [68] Ki is the dissociation constant for the enzyme-inhibitor complex. The inhibitor has advantageous properties such as low molecular weight and high aqueous solubility; 2-PMPA can serve as a tool to reveal the physiological role and mechanism of

GCP II. [68] Other similar compound is 2-(hydroxypentafluorophenyl methylphosphinoylmethyl) pentanedioic acid (GPI 5232) which has also high selectivity to GCP II and solubility in water (Fig. 13, p. 24). [68] Nevertheless, to be absorbed orally or to cross the blood brain barrier is difficult for molecules containing polar groups such as phosphonate and phosphinate groups; it limits their usage as therapeutic agents significantly. [70] To reduce polarity and improve oral bioavailability, phosphorous containing group can be substituted by a less polar thiol group. Thiol derivatives of 2-PMPA are, indeed, not as effective as 2-PMPA. The efficiency of inhibition of GCP II by thiol derivatives is dependent on the number of methylene units between pentanedioic acid and a thiol group. 2-(3-mercaptopropyl)pentanedioic acid (2-MPPA) (Fig. 13, p. 24) is considered to be the most favorable thiol analogue of 2-PMPA. 2-MPPA also works as a competitive inhibitor with K_i 30 nM. [70]

The effect of phosphonate analogue 2-PMPA was studied on various neurological diseases for which a high level of glutamate is characteristic. It has been shown that 2-PMPA has neuroprotective effects in animal models in the case of neonatal ischemia [73,74] or neuropathic pain. [75] Similar effects *in vivo* has been observed in the case of GPI 5232, 2-MPPA and urea-based analogues. [71] For example, GPI 5232 decrease consequences of brain injury and also improve electroencephalographic signal recovery; it can thus be used as post-injury treatment of stroke. [76]

The possibility to employ inhibitors of GCP II in the oncology field is opened up. As mentioned above, the other name of GCP II is prostate-specific membrane antigen. It is overexpressed in prostate tumors. Inhibitors of GCP II can target membranes of cancer cells and bind to them specifically. For this purpose, Tang *et al* synthetized inhibitor 2-PMPA modified with fluorescein dye. This derivative was incubated with cells which express GCP II (LNCaP cell line) and cells which do not (DU-145 cell line). Confocal microscopy and flow cytometry revealed that the derivative of 2-PMPA binds GCP II specifically, since no fluorescence on DU-145 was observed in contrast to fluorescently labeled LNCaP cells. [77] Effort has been made to synthetize conjugate of GCP II inhibitor and anticancer drug doxorubicin. This analogue was proved to have high binding affinity to GCP II, but low *in vitro* antitumor activity. The observation that a large group can be

attached to inhibitors without a loss of binding activity is a promising result for diagnostics and targeted therapy. [69]

2.3.2.4. Nanoparticles and PSMA:

Since it is known that GCP II can be used for diagnostics and targeted therapy to deliver some drugs to cancer cells, engaging nanoparticles for this purpose represents the next logical step. Sanna *et al* used biocompatible nanoparticles built from copolymer poly(lactide-co-glycolide)-block-poly(ethylene glycol) (PLGA-PEG). High-affinity urea-based GCP II inhibitor N-[N-[(S)-1,3-dicarboxypropyl]carbamoyl]-(S)-lysin (DCL), which was connected to the surface via amidic bond to PEG-COOH chain, was chosen as a targeting compound. (-)-epigallocatechin 3-gallate, compound which is present in green tea, was used as a chemotherapeutic agent attached to the surface. Targeted nanoparticles with inhibitor were more cytotoxic for LNCaP cells than non-targeted nanoparticles. On the other hand, no cytotoxicity was observed in normal cells (Human umbilical vein endothelial cell line, HUVEC). [78] This fact confirms the efficiency of targeting GCP II with nanoparticles. Similar system with similar results has been introduced by Chandran *et al*. Urea-based inhibitor and chemotherapeutic agent (docetaxel) was attached to poly(lactic acid)-block-polyethylene glycol (PLA-PEG) copolymer in this particular case. [79] Nanoparticles, which are targeted to prostate cancer cells using antibody or, rather aptamer on the surface, are considered as another possibility. Aptamer is a part of oligonucleic acid or peptide which interacts with a specific molecule with high affinity and specificity. The conjugate of PLGA-PEG-aptamer with cisplatine was proved to have a toxic effect and prolonged drug resistance in blood circulation both *in vitro* [80] and *in vivo* [81]. Apart from nanoparticles constituted of various polymers, gold nanoparticles using both oligonucleotidic aptamer [82] and phosphoramidate inhibitor [83] have been used recently for targeting of GCP II on prostate cancer cells. Using of NDs for GCP II targeting has not been described yet.

3. OBJECTIVES

- Modify transferrin for further bioconjugation
- Modify nanodiamond particles with silica and polymer coating
- Prepare a nanodiamond conjugate with transferrin
- Prepare a nanodiamond conjugate with inhibitor of glutamate carboxypeptidase II
- Characterize nanodiamond conjugates with these biomolecules
- Investigate a potential of these conjugates to target the cancer cells

4. MATERIALS AND METHODS

4.1 INSTRUMENT AND CHEMICALS

Sonication probe and ultrasonic processor 750 W (Cole Parmer Instrument., Illinois, USA)

Ultrasonic bath – Elmasonic P 60 H 37 kHz (Elma-Ultrasonic, Germany)

Flow cytometer BD LSR II equipped with 488 nm laser (Coherent Sapphire 488-20 DPSS laser) and emission filter 525/50 (Becton Dickinson, New Jersey, USA)

Confocal microscope FV-1000 equipped with the solid state laser (473 nm) and objective 40x/0.95 dry (Olympus, Japan)

Confocal microscope LSM 780 equipped with the argon laser (488 nm) or In-Tune laser tuned to 532 nm and an oil-immersion objective (Plan-Apochromat 63x/1.40 Oil DIC M27) (Zeiss, Germany)

Flow cytometer BD LSRFortessa equipped with 488 nm laser and emission filter 530/30 (Becton Dickinson, New Jersey, USA)

ZetaSizer Nano ZS (Malvern Instruments, Great Britain)

UV-Vis spektrofotometer Specord 250 Plus (Analytic Jena, Germany)

Luminiscence spectrometer: AMINCO Bowman Series 2 (Thermo Scientific Spectronic, Massachusetts, USA)

HPLC: 1200 Series Agilent Technologies (California, USA), Reversed-Phase column - C18, pore size 100Å, particle size 1.8 µm, 2.1 mm x 100 mm (Waters, Massachusetts, USA)

Monochrome scientific grade camera Quantum ST4 (Vilber Lourmat, France)

ThermoVac Sample Degassing and Thermostat Unit (MicroCal, Pennsylvania, USA)

SPR instrument: Plasmon IV and thin gold nanosenzor (Institute of Photonics and Electronics, Czech Republic)

IPC High Precision Multichannel Dispenser (Ismatec, Germany)

pH meter Jenway 3505 (Stone, Velká Británie)

Centrifugal filter tubes, cut off 300,000 Da (Millipore, Massachusetts, USA)

Ultrafiltration cell, cut off 30,000 (Millipore, Massachusetts, USA)

Analytical balance BBC-22 (Boeco, Germany)

Balance BBI-41 (Boeco, Germany)

Centrifuges with fixed angle rotors:

Centrifuge Allegra X-15R (Beckman Coulter Co., California, USA)

Centrifuge Hermle Z383K (Hermle LaborTechnik, Germany)

Centrifuge 5430 (Eppendorf, Germany)

Centrifuge Minispin plus (Eppendorf, Germany)

Centrifuge Hermle Z36HK (Hermle LaborTechnik, Germany)

Chemicals, if not stated otherwise, were purchased from standard supplier Sigma Aldrich (Missouri, USA). The high purity solvents (puriss grade, over molecular sieve) were used.

Nanodiamonds (Microdiamant, Switzerland)

Ethylalcohol 99.8% for UV spectroscopy (Lach-ner, Czech Republic)

α-Succinimidyl ester-ω-propargylacetamido poly(ethylene glycol) NHS-PEG-alkyne (Iris Biotech, Deutschland)

Alexa Fluor 488 alkyne, Alexa Fluor 488 azide, Alexa Fluor 488 sulfodichlorophenyl ester (Life technologies, California, USA)

Pteroyldi-γ-L-glutamic acid (Schircks laboratories, Switzerland)

Pierce Coomassie Plus Bradford Protein Assay (Thermo Scientific, Massachusetts, USA)

Roswell Park Memorial Institute medium (RPMI 1640) (Sigma Aldrich, Missouri, USA)

Minimum Essential Medium with HEPES (H-MEMd) (Institute of Molecular Genetics of the ASCR, v. v. i., Czech Republic)

Improved Minimal Essential Medium (Opti-MEM) (Life Technologies, California, USA)

Chemicals available in the laboratory (synthetized by co-workers or achieved from collaborating laboratories):

Fluorescein-alkyne; Tris(3-hydroxypropyltriazolylmethyl)amine (THPTA) [50]; 3-aminooxypropyl-1-azide [84]; N-(2-hydroxypropyl)methacrylamide (HPMA); 3-azidopropylacrylamide; Biotinylated extracellular domain of GCP II (44-750) synthetized with Avi-Tag (GCP II); 2-(phosphonomethyl)pentanedioic acid (2-PMPA); GCP II inhibitor-alkyne

4.2 METHODS

4.2.1 Standard protocol for azide-alkyne cycloaddition reaction

The stock solutions (c_{stock}) for copper(I) ions catalyzed azide-alkyne cycloaddition reaction (CuAAC) were prepared according to respective tables. Solutions were prepared in H_2O except of dye solutions (Fluorescein (Fl), Alexa Fluor 488 (A_{488})) prepared in DMSO. The solutions were mixed in the final concentrations (c_{final}) according to pipetting volumes and sequence in respective tables. The solutions of $CuSO_4 \cdot 5H_2O$ and tris(3-hydroxypropyltriazolylmethyl)amine (THPTA) were premixed (in concentration ratio 1:2 or 1:5 in reactions of Tf with NDs) before adding to the reaction mixture. The mixtures were filled to the final volume with H_2O. The reaction mixtures were well-sealed after adding sodium ascorbate, mixed and reacted with no stirring.

4.2.2 Preparation of ND conjugate with Tf

4.2.2.1 Preparation of transferrin-azide (Tf-N_3)

Human hTf (30 mg, 390 nmol) was diluted in acetate buffer (0.1 M, pH 5.5) in concentration 2 mg/ml. $NaIO_4$ solution was slowly added to cooled Tf solution (the final concentration 1 mM). Mixture was incubated on ice in the dark for 30 minutes (Fig. 14).

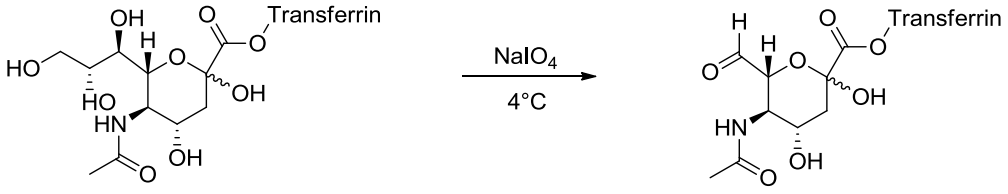

Fig. 14 **Reaction of Tf with $NaIO_4$.** The C-C bond of sialic acid is cleaved to obtain the Tf-aldehyde.

The solution containing Tf-aldehyde was six-times concentrated in ultrafiltration cell (from 70 ml to 5 ml). 4-(2-hydroxyethyl)-1-piperazineethanesulfonic acid (HEPES) buffer (0.1 M, pH 7.2) was used to refill the volume. Tf-aldehyde was incubated with 3-aminooxypropyl-1-azide (16.2 mg, 140 µmol) in HEPES buffer with dimethyl sulfoxide (DMSO, 20%, total volume 17 ml) for 5 h at room temperature (RT) at gentle mixing (Fig. 15, p. 31). The removal of 3-aminooxypropyl-1-azide excess was performed by the ultrafiltration (70 ml to 5 ml, six-times) in HEPES buffer (0.1 M, pH 8). Solution was freeze-dryed to obtain Tf-N_3. [48]

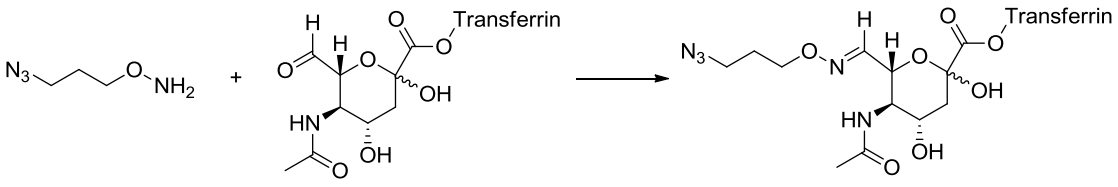

Fig. 15 **Oxime ligation.** The reaction of the aldehyde group of Tf with the aminooxy group of 3-aminooxypropyl-1-azide to obtain Tf-N_3.

4.2.2.2 Reaction of Tf-N_3 with Fl-alkyne to obtain Tf-Fl and subsequent SDS-PAGE

Tf-N_3 and Fl-alkyne were reacted 2 hours using CuAAC (Fig. 16, Tab. 1).

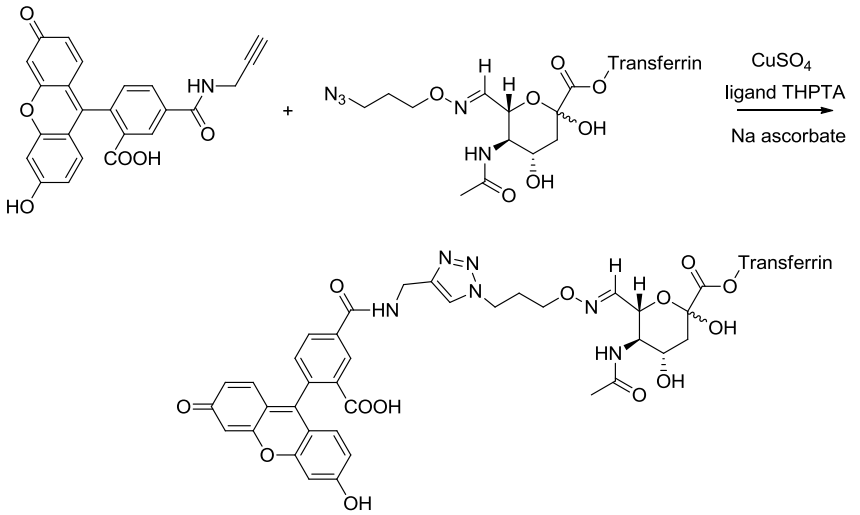

Fig. 16 **Reaction of Tf-N_3 with Fl-alkyne using CuAAC**

Tab. 1 **Preparation of the solutions for CuAAC of Tf-N_3 and Fl-alkyne.**

	M (g/mol)	m (mg)	V (µL)	c_{stock} (mM)	c_{final} (mM)
Tf-N_3	77,000	0.18	33	0.071	0.020
Fl-alkyne	413.4	3.0	7,257	1	0.075
$CuSO_4 \cdot 5H_2O$	249.7	12.5	5,000	10	0.17
THPTA	434.5	1.4	322	10	0.33
Sodium ascorbate	198.1	9.9	1,000	50	5

The reaction product (Tf-Fl) was analyzed by SDS-PAGE. Gels (14% resolving gel, 6.6% stacking gel, see below) were prepared and placed into a vertical electrophoresis apparatus. The upper and lower reservoirs of the apparatus were filled with the 5-times diluted running buffer. 25 µl of twice diluted samples (Tf, Tf-N_3 and Tf-Fl, 0.01 mM) was mixed with 5 µl of the sample buffer and boiled for 5 minutes. 4 µl of the boiled mixture was loaded to gel holes. Precision Plus Protein All blue standards were used as the

standard of a molecular weight. SDS-PAGE was run at 140 V. Photograph of gel under UV lamp was taken after SDS-PAGE and gel was then colored 10 minutes by Coomassie Brilliant Blue and destained overnight.

Resolving gel (14%): 313mM Tris-HCl (pH 8.8); 13.3% acrylamide; 0.37% N,N´-methylene-bisacrylamide; 0.1% sodium dodecylsulfate (SDS); 0.001% tetramethylethylendiamine; 0.1% ammonium persulfate

Stacking gel (6.6%): 250mM Tris-HCl (pH 6.8); 6.42% acrylamide, 0.18% N,N´-methylene-bisacrylamide; 0.1% SDS; 0.005% tetramethylethylendiamine; 0.1% ammonium persulfate

Sample buffer: 50mM Tris-HCl (pH 6.8); 30% glycerol; 10% SDS; 6% 2-mercaptoethanol; 0.012% bromphenol blue

Running buffer: 125mM Tris-HCl; 1.25M glycine; 0.5% SDS; pH 8.8

Coomassie solution for staining: 0.5% Coomassie Brilliant Blue; 50% methanol; 10% acetic acid; Destaining solution: 10% acetic acid

4.2.2.3 Reaction of Tf-N_3 with A_{488}-5-sulfodichlorophenyl ester to obtain Tf-A

The reaction was performed according to the procedure recomended by producer. Tf-N_3 (20 mg, 260 nmol) was dissolved in sodium bicarbonate buffer (0.1 M, pH 8.3) in concentration 10 mg/ml. A_{488}-5-sulfodichlorophenyl ester (0.55 mg, 666 nmol) was dissolved in DMSO (100 µl), slowly added to Tf-N_3 solution and incubated 5 hours at RT by gentle mixing. The mixture was 5-times concentrated in the ultrafiltration cell from approximately 70 ml to 5 ml. Phosphate buffered saline (PBS) was used to refill the volume after the ultrafiltration. The solution was freeze-dryed to obtain Tf-A as an orange powder. The absorption spectrum of Tf-A was determined. The Bradford assay was performed. 50 µl of protein solution (Tf or Tf-A in concentration 0.74 mg/ml; fatty acid free human serum albumin (HSA) in various concentrations) was mixed with 1,500 µL of the Bradford reagent for exactly 10 minutes and measured at 595 nm. The control experiment using H_2O instead of protein was performed under the same conditions.

4.2.2.4 Binding activity comparison of modified Tf (Tf-A) and unmodified Tf

K562 (non-adherent human myelogenous leukemia cell line) and HT-29 (adherent human colon carcinoma cell line) were grown in RPMI with 10% fetal serum albumine (FBS)

addition on Petri dishes at 37 °C in a humidified 5% CO_2 atmosphere. After 24 hours of cell seeding, trypsin-ethylenediaminetetraacetic acid (EDTA) solution (0.25% trypsin, 0.01% EDTA in PBS) was added to adherent cells and incubated for 20 minutes (at 37 °C). The solutions of Tf-A and Tf in PBS were added to the cells in various concentration ratios (Tab. 2) in the total final concentration 0.2 mg/ml and incubated for 30 minutes at 37 °C. After the incubation and washing the cells with PBS, the cell fluorescence was analyzed by flow cytometry (BD LSR II). The fluorescence of A_{488} was collected in the range 500-550 nm upon excitation at 488 nm.

Tab. 2 **Various concentration ratios for the incubation of K562 and HT-29 cells with Tf-A and Tf.** F – pipetting ratios of Tf-A; N – pipetting ratios of Tf

Sample	**1**	**2**	**3**	**4**	**5**	**6**	**7**	**8**	**9**	**10**
F	1	0,95	0,89	0,81	0,71	0,6	0,48	0,35	0,23	0,11
N	0	0,05	0,11	0,19	0,29	0,4	0,52	0,65	0,77	0,89

4.2.2.5 Preparation of carboxyl-modified ND (ND-COOH) – the ND pretreatment

Purified ND particles (irradiated, annealed and partially oxidized) were achieved from co-worker in laboratory. The NDs were then treated with a mixture of HNO_3 and H_2SO_4 (85 °C, 3 days), washed with 0.1M NaOH and 0.1M HCl, washed 5-times with H_2O and freeze-dried. The particles were dissolved in H_2O (2 mg/ml) and sonicated with a probe for 30 minutes. The resulting transparent colloid was filtered using a 0.2 µm poly(1,1-difluoroethylene) (PVDF) microfilter to provide the colloidal solution of the carboxyl-modified ND-COOH particles.

4.2.2.6 Preparation of silica-coated NDs and subsequent grafting of the PEG-alkyne chains to obtain C_1ND particles

Polyvinylpyrrolidone (M = 10,000, 96 mg, 9.6 µmol) was dissolved in H_2O (204 ml) and sonicated for 10 minutes in an ultrasonic bath. ND-COOH colloid (6 ml, 2 mg/ml) was added and the mixture was stirred for 24 hours. The colloid was then concentrated by the centrifugation in 2 steps. In the first step (40,000 rcf, 1 hour), the volume was reduced to approximately 12 ml. The second centrifugation step (30,000 rcf, 30 min) was performed in microvials and the solvent volume was reduced to approximately 0.2 ml. Sedimented

ND were resuspended in ethanol (12 ml) in a round bottom flask and sonicated in ultrasonic bath for 2-4 min. Tetraethyl orthosilicate (112 mg, 539 µmol) was added. After 2 minutes of vigorous stirring, ammonia solution (25%, 500 µl) was added. The reaction mixture was stirred for 14 hours. After reaction period 1,2-bis(triethoxysilyl)ethane (12 mg, 34 µmol) and (3-aminopropyl)triethoxysilane (12 mg, 54 µmol) were added to the solution (Fig. 4, p. 12). The reaction mixture was stirred for 24 hours. The product was purified by the centrifugation (14,000 rcf, 5 min) with ethanol (12 ml, 4-times) and acetonitrile (12 ml, 2-times) and was suspended in 6 ml of acetonitrile.

α-Succinimidyl ester-ω-propargylacetamido poly(ethylene glycol) (84 mg, 16.8 µmol), 2-ethoxy-1-ethoxycarbonyl-1,2-dihydroquinoline (16.8 mg, 68 µmol), and 4-dimethylaminopyridine (8.2 mg, 68 µmol) were dissolved together in 12.8 ml acetonitrile. The resulting solution was placed into an ultrasonic bath cooled to 18 °C. Silica-coated NDs (12 mg, 2 mg/ml) were slowly added to the reaction mixture in 30 minutes using a syringe pump. The mixture was sonicated at 18 °C for an additional 2.5 hours and then gently shaken for 16 hours. The product was purified by the centrifugation (14,000 rcf, 5 min) with acetonitrile (12 ml, 3-times), ethanol (24 ml, 1-times), H_2O (12 ml, 2-times) and was storaged in acetonitrile at -18 °C. Agglomeration state of colloid was determined in PBS by dynamic light scattering (DLS).

4.2.2.7 Attachment of NDs with Tf-A for subsequent cancer cell targeting (C_1ND-Tf)

4.2.2.7.1 Reaction of C_1ND with Tf-A to obtain C_1ND-Tf

C_1ND and Tf-A were reacted 2 hours using CuAAC (Tab. 3).

Tab. 3 **Preparation of the solutions for CuAAC of C_1ND and Tf-A.**

	M (g/mol)	m (mg)	V (uL)	c_{stock} (mM)	c_{final} (mM)	pipetting (ul)
C_1ND		2	1,000			250
Tf-A	77,000	0.04	30.72	0.017	0.00041	15.36
$CuSO_4.5H_2O$	249.7	31.2	5,000	25	0.32	28.6
THPTA	434.5	2.17	100	50	1.60	
Aminoguanidin	110	11	1,000	100	5	32
Sodium ascorbate	198.1	20	1,000	100	5	32
H_2O						282

The mixture was diluted to 3.5 ml and concentrated using centrifugal filter tubes. The reaction mixture was centrifuged (14,000 rcf, 5 min) and washed with PBS buffer (14,000 rcf, 10 min, 1 ml, 4-times). The resulting concentration of colloid was 1 mg/ml. Agglomeration state of colloid in PBS was determined by DLS.

4.2.2.7.2 Reaction of C_1ND with fluorescein-azide (Fl-N_3) to obtain C_1ND-Fl

C_1ND and Fl-N_3 were reacted 2 hours using CuAAC (Tab. 4).

Tab. 4 **Preparation of the solutions for CuAAC of C_1ND and Fl-N_3.**

	M (g/mol)	m (mg)	V (uL)	c_{stock} (mM)	c_{final} (mM)	pipetting (ul)
C_1ND		2	1,000			250
Fl-N_3	576	0.5	500	1.74	0.016	5.90
$CuSO_4.5H_2O$	249.7	31.2	5,000	25	0.32	16.4
THPTA	434.5	2.17	100	50	0.64	
Aminoguanidin	110	11	1,000	100	5	32
Sodium ascorbate	198.1	20	1,000	100	5	32
H_2O						303.7

The reaction mixture was centrifuged (14,000 rcf, 5 min) and washed with PBS buffer (14,000 rcf, 10 min, 1 ml, 4-times). The resulting concentration of colloid was 1 mg/ml.

4.2.2.7.3 Targeting of cancer cells by Tf-A and C_1ND-Tf

K562 were grown in RPMI medium containing 10% FBS on Petri dish at 37 °C in a humidified 5% CO_2 atmosphere. After 24 hours of cell seeding, the culture medium was replaced by PBS containing Tf-A (the final concentration 100 µg/ml) or NDs (C_1ND-Tf or C_1ND-Fl, the final concentration 1 mg/ml). After 1 hour of incubation, cells were washed twice with PBS. The cell culture medium was replaced by PBS containing Tf (the final concentration 100 µg/ml) for 30 minutes, simultaneously to previous experiments. Tf-A was added for additional 1 hour to Tf pre-incubated cells. Confocal microscopy was performed (confocal microscope FV-1000). Fluorescence was collected using spectral detector in range 485-585 nm upon excitation at 473 nm.

4.2.2.8 Attachment of NDs with Tf-A for subsequent cancer cell targeting (C_1ND-A-Tf)

4.2.2.8.1 Reaction of C_1ND with A_{488}-azide (A_{488}-N_3) to obtain C_1ND-A

C_1ND particles and A_{488}-N_3 were reacted 3 hours using CuAAC (Tab. 5, p. 36).

Tab. 5 **Preparation of the solutions for CuAAC of C_1ND and A_{488}-N_3.**

	M (g/mol)	m (mg)	V (uL)	c_{stock} (mM)	c_{final} (mM)	pipetting (ul)
C_1ND		2.00	1,000			1000
A_{488}-N_3	861.04	1	100	11.60	0.054	12
$CuSO_4.5H_2O$	249.7	31.20	5,000	25	0.32	65.5
THPTA	434.5	2.17	100	50	0.64	
aminoguanidin	110	11	1,000	100	5	128
sodium ascorbate	198.1	20	1,000	100	5	128
H_2O						1226.5

The reaction mixture was centrifuged (14,000 rcf, 5 min) and washed with H_2O (14,000 rcf, 10 min, 1 ml, 3-times) and ethanol (14,000 rcf, 10 min, 1 ml, 2-times). The resulting colloid concentration was 0.5 mg/ml. Agglomeration state of colloid was determined by DLS.

4.2.2.8.2 Reaction of C_1ND-A with Tf-A to obtain C_1ND-A-Tf

C_1ND-A and Tf-A were reacted 4 hours using CuAAC (Tab. 6).

Tab. 6 **Preparation of the solutions for CuAAC of C_1ND-A and Tf-A.**

	M (g/mol)	m (mg)	V (uL)	c_{stock} (mM)	c_{final} (mM)	pipetting (ul)
C_1ND-A		2.00	1,000			800
Tf-A	77,000	0.64	50	0.17	0.00408	46.08
$CuSO_4.5H_2O$	249.70	31.20	5,000	25	0.32	86.02
THPTA	434.5	2.17	100	50	1.6	
aminoguanidin	110.0	11.0	1,000	100	5	96
sodium ascorbate	198.1	20	1,000	100	5	96
H_2O						795.8

The reaction mixture was centrifuged (14,000 rcf, 5 min) and washed with PBS (14,000 rcf, 10 min, 1 ml, 5-times). The resulting concentration of colloid was 0.5 mg/ml. The agglomeration state of colloid was determined by DLS. The fluorescence spectra of C_1ND-A and C_1ND-A-Tf were analyzed to compare the fluorescence of particles.

4.2.2.8.3 Targeting of cancer cells by Tf-A and C_1ND-A-Tf

K562 and HT-29 cells were grown in RPMI medium containing 10% FBS on Petri dishes at 37 °C in a humidified 5% CO_2 atmosphere. The cells were transferred to serum-free

medium H-MEMd 24 hours before experiment. The adherent cells were transferred to a suspension by incubation with trypsin-EDTA for 20 minutes (at 37 °C). The experiment was performed in microvials. The culture medium was replaced by same medium containing Tf-A or NDs (C_1ND-A, C_1ND-A-Tf, the final concentration 10 μg/ml). The cells were washed twice with PBS after incubation at 37 °C. 1; 3; 6 and 24 hours were various times used for incubation. Another alternative was performed with the incubation 2 hours at 4 °C and then another 1 hour at 37 °C. Tf-A was incubated for 1 hour in the cells. Confocal microscopy measurement and flow cytometry were performed in the similar manner as described in the paragraphs 4.2.2.4 and 4.2.2.7.3.

4.2.3 Preparation of ND conjugate with GCP II - inhibitor

4.2.3.1 Preparation of NDs coated by thin silica layer and acrylamide copolymer (C_2ND1)

ND-COOH preparation and the reaction of ND-COOH with polyvinylpyrrolidone were performed in the same manner as was written in the paragraphs 4.2.2.5 and 4.2.2.6. Tetraethyl orthosilicate (84.06 mg, 405 μmol) and 3-(Trimethoxysilyl)propylmethacrylate (31.35 mg, 126 μmol) were added to a round bottom flask (Fig. 6, p. 13). NH_3 (25%, 498 ul) was added after 20 second sonication in an ultrasonic bath. The reaction mixture was stirred for 14 hours. The product was purified by the centrifugation (14,000 - 25,000 rcf, 15 min) with ethanol (12 ml, 2-times). HPMA was twice recrystallized from mixture of aceton-hexan (boiling point approximately 70 °C, 1:3 v/v). The mixture was filtered at higher temperature before the first recrystallization. HPMA (595 mg, 4.16 nmol) and AzpAAm (105 mg, 0.61 nmol) were dissolved in ethanol (17 ml). 2,2'-Azobis(2-methylpropionitrile) (200 mg, 1.22 nmol, recrystallized by thickening ethanol solution on rotary evaporator, maximum temperature 30 °C) was added to the mixture. Mixture was filtered using a 0.2 μm polytetrafluorethylen microfilter. ND-COOH colloid (2 mg, 2 mg/ml) was added and the mixture was reacted 12 hours at 70 °C under argon. The product was centrifuged (18,000, 30 min) and purified by the centrifugation with ethanol (25,000 rcf, 30 min, 1 ml, 3-times), H_2O (30,000 rcf, 30 min, 1 ml, 3-times) and methanol (30,000 rcf, 30 min, 1 ml, 2-times). The ND particles (C_2ND1, Fig. 19, p. 46) were stored in the freezer.

4.2.3.2 Reaction of C_2ND1 particles with Fl-alkyne to obtain C_2ND1-Fl or with GCP II inhibitor-alkyne to obtain C_2ND1-I

C_2ND1 were reacted 3 hours using CuAAC with Fl-alkyne or GCP II inhibitor-alkyne (Fig. 17, Tab. 7).

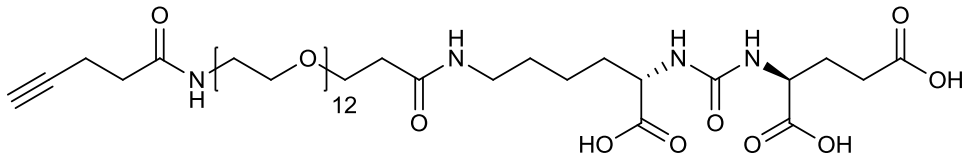

Fig. 17 **Structure of GCP II inhibitor-alkyne capable of reacting with azide-modified moieties.**

Tab. 7 **Preparation of solutions for CuAAC of C_2ND1 and Fl-alkyne or GCP II-inhibitor-alkyne.**

	M (g/mol)	m (mg)	V (uL)	c_{stock} (mM)	c_{final} (mM)	pipetting (ul)	
C_2ND1		2.00	1,000			500	500
Fl-alkyne	413.4	3	145	50.05	0.16	3.84	-
GCP II inhibitor-alkyne	1000	10.5	525	20	0.16	-	9.6
$CuSO_4.5H_2O$	249.7	31.20	5,000	25	0.32	30.72	30.72
THPTA	434.5	2.17	100	50	0.64		
aminoguanidin	110	11	1,000	100	5	60	60
sodium ascorbate	198.1	20	1,000	100	5	60	60
H_2O						545.5	540

The reaction mixtures were centrifuged (20,000 rcf, 15 min) and purified by the centrifugation with H_2O (30,000 rcf, 20 min, 1 ml, 4-times). The resulting concentrations of colloids were 1 mg/ml. Agglomeration state of colloids was determined by DLS in concentration 0.1 mg/ml. Absorption spectrum of C_2ND1-Fl was analyzed. Absorption spectra of various concentrations of fluorescein solutions (2 µg/ml, 1 µg/ml and 0.5 µg/ml) were determined.

4.2.3.3 Reaction of C_2ND1-I or C_2ND1 with A_{488}-alkyne to obtain C_2ND1-A1, C_2ND1-A2, C_2ND1-I-A1, C_2ND1-I-A2

C_2ND1 (Tab. 8, p. 39) or C_2ND1-I (Tab. 9, p. 39) particles were reacted 2 hours using CuAAC with A_{488}-alkyne under two various conditions – with lower (0.002 mM) and higher (0.08 mM) concentration of A_{488}-alkyne (Fig. 19, p. 46).

Tab. 8 **Preparation of the solutions for CuAAC of C_2ND1 and A_{488}-alkyne.**

	M (g/mol)	m (mg)	V (uL)	c_{stock} (mM)	c_{final} (mM)	pipetting (ul)	
C_2ND1		2.00	1,000			100	100
A_{488}-alkyne	773.9	0.5	250	2.58	0.002 or 0.08	0.19	9.29
$CuSO_4.5H_2O$	249.7	31.20	5,000	25	0.32	7.68	7.68
THPTA	434.5	2.17	100	50	0.64		
aminoguanidin	110	11	1,000	100	5	15	15
sodium ascorbate	198.1	20	1,000	100	5	15	15
H_2O						162.1	153

Tab. 9 **Preparation of the solutions for CuAAC of C_2ND1-I and A_{488}-alkyne.**

	M (g/mol)	m (mg)	V (uL)	c_{stock} (mM)	c_{final} (mM)	pipetting (ul)	
C_2ND1-I		2.00	1,000			100	100
A_{488}-alkyne	773.9	0.5	250	2.58	0.002 or 0.08	0.19	9.29
$CuSO_4.5H_2O$	249.7	31.20	5,000	25	0.32	7.68	7.68
THPTA	434.5	2.17	100	50	0.64		
aminoguanidin	110	11	1,000	100	5	15	15
sodium ascorbate	198.1	20	1,000	100	5	15	15
H_2O						162.1	153

The reaction mixtures were centrifuged (20,000 rcf, 15 min) and washed with H_2O (30,000 rcf, 20 min, 1ml, 3-times). The resulting concentrations of colloids were 1 mg/ml. The absorption spectra of colloids were analyzed. The absorption spectra of various concentrations of A_{488} (2 µg/ml, 1 µg/ml and 0.5 µg/ml) were determined.

4.2.3.4 Preparation of NDs coated by thin silica layer and acrylamide copolymer – the procedure optimization (to obtain C_2ND2, C_2ND3 and C_2ND4 particles)

The coating of NDs by the thin silica layer was performed in the same manner as described in paragraph 4.2.3.1. Polymerization procedure was performed in the similar manner. HPMA (689.5 mg, 4.82 nmol) and AzpAAm (10.5 mg, 0.06 nmol) were dissolved in ethanol (18 mL) or DMSO (8.8 mL or 2.2 mL), respectively. 2,2'-Azobis(2-methylpropionitrile) (200 mg, 1.22 nmol) was added to the mixture. ND-COOH colloid (2 mg, 10 mg/ml) was added. The mixture was reacted for 3 days under argon at 70 °C, 60 °C and 55 °C, respectively. C_2ND2, C_2ND3 and C_2ND4 particles were prepared (Fig. 19,

p. 46). The C_2ND4 particles were centrifuged (30,000, 40 min). Supernatant was coagulated by acetonitrile (1:1 v:v) and centrifuged (15,000 rcf, 10 min). Supernatant was removed again and the sediment was dissolved in H_2O and centrifuged (25,000 rcf, 20 min). C_2ND2, C_2ND3 and C_2ND4 particles were centrifuged (18,000 rcf, 30 min) and purified by the centrifugation with ethanol (25,000 rcf, 30 min, 1 ml, 3-times) and H_2O (30,000 rcf, 30 min, 1 ml, 5-times).

4.2.3.5 C_2ND2, C_2ND3 and C_2ND4 particles – the stability study and the reaction with HSA

C_2ND2, C_2ND3 and C_2ND4 and ND-COOH particles were used (Fig. 19, p. 46). ND particles (50 µL, 2 mg/ml in H_2O), PBS (245 µL) and HSA solution (5 µL, 2 mg/mL) were mixed for 30 minutes. The mixture was centrifuged (30,000 rcf, 30 min). 200 µL of supernatant was mixed with 1,500 µL of the Bradford reagent for exactly 10 minutes and measured at 595 nm. The control experiment using H_2O instead of ND particles was performed under the same conditions. C_2ND2, C_2ND3 and C_2ND4 were measured by DLS in the final concentration 0.1 mg/ml in H_2O and in NaCl solution (0.5 M or 1 M).

4.2.3.6 Reaction of C_2ND4 particles with A_{488}-alkyne to obtain C_2ND4-A1 and with GCP II inhibitor-alkyne to obtain C_2ND4-I particles

C_2ND4 were reacted 4 hours using CuAAC either with A_{488}-alkyne or with GCP II inhibitor-alkyne (Tab. 10) under the same conditions.

Tab. 10 **Preparation of the solutions for CuAAC of C_2ND4 and A_{488}-alkyne or GCP II-inhibitor-alkyne.**

	M (g/mol)	m (mg)	V (uL)	c_{stock} (mM)	c_{final} (mM)	pipetting (ul)	
C_2ND4		2.00	1,000			100	750
A_{488}-alkyne	773.9	0.5	250	2.6	0.16	15.84	
GCP II inhibitor-alkyne	1000	10.5	525	20	0.16		15.36
$CuSO_4.5H_2O$	249.7	31.20	5,000	25	0.32	6.55	49.2
THPTA	434.5	2.17	100	50	0.64		
aminoguanidin	110	11	1,000	100	5	12.8	96
sodium ascorbate	198.1	20	1,000	100	5	12.8	96
H_2O						108	914

The reaction mixtures were centrifuged (20,000 rcf, 15 min + 27,000 rcf, 4 min) and washed with H_2O (25,000 rcf, 10 min + 30,000 rcf, 5 min, 1ml, 4-times). The resulting

concentrations of colloids were 1 mg/ml. The absorption spectrum of C_2ND4-A1 was analyzed.

4.2.3.7 Reaction of C_2ND4 particles with A_{488}-alkyne to obtain C_2ND4-A2 and subsequently with GCP II inhibitor-alkyne to obtain C_2ND4-A2-I

C_2ND4 particles and A_{488}-alkyne were reacted 2 hours using CuAAC (Tab. 11).

Tab. 11 **Preparation of the solutions for CuAAC of C_2ND4 and A_{488}-alkyne**

	M (g/mol)	m (mg)	V (uL)	c_{stock} (mM)	c_{final} (mM)	pipetting (ul)
C_2ND4		2.00	1,000			200
A_{488}-alkyne	773.9	0.5	250	2.6	0.04	7.92
$CuSO_4.5H_2O$	249.7	31.20	5,000	25	0.32	13.11
THPTA	434.5	2.17	100	50	0.64	
aminoguanidin	110	11	1,000	100	5	25.6
sodium ascorbate	198.1	20	1,000	100	5	25.6
H_2O						239.8

The reaction mixture was centrifuged (24,000 rcf, 10 min + 30,000 rcf, 2 min) and washed with H_2O (24,000 rcf, 9 min + 30,000 rcf, 3 min, 1ml, 4-times). C_2ND4-A2 particles reacted subsequently with GCP II-inhibitor 2 hours in CuAAC (Tab. 12).

Tab. 12 **Preparation of the solutions for CuAAC of C_2ND4-A2 particles and inhibitor-alkyne**

	M (g/mol)	m (mg)	V (uL)	c_{stock} (mM)	c_{final} (mM)	pipetting (ul)
C_2ND4-A2		2.00	1,000			100
Inhibitor-alkyne	1000	11	525	20	0.16	2.05
$CuSO_4.5H_2O$	249.7	31.20	5,000	25	0.32	6.55
THPTA	434.5	2.17	100	50	0.64	
aminoguanidin	110	11	1,000	100	5	12.8
sodium ascorbate	198.1	20	1,000	100	5	12.8
H_2O						121.8

The reaction mixture was centrifuged (24,000 rcf, 9 min + 30,000 rcf, 3 min) and purified by the centrifugation with H_2O (24,000 rcf, 12 min, 1ml, 4-times). The resulting concentration of colloid was 1 mg/ml.

4.2.3.8 Surface plasmon resonance study of C_2ND1-I conjugate

The thin gold sensor stored in the solution of thiols (HS-$(CH_2)_{11}$-PEG_4-OH and HS-$(CH_2)_{11}$-PEG_6-OCH_2-COOH, 3:7) was washed with ethanol and H_2O and inserted into the surface plasmon resonance (SPR) instrument. The accurate preparation of GCP II layer with times of the solutions addition can be seen on Fig. 18. Solution flow was set to 30 µl/min. Oxygen was removed from H_2O, PBS and sodium acetate buffer (SA10 10 mM, pH 5.0). To three different flow cells (channels) was added H_2O. The carboxyl groups present on the gold thin sensor were activated by solution of N-hydroxysuccinimide/1-ethyl-3-[3-dimethylaminopropyl]carbodiimide (NHS/EDC, 12.5 mM/60 mM). The streptavidin solution in SA10 (10 ng/µl, pre-incubated at 37 °C) was added to the activated carboxyl groups. The non-covalently bound streptavidin was unbound by the solution of PBS (with 0.5M NaCl addition). 1M ethanolamine and bovine serum albumine (BSA) reacted with the rest of activated carboxyl groups. Biotinylated extracellular domain of GCP II protein (GCP II, 0.24 ng/µl) was bound to the surface of the gold sensor (in channel 2 and 3). C_2ND1-I and C_2ND1 (500 pM) were added to the sensor after the preparation of GCP II layer.

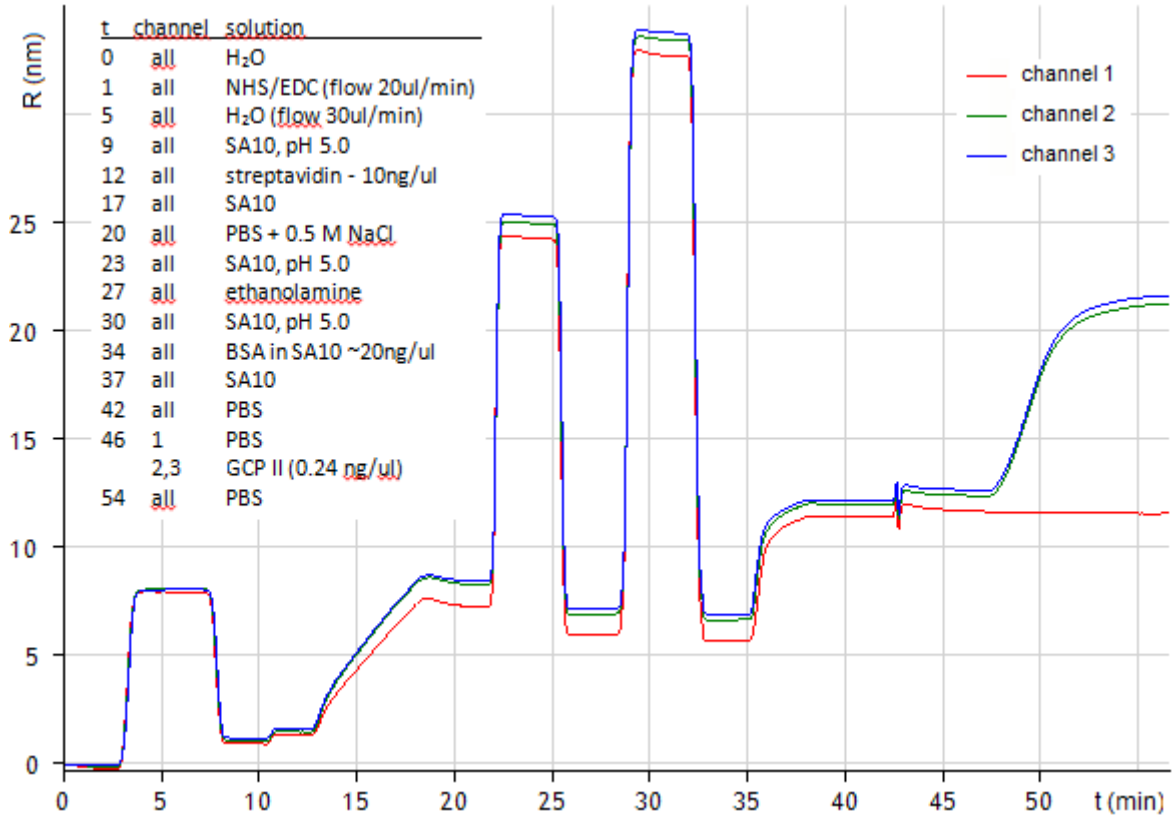

Fig. 18 **Preparation of GCP II layer on the gold sensor with solutions´ addition times.** Relative change of local refraction index (R) is plotted versus time (t). For experimental details see the paragraph 4.2.3.8.

4.2.3.9 SPR study of C_2ND4-I conjugate

SPR was performed in the similar manner as described in the paragraph 4.2.3.8 with few differences. Neutravidin (25 ng/µl, pre-incubated at 37 °C) was used instead of the streptavidin solution. BSA was not used for blocking the activated carboxyl groups. Biotin (50 nM) was added with GCP II (50 nM) to three out of four channels. C_2ND4-I particles (500 pM, 250 pM) and C_2ND4 particles (500 pM) were added.

Preparation of gold sensor covered with GCP II was repeated with the addition of GCP II and biotin (molar ratio 1:6 24 nM/144 nM) in all channels. C_2ND4-I particles were added in various concentrations (3 nM, 9 nM, 27 nM and 83 nM) at flow 20 µl/min.

4.2.3.10 Inhibition assay of C_2ND1-I-A1 conjugate

Following solutions were used for the inhibition assay: reaction buffer (RB, 25mM Bis-tris propane + 50mM NaCl, pH 7.4); GCP II (120 ng/µL) as enzyme; C_2ND1-I-A1 colloids as inhibitor; pteroyldi-γ-L-glutamic acid as substrate (PteGlu2, 2 µM) and stopping buffer (7% H_3PO_3 + 30 µM 2-PMPA). 193.5 µl of RB was added to wells A1, B1 of a MicroWell. 193.5 µL of GCP II (1,000-fold diluted in RB, 24 ng/well) was added to the wells A2, B2. 172 µL of GCP II (86,000-fold diluted in RB, 0.24 ng/well) and 21.5 µL of RB were added to the wells A3, B3. 172 µL of GCP II (86,000-fold diluted in RB, 0.24 ng/well) and 21.5 µL of C_2ND1-I-A1 colloids (Tab. 13) were added to the A4-A12, B4-B12 wells.

Tab. 13 **Final concentrations of C_2ND1-I-A1 in the inhibition reaction.** All concentrations are in pM units. Stock solutions were prepared 10-fold concentrated.

A1	**A2**	**A3**	**A4**	**A5**	**A6**	**A7**	**A8**	**A9**	**A10**	**A11**	**A12**
			5,000	500	50	5	0.5	0.05	$5{\cdot}10^{-3}$	$5{\cdot}10^{-4}$	$5{\cdot}10^{-5}$
B1	**B2**	**B3**	**B4**	**B5**	**B6**	**B7**	**B8**	**B9**	**B10**	**B11**	**B12**
			$5{\cdot}10^{-6}$	$5{\cdot}10^{-7}$	$5{\cdot}10^{-8}$	$5{\cdot}10^{-9}$	$5{\cdot}10^{-10}$	$5{\cdot}10^{-11}$	$5{\cdot}10^{-12}$	$5{\cdot}10^{-13}$	$5{\cdot}10^{-14}$

C_2ND1-A1 particles (5 nM) were used as negative control. The MicroWell was incubated for 5 minutes at 37 °C. 21.5 µL of PteGlu2 (the final concentration 200 nM) was added to all wells and incubated 20 minutes at 37 °C. Then 10 µL of stopping buffer was added. The MicroWell was centrifuged (5,200 rcf, 5 min) and 120 µL of every mixture was replaced in another MicroWell. Mixtures were analyzed by HPLC in reversed phase using absorption

detector. 97.9% phosphate buffer and 2.1% acetonitrile were used as a mobile phase. Flow was set to 0.4 mL/min.

4.2.3.11 Inhibition assay of C_2ND4-I conjugate

The following solutions were used for inhibition assay: reaction buffer (RB, 25mM Bis-tris propane + 50mM NaCl, pH 7.4) with detergent octaethylene glycol monododecyl ether $C_{12}E_8$ (det, 10^{-3} weight % in RB); GCP II (diluted in RB with detergent, the final concentration 0.14 ng/well) as enzyme; C_2ND4-I as inhibitor; C_2ND4 as negative control, PteGlu2 as substrate (the final concentration 200 nM) and stopping buffer (50µM 2-PMPA in RB) (Tab. 14).

Tab. 14 **Preparation of the mixtures for inhibition assay**. Numbers express the final concentrations of C_2ND4-I (row A+B) and C_2ND4 (row C+D) in reaction. Concentrations are in pM units. Stock solutions were prepared 10-fold concentrated. H_2O was added to the first and second well in each row instead of ND.

V (µL)	**A1**	**A2**	**A3**	**A4**	**A5**	**A6**	**A7**	**A8**	**A9**	**A10**	**A11**	**A12**
160	RB+det	Enzyme GCP II in RB with detergent										
20	H_2O	H_2O	$3{\cdot}10^4$	$8.6{\cdot}10^3$	$2.5{\cdot}10^3$	700	200	57.1	16.3	4.66	1.33	0.38
	B1	**B2**	**B3**	**B4**	**B5**	**B6**	**B7**	**B8**	**B9**	**B10**	**B11**	**B12**
160	RB+det	enzyme GCP II in RB with detergent										
20	H_2O	H_2O	$3{\cdot}10^4$	$8.6{\cdot}10^3$	$2.5{\cdot}10^3$	700	200	57.1	16.3	4.66	1.33	0.38
	C1	**C2**	**C3**	**C4**	**C5**	**C6**	**C7**	**C8**	**C9**	**C10**	**C11**	**C12**
160	RB+det	enzyme GCP II in RB with detergent										
20	H_2O	H_2O	$3{\cdot}10^4$	$8.6{\cdot}10^3$	$2.5{\cdot}10^3$	700	200	57.1	16.3	4.66	1.33	0.38
	D1	**D2**	**D3**	**D4**	**D5**	**D6**	**D7**	**D8**	**D9**	**D10**	**D11**	**D12**
160	RB+det	enzyme GCP II in RB with detergent										
20	H_2O	H_2O	$3{\cdot}10^4$	$8.6{\cdot}10^3$	$2.5{\cdot}10^3$	700	200	57.1	16.3	4.66	1.33	0.38

The enzyme solution was mixed with C_2ND4-I (row A, B) or C_2ND4 (row C, D) (Tab. 14) and incubated 5 minutes at 37 °C. 20 µL of PteGlu2 was added to all wells and incubated 20 minutes at 37 °C. 10 µL of stopping buffer was added. The MicroWell was centrifuged (5 min, 5,200 rcf) and 120 µL of every mixture was replaced in another MicroWell. Mixtures were analyzed by HPLC on reversed phase using absorption detector. 97.1% phosphate buffer and 2.9% acetonitrile were used as a mobile phase. Flow was set to 0.4 mL/min.

4.2.3.12 Targeting of cancer cells by the conjugate C_2ND1-I-A2

U373 (adherent human glioblastoma cell line) were grown in Opti-MEM medium on Petri dish at 37 °C in a humidified 5% CO_2 atmosphere. U373 cells which express GCP II and without the GCP II expression (compound doxycycline present in medium to block the GCP II expression) were used. After 24 hours of cell seeding, the cells were washed with PBS. PBS containing NDs (C_2ND1-I-A2 and C_2ND1-A2, the final concentration 100 μg/ml) was added to the cells. The cells were incubated 1 hour at 37 °C, washed twice with PBS and cultured 24 hours in medium. The fluorescence of A_{488} was collected by Zeiss LSM 780 at 499-552 nm upon excitation at 488 nm.

4.2.3.13 Targeting of cancer cells by the conjugate C_2ND4-A2-I

U373 were grown in RPMI medium containing 10% FBS on Petri dish at 37 °C in a humidified 5% CO_2 atmosphere. U373 cells with and without the GCP II expression were used. After 24 hours of cell seeding, NDs (C_2ND4-A2-I and C_2ND4-A2 particles, the final concentration 100 μg/ml) were added. After 24 hour incubation at 37 °C, the cells were washed twice with PBS. The fluorescence of A_{488} was collected by Zeiss LSM 780 at 499-552 nm upon excitation at 488 nm. Solution of trypsin-EDTA was added to adherent cells for 5 minutes (37 °C). The cells were washed with RPMI medium and PBS. Flow cytometry was performed (BD LSRFortessa). The fluorescence of A_{488} was collected in the range 515-545 nm upon excitation at 488 nm.

4.2.4 Visualization of NDs in cancer cells

LNCaP cells (human lymph node carcinoma of the prostate cells) were grown in RPMI medium containing 10% FBS serum in Petri dish at 37 °C in a humidified 5% CO_2 atmosphere. After 24 hours of cell seeding, the medium was replaced by the same medium containing NDs (C_1ND or ND-COOH) at concentration 200 μg/ml. NDs were pre-incubated either half an hour in RPMI medium or one hour in PBS before adding to the cells. After 1 hour incubation, the cells were washed twice with RPMI medium. After additional 23 hours of incubation, cells were fixed by 2% formaldehyde solution in PBS at 4 °C. Time of fixation was 2 days (fixation time was 10 minutes in case of C_1ND pre-incubated in PBS). After fixation, cells were washed twice with PBS. The ND fluorescence was collected by Zeiss LSM 780 at 639-758 nm upon excitation at 532 nm (100% laser) with master gain set to 1200 V (or 850 V in case of ND-COOH pre-incubated in PBS).

4.2.5 Preparation of samples – summary

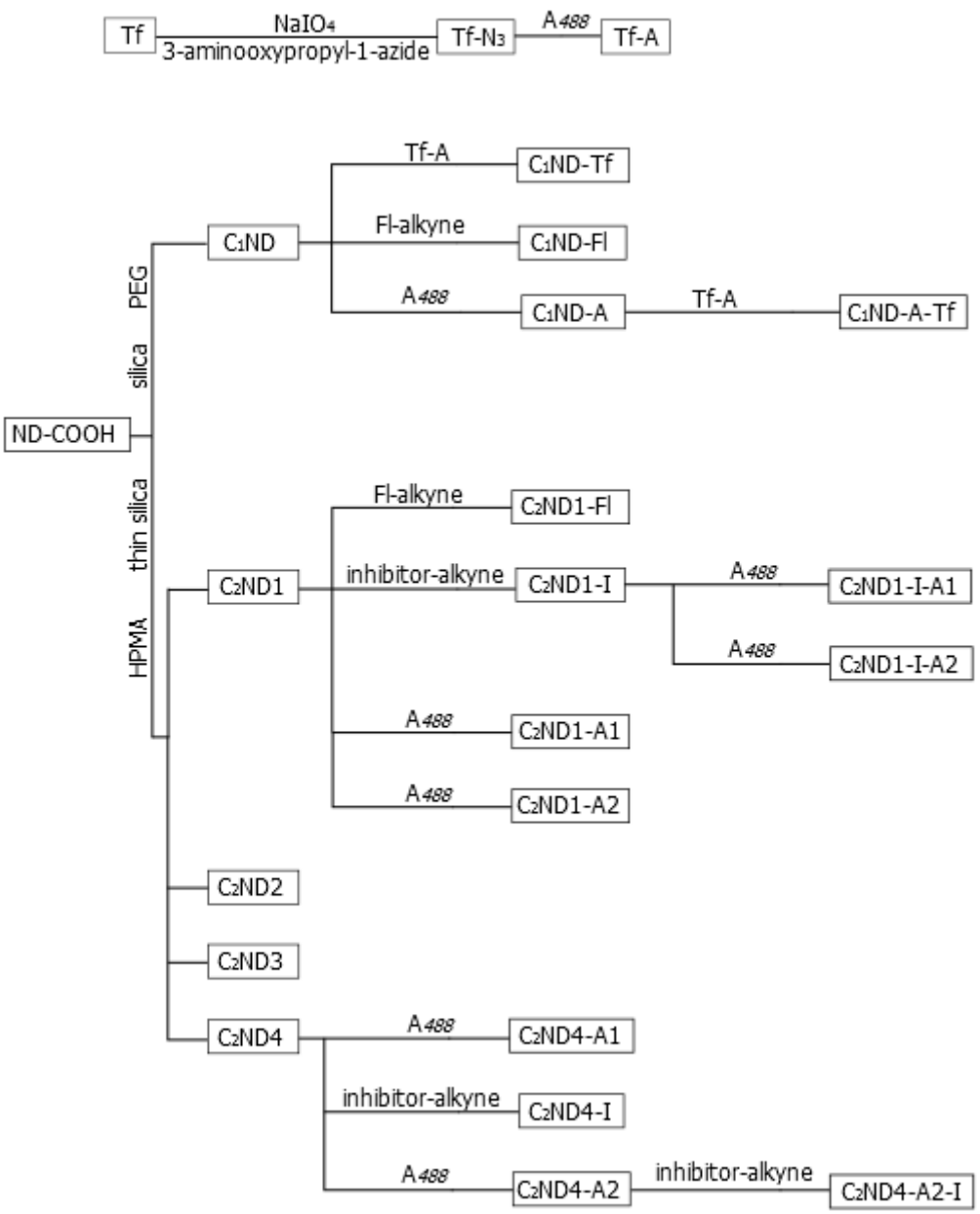

Fig. 19 **Scheme of all samples preparation and their nomenclature.** Lines represent relations between samples. ND-COOH sample in first column was initial material for preparation of all further ND samples. Samples present in next columns were prepared from samples in the previous columns connected with a line. Samples were modified with various substances labeled above the line. For example: C_2ND1-I-A2 sample was prepared from oxidized naked NDs (ND-COOH) coated with thin layer of silica and HPMA layer under first conditions out of four (C_2ND1) and modified with inhibitor-alkyne (C_2ND1-I) and subsequent A_{488} under second conditions out of two (C_2ND1-I-A2).

5. RESULTS

5.1 PREPARATION OF ND CONJUGATE WITH Tf

5.1.1 SDS-PAGE of Tf-Fl

Tf-Fl (the reaction product from CuAAC of Tf-N_3 and Fl-alkyne) was analyzed by SDS-PAGE. All samples (Tf, Tf-N_3 and Tf-Fl) have a molecular weight approximately 75 kDa (Fig. 20A). Only the Tf-Fl stain can be seen on photograph taken under UV-lamp (Fig. 20B).

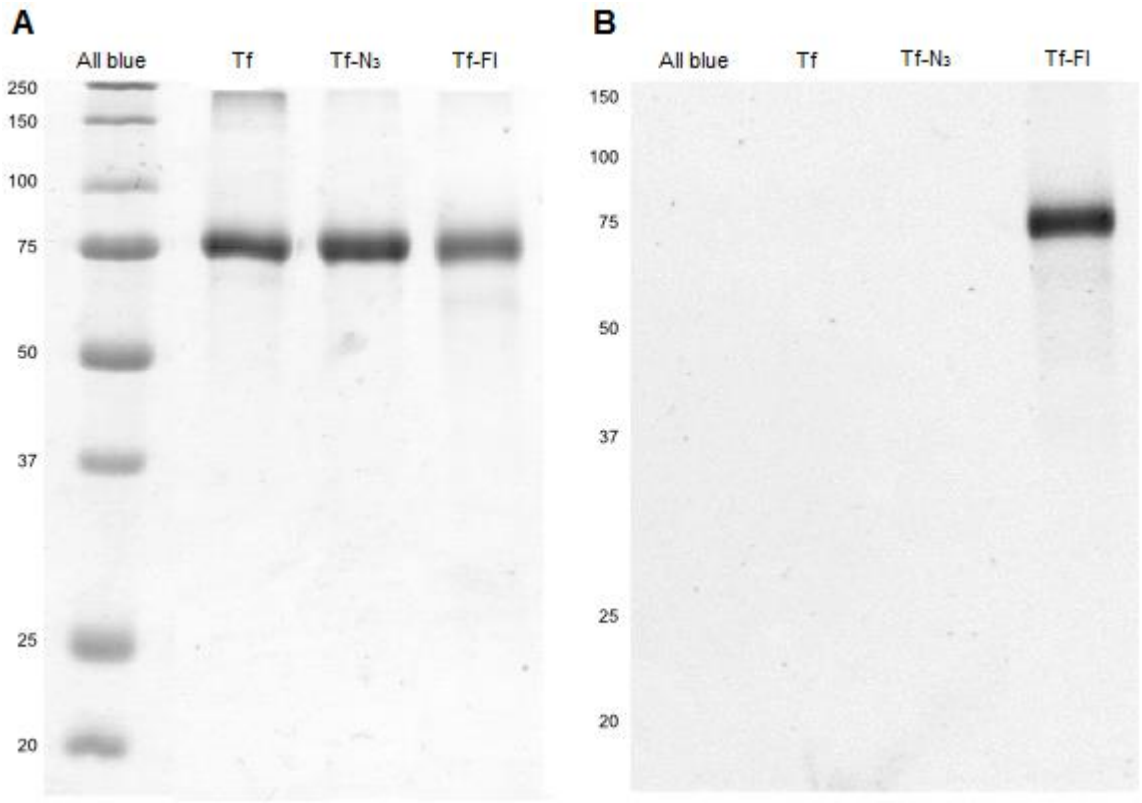

Fig. 20 **SDS-PAGE of Tf-A.** (A) 14% gel colored by the staining solution of Coomassie Brilliant Blue. (B) Photograph of gel before staining under UV lamp. In four colums are 4 ul of Precision Plus Protein All blue standards, Tf, Tf-N_3 and Tf-Fl, respectively. SDS-PAGE was run at 140 V. Figures were processed in The GNU Image Manipulation Program. Experimental details are given in the paragraph 4.2.2.2.

5.1.2 Evaluation of the reaction product Tf-A

The absorption spectrum of Tf-A (Fig. 21, p. 48) was analyzed for the purpose of determining the degree of protein labeling according to protocol “Calculate dye: protein molar ratios” (Thermo-scientific). The tabled values were taken from the manual used for the labeling reaction with A_{488} (Invitrogen).

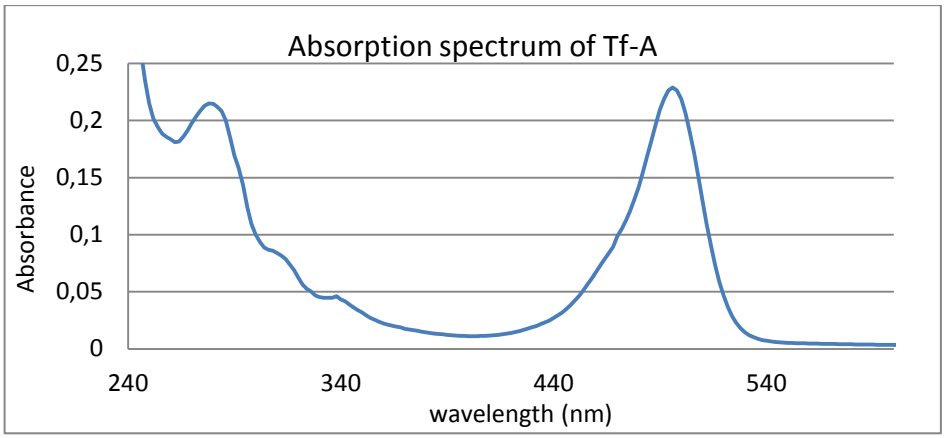

Fig. 21 **Absorption spectrum of Tf-A for determining degree of protein labeling by dye A_{488}.**

For determining the degree of Tf labeling with the dye A_{488} several pieces of information are required: absorbance at 280 nm (A_{280} = 0,215) and at the dye A_{488} maximum wavelength 495 nm (A_{495} = 0,229), the correction factor which adjusts the amount of absorbance at 280 nm caused by A_{488} (tabled value CF = 0.11) and the molar absorption coefficient both for the protein (ε = 103,900 M^{-1} cm^{-1}) and the dye (ε´ = 71,000 M^{-1} cm^{-1}).

$$\text{Protein concentration (M)} = \frac{A_{280} - (A_{495}\ CF)}{\varepsilon} = \frac{0.215 - (0.229 \cdot 0.11)}{103900}$$

$$= 1.83 \cdot 10^{-6}\ \text{M}$$

$$\text{Moles of the dye per mole of the protein} = \frac{A_{495}}{\varepsilon' \cdot \text{protein concentration}}$$

$$= \frac{0.23}{71{,}000 \cdot 1{,}83^{-6}} = 1.77$$

Approximately two A_{488} molecules are bound to one molecule of Tf.

The calculated weight of protein:

$$m = cVM = 1.83 \cdot 10^{-6} \cdot 10^{-3} \cdot 77{,}000 = 1.41 \cdot 10^{-4}\ g = 0.141\ mg$$

Tf-A was freeze-dryed in buffer; mass fraction (the ratio of the protein weight to the total weight) for Tf-A is 0.11 according to the labeling protocol, 0.10 according to the aminoacid analysis (AAA) and 0.09 according to the Bradford assay. The mass fraction of Tf is 0.74 from AAA and 0.65 according to the Bradford assay. Absorbance of the negative control (H_2O) was subtracted from the absorbance of Tf-A and Tf in Bradford assay. Tf-A and Tf concentration was calculated according to HSA calibration curve.

5.1.3 Binding affinity comparison of modified Tf (Tf-A) and unmodified Tf

Association of Tf-A (F) with TfR (R) can be expressed by equation $\mathrm{F} + \mathrm{R} \rightleftarrows \mathrm{FR}$ with binding constant $\mathrm{K_F} = \frac{[\mathrm{FR}]}{[\mathrm{F}][\mathrm{R}]}$ where [F], [R] and [FR] are concentrations of Tf-A, TfR and complex of Tf-A and TfR, respectively. Association of Tf (N) with TfR (R) can be expressed by equation $\mathrm{N} + \mathrm{R} \rightleftarrows \mathrm{NR}$ with binding constant constant $\mathrm{K_N} = \frac{[\mathrm{NR}]}{[\mathrm{N}][\mathrm{R}]}$ where [N], [R] and [NR] are concentrations of Tf, TfR and complex of Tf and TfR, respectively.

Under the condition of TfR saturation, [F] and [N] can be substituted for c_F and c_N – the final concentrations of Tf-A and Tf in the solution. Fluorescence intensity can be expressed as I, I_{max} is fluorescence intensity for full saturation of TfR with Tf-A. I_{max} and I were determined using flow cytometry (Fig. 22). Relationship between these quantities can be expressed in equation:

$$\mathrm{I} = \frac{\mathrm{K_F I_{max} c_F}}{\mathrm{K_N c_N} + \mathrm{K_F c_F}}$$

This relationship can be modified in form of linear equation, where the slope of a line is desired ratio of binding constants $\frac{\mathrm{K_N}}{\mathrm{K_F}}$:

$$\frac{\mathrm{I_{max}}}{\mathrm{I}} = \frac{\mathrm{K_N}}{\mathrm{K_F}} \frac{\mathrm{c_N}}{\mathrm{c_F}} + 1$$

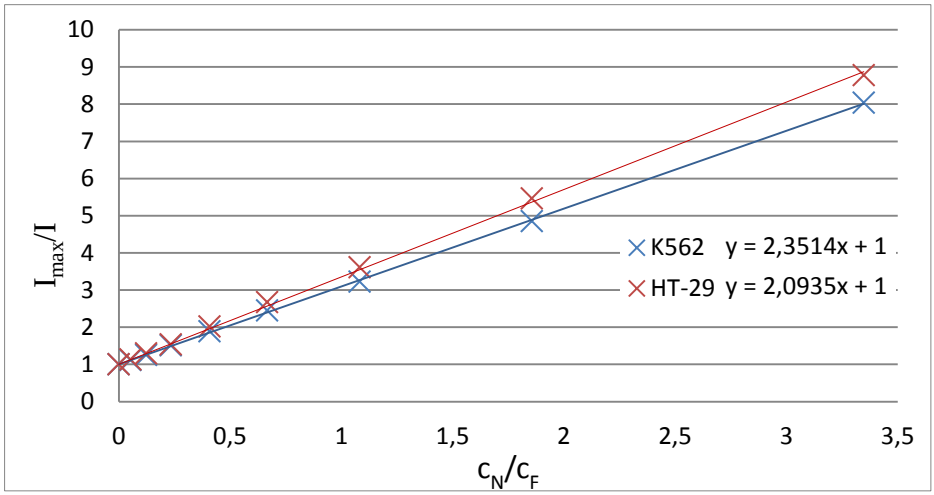

Fig. 22 **Ratio of maximal fluorescence intensity and fluorescence intensity (I_{max}/I) for various concentration ratios of Tf and Tf-A (c_N/c_F).** Tf-A and Tf were incubated with K562 and HT-29 cells for 30 minutes. The slopes of the lines are ratio of binding constants K_N/K_F. For experimental details see the paragraph 4.2.2.4

Software FlowJO 9 was used for the analysis of flow cytometry data. Gating using the forward scatter and the side scatter was performed to exclude death cells or cells with outlying size. Measured mean fluorescence intensity is a relative number – the amount of the label on the cell surface or in the cell. The cell auto-fluorescence has to be subtracted from mean fluorescence intensity to calculate fluorescence intensity. Ratio of binding constant is then calculated from the slope of a line. The binding constant of unmodified Tf is 2.1-fold higher than Tf-A for K562 cell line and 2.4-fold higher for HT-29 cell line.

5.1.4 Attachment of NDs with Tf-A for subsequent cancer cell targeting (C_1ND-Tf)

5.1.4.1 DLS of C_1ND-Tf

The agglomeration state of C_1ND and C_1ND-Tf particles was determined by DLS (Fig. 23). The average size of C_1ND-Tf in PBS is approximately 190 nm.

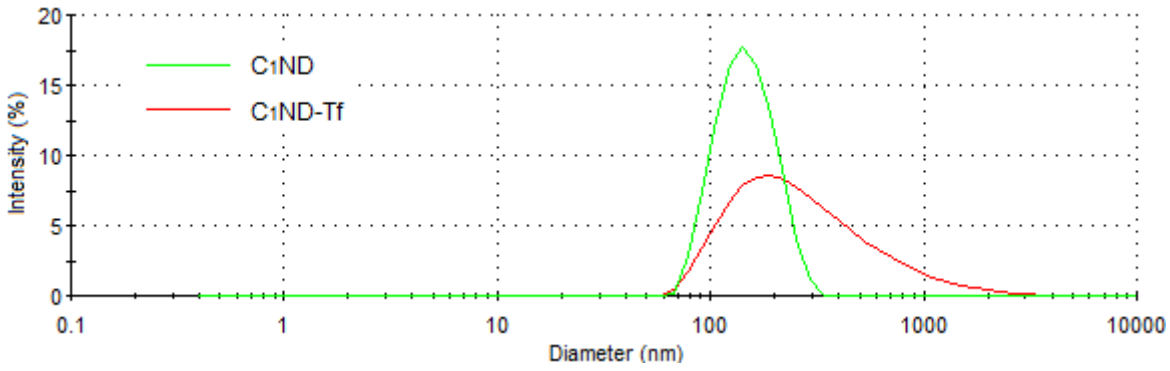

Fig. 23 **Dynamic light scattering (DLS) of the size distribution of C_1ND and C_1ND-Tf particles.** The concentration of studied colloids in PBS was 1 mg/ml.

5.1.4.2 Targeting of cancer cells by Tf-A and C_1ND-Tf - confocal microscopy

The result of the targeting of K562 cancer cells by Tf-A is displayed on Fig. 24, 1B, p. 51. Fluorescence can be seen inside the cells in contrary to cells pre-incubated by Tf before adding Tf-A (Fig. 24, 1C, p. 51). Only little fluorescence can be seen in the cells with no Tf-A or particle incubation. The result of the targeting of K562 cancer cells by C_1ND-Tf is displayed on Fig. 24, 2A,B, p. 51. Fluorescence can be seen inside the cells contrary to the cells incubated with C_1ND-Fl and fluorescence on the cell membrane (Fig. 24, 2C, p. 51).

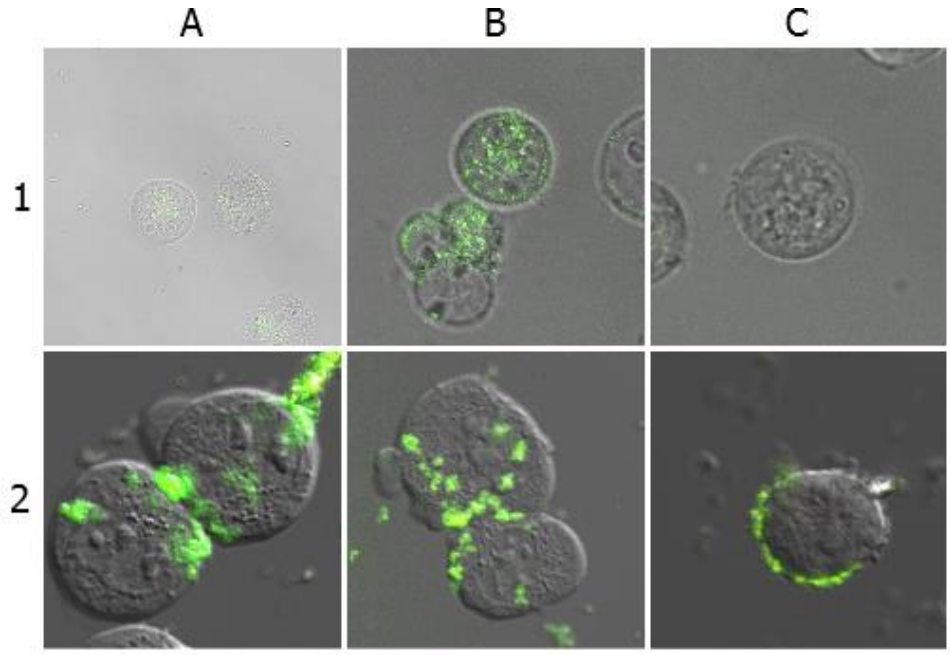

Fig. 24 **Confocal microscopy of K562 cells incubated with Tf-A, C_1ND-Tf and C_1ND-Fl.** (1A) The cells incubated with no particles. (1B) The cells incubated with Tf-A. (1C) The cells after 30 minutes pre-incubation with Tf and subsequent incubation with Tf-A. (2A, B) The cells incubated with C_1ND-Tf. (2C) The cells incubated with C_1ND-Fl. The final concentration was 100 µg/ml (Tf and Tf-A) and 1 mg/ml (NDs). Incubation time was 1 hour. The fluorescence of A_{488} was collected by Olympus FV-1000 at 485-585 nm upon excitation at 473 nm.

5.1.5 Attachment of NDs with Tf-A for subsequent cancer cell targeting (C_1ND-A-Tf)

5.1.5.1 DLS, AAA and fluorescence spectroscopy of C_1ND-A-Tf

The average diameter of C_1ND, C_1ND-A and C_1ND-A-Tf changes from 140 nm to 190 nm (Fig. 25).

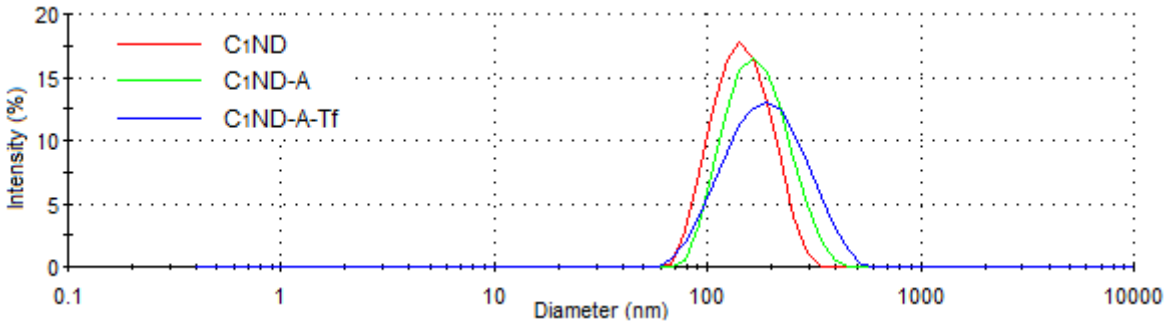

Fig. 25 **DLS of the size distributions of C_1ND, C_1ND-A and C_1ND-A-Tf.** The concentration of studied colloids in PBS was 0.5 mg/ml.

Quantity of Tf on NDs (C_1ND-A-Tf) was determined from the AAA as 7.63 µg Tf/mg NDs. The number of Tf molecules present on one particle was calculated as follows. Amount of

substance (n) was calculated as the ratio of weight (m) and molecular weight (M):

$$n = \frac{m}{M} = \frac{7.63 \cdot 10^{-6}}{77000} = 100\ \text{pmol}$$

The number of Tf molecules presents on 1 mg NDs (N_{sum}):

$$N_{sum} = nN_A = 100 \cdot 10^{-12} \times 6.022 \cdot 10^{23} = 6{,}022 \cdot 10^{13}$$

Weight of one ND particle is assumed to be $3.3 \cdot 10^{-20}$ kg, therefore number of Tf molecules present on one ND particle can be calculated as:

$$N = \frac{3.3 \cdot 10^{-20}}{10^{-6}} \cdot 6.022 \cdot 10^{13} = 2.0$$

The fluorescence ratio of C_1ND-A to C_1ND-A-Tf was calculated as 2.17 from the fluorescence spectra measurement.

5.1.5.2 Targeting of cancer cells by C_1ND-A-Tf – flow cytometry and confocal microscopy

Fluorescence intensity was determined using flow cytometry after the incubation of K562 and HT-29 cells with various ND particles for various incubation times and temperatures (Tab. 15). Incubation alternatives with the higher fluorescence of C_1ND-A-Tf than C_1ND-A, e.i. the alternatives suggesting effective targeting, are highlighted in blue.

Tab. 15 **Fluorescence intensity measurements of K562 and HT-29 cells incubated with C_1ND-A-Tf and C_1ND-A using flow cytometry.** The final concentration of C_1ND-A-Tf and C_1ND-A was 10 μg/ml. For experimental detail see the paragraph 4.2.2.8.3.

	I (A_{488})	
sample	**K562**	**HT-29**
1h 37 °C_ C_1ND-A	5227	10858
1h 37 °C _ C_1ND-A-Tf	5574	9200
2h 4 °C and 1h 37 °C _ C_1ND-A	5120	8988
2h 4 °C and 1h 37 °C _ C_1ND-A-Tf	3757	5276
3h 37 °C _ C_1ND-A	3829	12028
3h 37 °C _ C_1ND-A-Tf	5806	10132
6h 37 °C _ C_1ND-A	4406	12018
6h 37 °C _ C_1ND-A-Tf	52286	13138
24h 37 °C _ C_1ND-A	15498	18716
24h 37 °C _ C_1ND-A-Tf	26652	16882

The result of the targeting of K562 and HT-29 cancer cells by C_1ND-A-Tf and C_1ND-A is displayed on Fig. 26. C_1ND-A particles are found more on the cell membrane then C_1ND-A-Tf after 1 hour in K562 cells. Difference between C_1ND-A-Tf and C_1ND-A is not so evident for 1 hour incubation of HT-29 cells. C_1ND-A particles and C_1ND-A-Tf are present after 3 hour incubation with K562 cells partially on the cell membrane and inside the cell. C_1ND-A particles are present after 3 hour incubation with HT-29 only on the cell membrane, few C_1ND-A-Tf particles are inside the cells. Other incubation variants (incubation for 6 and 24 hours at 37 °C and 2 hours at 4 °C and subsequently 1 hour at 37 °C) are not shown. The cells incubated 2 hours at lower temperature exhibited similar features as displayed figures. The great amount of the cells, including the negative control with no particles, incubated for 6 and 24 hours were death. Tf-A was found in the cells and showed similar manner as in the Fig. 24, p. 51 (data not shown).

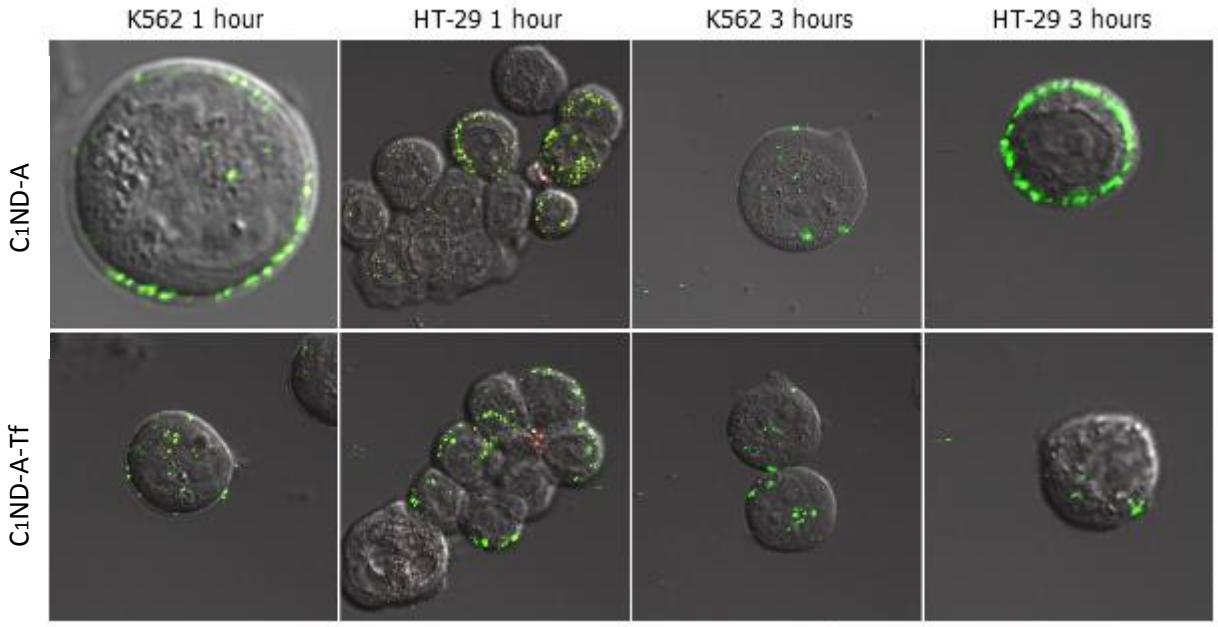

Fig. 26 **Confocal microscopy analysis of C_1ND-A-Tf and C_1ND-A particles internalized by K562 cells and HT-29 cells.** All the cells were incubated with ND in the final concentration 10 µg/ml for 1 or 3 hours and were subsequently washed twice with PBS. The fluorescence from A_{488} was collected by Olympus FV-1000 at 485-585 nm upon excitation at 473 nm.

5.2 PREPARATION OF ND CONJUGATE WITH GCP II - INHIBITOR

5.2.1 Evaluation of the reaction product C_2ND1-I

The average diameter of all C_2ND1, C_2ND1-I and C_2ND1-Fl particles was 120 nm (Fig. 27, p. 54).

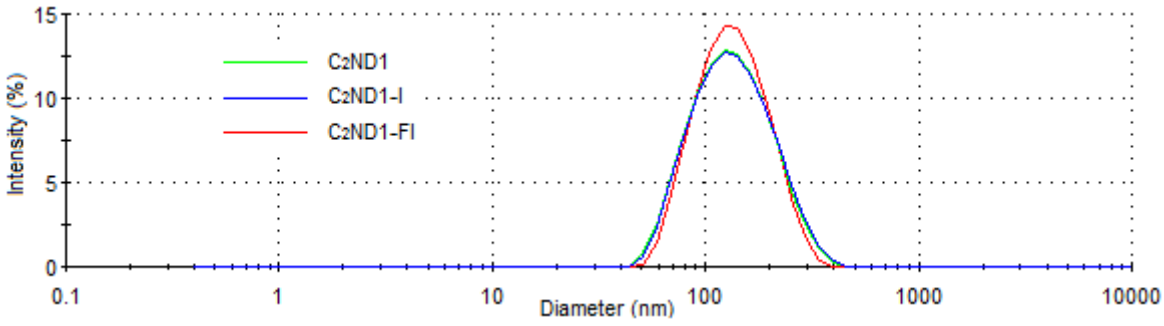

Fig. 27 **DLS of the size distributions of C_2ND1, C_2ND1-I and C_2ND1-Fl particles.** The concentration of studied colloids in PBS was 0.1 mg/ml.

Linear equation y = 0.146 x expressing the relation between absorbance (y) and concentration (x) at 495 nm was calculated from the absorption spectra of the fluorescein solution in various concentrations (Fig. 28). The number of 250 fluorescein molecules per one ND particle was calculated from linear equation after the subtraction the ND scattering from C_2ND1-Fl absorption spectrum (according to the paragraph 5.1.5.1).

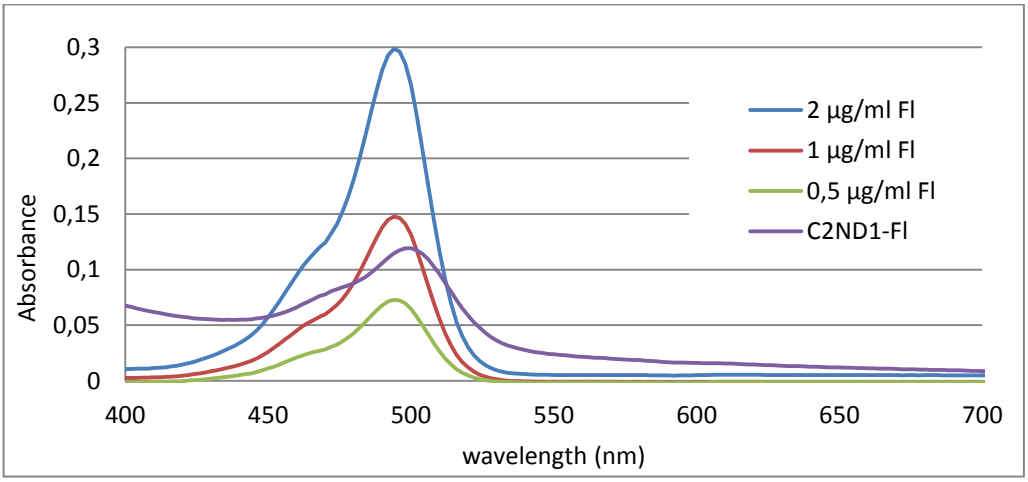

Fig. 28 **Absorption spectra of C_2ND1-Fl and fluorescein (Fl) solutions in various concentrations.**

5.2.2 Reaction of C_2ND1-I or C_2ND1 with A_{488}-alkyne to obtain C_2ND1-I-A1, C_2ND1-I-A2, C_2ND1-A1 or C_2ND1-A2

The absorption spectra of C_2ND1-I-A1, C_2ND1-I-A2 and C_2ND1-A1 C_2ND1-A2 (Fig. 19, p. 46) colloids were analyzed. Calibration curve was calculated from absorbance values of various A_{488}-alkyne concentrations. The reaction of C_2ND1-I or C_2ND1 with A_{488}-alkyne was performed in two different A_{488}-alkyne concentrations. The number of A_{488}-alkyne molecules bound to one C_2ND1-A1 and C_2ND1-A2 particle was calculated (according to

the paragraph 5.1.5.1) as 24 and 79, respectively. 12 and 53 molecules of A_{488}-alkyne are present on one C_2ND1-I-A1 and C_2ND1-I-A2 particle, respectively.

5.2.3 Evaluation of C_2ND2, C_2ND3, C_2ND4 particles – the Bradford assay

The Bradford assay was used for the determination of the non-covalent absorption of HSA on the ND surface (Fig. 29). The non-covalent absorption of HSA on the ND surface (expressed in %) was determined indirectly from amount of HSA in supernatant after the centrifugation. The amount of HSA in the reaction with no ND particles was established as 100% value. Almost 60% of HSA from the reaction was absorbed on the surface of ND-COOH. On the other hand, negligible amount of HSA was absorbed on the surface of C_2ND3 and C_2ND4. Difference between these particles is in the range of measurement error and therefore undetectable. C_2ND2 particles were analyzed in the different measurement and showed the same behavior as C_2ND3 and C_2ND4.

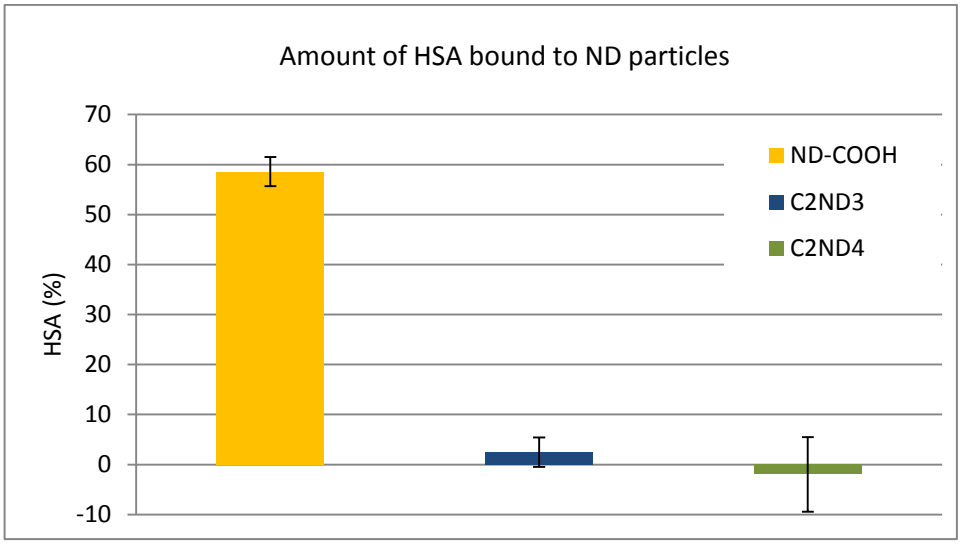

Fig. 29 **Amount of non-covalently absorbed HSA to the ND surface.** The amount of HSA was determined as difference between 100% HSA in solution and amount of HSA in supernatant after centrifugation. For experimental data see the paragraph 4.2.3.5.

5.2.4 Evaluation of C_2ND2, C_2ND3, C_2ND4 particles – the stability study

ND colloids were analyzed for the stability study in H_2O and NaCl solution (0.5 M or 1 M) by DLS (Fig. 30, p. 56). C_2ND2 particles were according to determined diameters unstable in 0.5M NaCl immediately after mixing together (Fig. 30A, p. 56). C_2ND3 particles were more stable in 0.5M NaCl contrary to C_2ND2. The stability of C_2ND3 colloid was however

not sufficient and diameter was higher in the course of time (Fig. 30B). C_2ND4 particles were stable even in 1M NaCl after 24 hours (Fig. 30C,D).

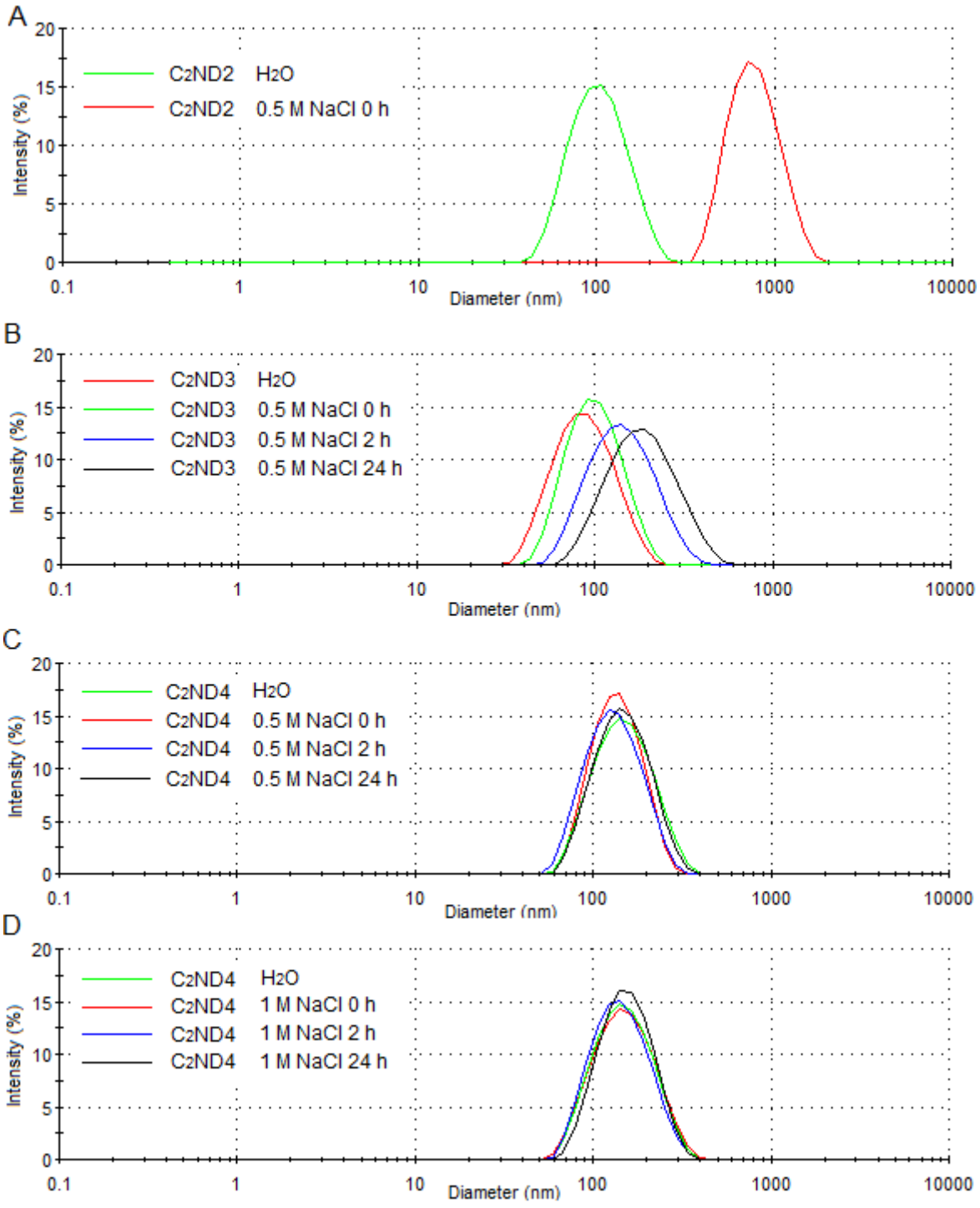

Fig. 30 **Stability study of various C_2ND particles.** DLS of the size distributions of (A) C_2ND2, (B) C_2ND3 and (C, D) C_2ND4 in NaCl in the course of time. The concentration of studied colloids was 0.1 mg/ml.

5.2.5 Reaction of C_2ND4 with A_{488}-alkyne to C_2ND4-A1

Absorption spectrum of C_2ND4-A1 colloid was analyzed. Calibration curve was calculated from absorbance values of various A_{488}-alkyne concentrations (in the paragraph 5.2.2). 360 molecules of A_{488}-alkyne bound to one C_2ND4-A1 particle was determined from linear equation after subtraction of ND scattering (according to the paragraph 5.1.5.1).

5.2.6 SPR study of C_2ND1-I conjugate

The binding response can be seen only for C_2ND1-I particles (green curve) (Fig. 31). No binding response is found for C_2ND1 particles (blue curve) and C_2ND1-I particles where GCP II was not bound to the surface of gold sensor (red curve).

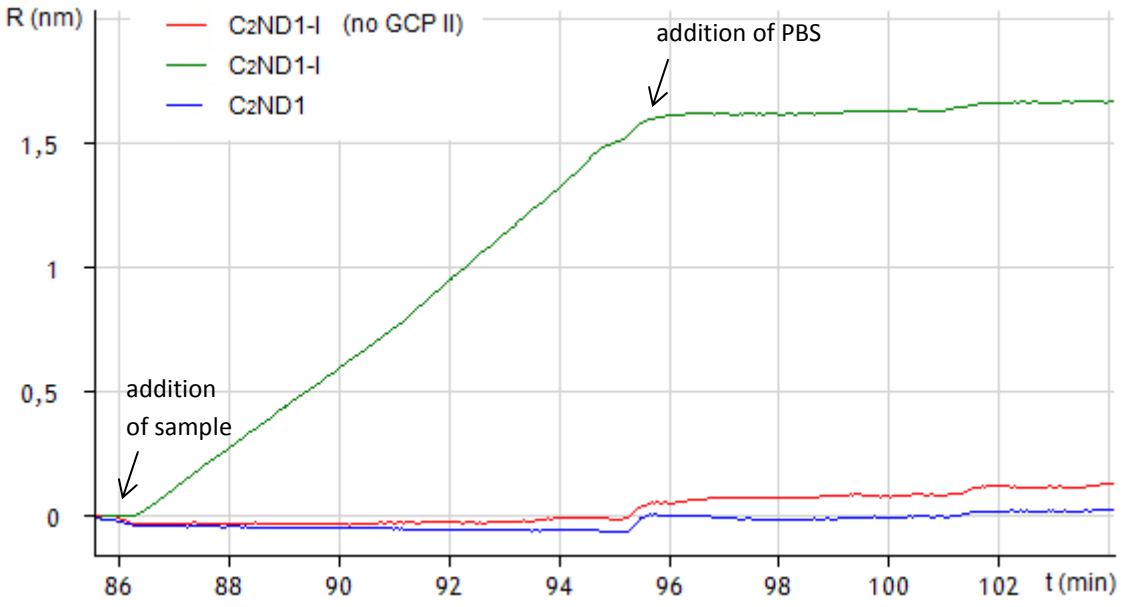

Fig. 31 **SPR sensogram of C_2ND1-I.** The relative change of local refractive index (R) plotted versus time (t). For experimental details see the paragraph 4.2.3.8.

5.2.7 SPR study of C_2ND4-I conjugate

Binding response of C_2ND4-I on gold sensor with GCP II is evident (green and red curve) (Fig. 32, p. 58). No binding response is found for C_2ND4 particles (blue curve) and C_2ND4-I particles where GCP II was not bound to the gold sensor (yellow curve). The result of the SPR with C_2ND4-I particles in various particle concentrations is displayed on Fig. 33, p. 58. Program TraceDrawer was used for kinetic fitting of curves, fit model one-to-one and diffusion correction was used. K_{on} (association rate constant) was determined as 33418 ± 468 $M^{-1}s^{-1}$. K_{off} (dissociation rate constant) value was determined as $5.2 \cdot 10^{-6} \pm 1.4 \cdot 10^{-6}$ s^{-1}.

K_{off} is, however, due to extremely strong binding and no dissociation under quantification limit and could not be determined precisely; the error is in the same order as result. Dissociation constant K_D can be calculated as $K_D = \frac{K_{off}}{K_{on}} = 160$ pM.

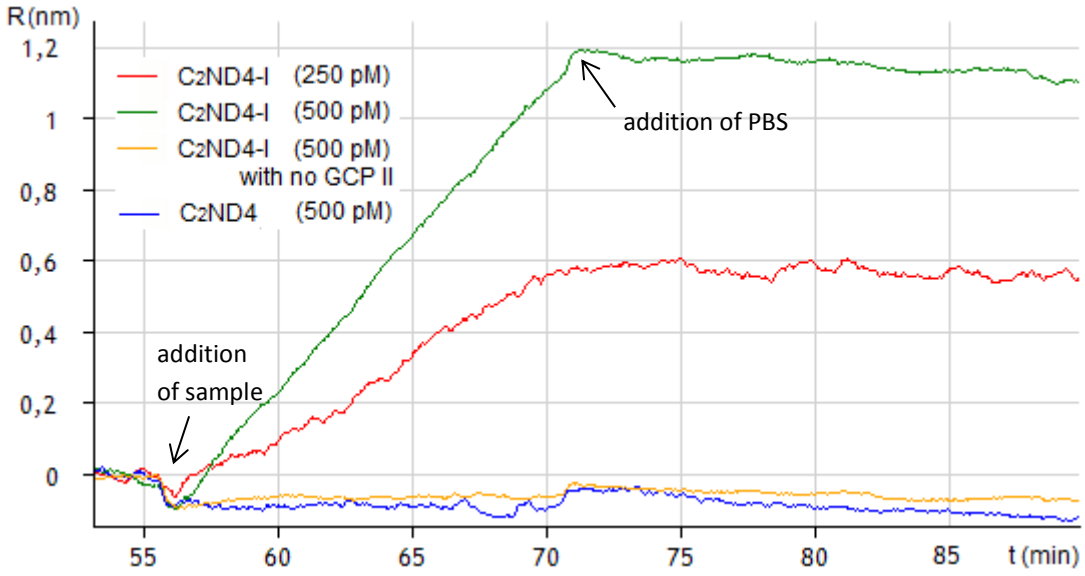

Fig. 32 **SPR sensogram of C_2ND4-I.** The relative change of local refractive index (R) plotted versus time. For experimental details see the paragraph 4.2.3.9.

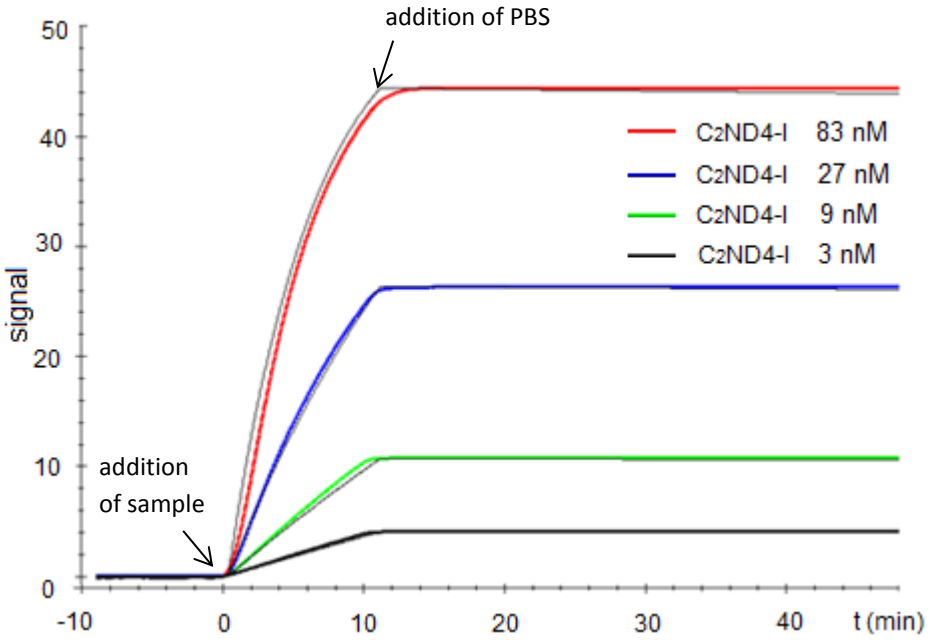

Fig. 33 **Fitted curves of SPR sensogram of C_2ND4-I.** The relative change of local refractive index (signal) plotted versus time. Program TraceDrawer was used for kinetic fitting of curves, fit model one-to-one corrected to diffusion was used. For experimental details see the paragraph 4.2.3.9.

5.2.8 Inhibition assay of C_2ND1-I-A1 conjugate

Every reaction was analyzed by HPLC on reversed phase using the absorption detector. Both the substrate and product absorb UV light. Reaction rate is linearly proportional to the amount of substrate and product in reaction (peak´s area after HPLC separation). The reaction conversion and the factor v_i/v_0 can be calculated as follows:

$$\text{reaction conversion } (\%) = \frac{\text{product area}}{(\text{substrate area} + \text{product area})}$$

$$\frac{v_i}{v_0} = \frac{\text{reaction conversion}}{\text{conversion of reaction without inhibitor}}$$

The factor v_i/v_0 of the reaction mixture with the highest inhibitor concentration is 0 (Fig. 34). All C_2ND1-I-A1 concentrations lower than 0.5 pM respond to v_i/v_0 approximately 0.92. The half maximal inhibitory concentration (IC_{50}) was calculated as 107 ± 46 pM by the program GraFit analysis data software. The factor v_i/v_0 of the reaction mixture with C_2ND1-A1 instead of C_2ND1-I-A1 in the concentration 5 nM is 0.56.

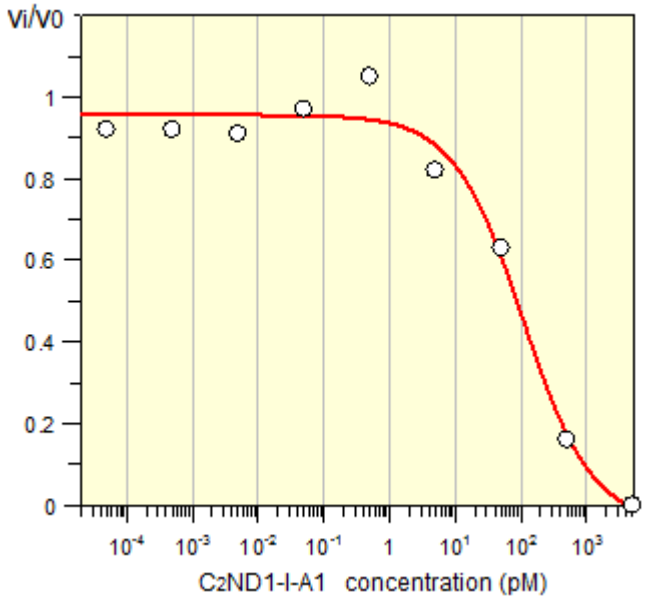

Fig. 34 **Inhibition of GCP II activity by C_2ND1-I-A1 analyzed by HPLC using PteGlu as a substrate.** For experimental details see the paragraph 4.2.3.10.

5.2.9 Inhibition assay of C_2ND4-I conjugate

The inhibition assay was evaluated in the similar manner as described in the paragraph 5.2.8. On graph (Fig. 35, p. 60) the factor v_i/v_0 is plotted versus C_2ND4-I concentration.

The factor v_i/v_0 of the mixture with the highest C_2ND4-I concentration ($3 \cdot 10^4$ pM) is 0. The lowest concentration of C_2ND4-I (0.38 pM) does not inhibit. IC_{50} was calculated as 56.3 ± 2.7 pM by the program GraFit analysis data software. The relation between IC_{50} and K_I is expressed by the equation:

$$K_I = \frac{IC_{50}}{1 + \frac{[S]}{[K_M]}}$$

K_M for GCP II and PteGlu2 was determined by co-workers as 100 nM; K_I was calculated as 18.8 pM. C_2ND4 particles do not reduce reaction conversion in any concentration.

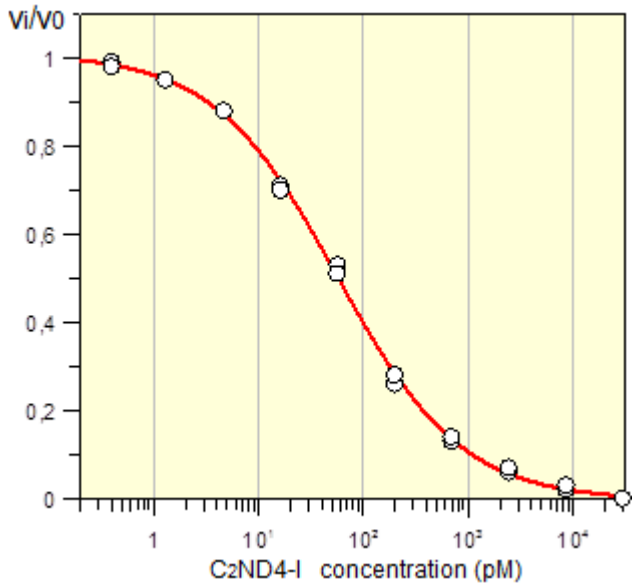

Fig. 35 **Inhibition of GCP II activity by C_2ND4-I analyzed by HPLC using PteGlu2 as a substrate.** For experimental details see the paragraph 4.2.3.11.

5.2.10 Targeting of cancer cells by conjugate C_2ND1-I-A2

Confocal microscopy was performed after 24 hours in Opti-MEM medium. C_2ND1-I-A2 and C_2ND1-A2 particles (Fig. 19, p. 46) were found inside the both cell types (with GCP II expression and without the GCP II expression) (Fig. 36, p. 61).

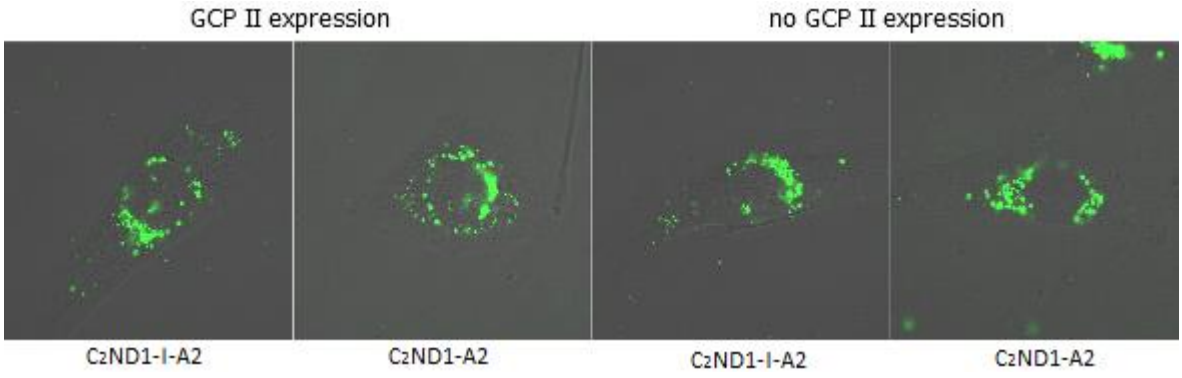

Fig. 36 **Confocal microscopy analysis of C_2ND1-I-A2 and C_2ND1-A2 internalized by U373 cells with and without the GCP II expression.** The cells were incubated 1 hour with NDs in the final concentration 100 µg/ml and were subsequently washed twice with PBS and incubated more 24 hours in Optim-MEM medium. The fluorescence of A_{488} was collected by Zeiss LSM 780 at 499-552 nm upon excitation at 488 nm.

5.2.11 Targeting of cancer cells by conjugate C_2ND4-A2-I

U373 cells with the GCP II expression and without the GCP II expression were used. Confocal microscopy was performed after 24 hours incubation. C_2ND4-A2-I and C_2ND4-A2 particles (Fig. 19, p. 46) were found inside the both cells types (Fig. 37).

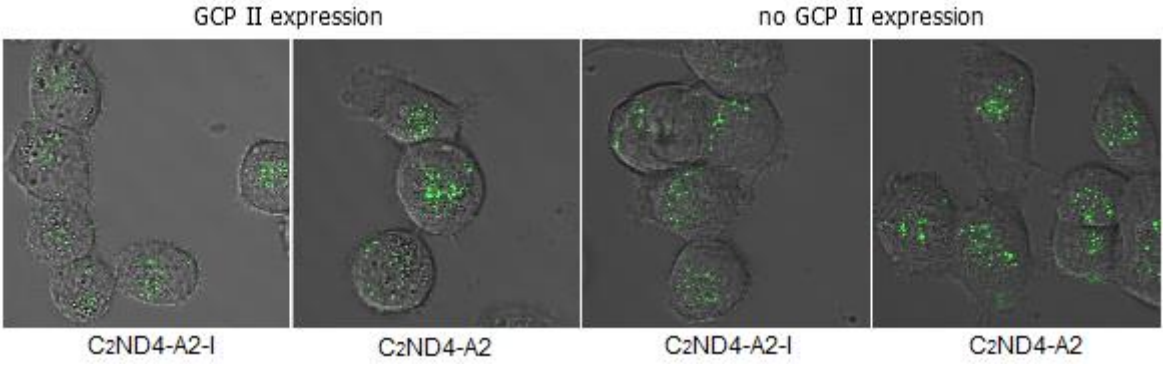

Fig. 37 **Confocal microscopy analysis of C_2ND4-A2-I and C_2ND4-A2 internalized by U373 cells with and without the GCP II expression.** The cells were incubated 24 hours with NDs (final concentration 100 µg/ml) and were subsequently washed twice with PBS. The fluorescence of A_{488} was collected by Zeiss LSM 780 at 499-552 nm upon excitation at 488 nm.

Quantification of fluorescence, measurement of fluorescence intensity, was performed using flow cytometry. The same intensity value was observed for both types of particles in both types of cells (U373+ with GCP II expression, U373- without GCP II expression) (Tab. 16, p. 62).

Tab. 16 **Results of fluorescence intensity measurement by the flow cytometry.**

sample	I (A_{488})
C_2ND4-A2-I _U373+ cells	12,510
C_2ND4-A2-I _U373- cells	12,120
C_2ND4-A2 _U373+ cells	14,070
C_2ND4-A2 _U373- cells	14,470

5.3 VISUALISATION OF ND IN CANCER CELLS

There is a significant difference between C_1ND particles pre-incubated in PBS which were internalized inside the cells and ND-COOH pre-incubated in PBS located mostly on the cell membrane (Fig. 38). However, in the case of ND pre-incubated in medium, there is no difference between C_1ND and ND-COOH and both particles are found inside the cells.

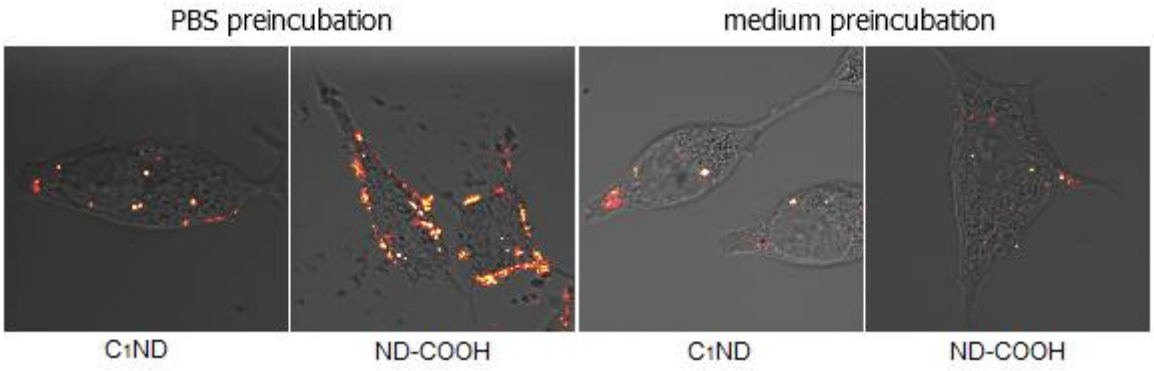

Fig. 38 **Confocal microscopy analysis of C_1ND and ND-COOH internalized by LNCaP cells.** The cells were washed by PBS after 1 hour incubation with NDs (final concentration 200 ug/ml), incubated for 23 hours and observed after fixation. Fluorescence of NDs was collected by Zeiss LSM 780 at 639-758 nm upon excitation at 532 nm. Fluorescence from NDs is displayed in red-to-white false colours.

6. DISCUSSION

6.1 PREPARATION OF ND CONJUGATE WITH Tf

6.1.1 Preparation of Tf-A

It is crucial for further applications (targeting of cancer cells, for example) to preserve biomolecules´ structure, properties and function after their immobilization on the ND surface. To know and control the biomolecule exposure, as little reacting groups as possible should be present in the biomolecule. Tf is usually connected to the ND surface by an amide bond. Tf includes 58 lysines and one terminal amino group. [55] 59 amino groups can formally react in amide bond formation, although not all amino groups are accessible on the Tf surface. In this work, oxime ligation was used to connect Tf to the ND surface. Oxime ligation is a reasonably efficient reaction applicable at mild conditions with a well-defined chemistry of attachment. [47,48] There are four sialic acids in glycosylated Tf located at the end of two branched carbohydrate structures. [48] The maximum of four aldehyde and subsequently azide groups is introduced to the Tf structure in the reaction with $NaIO_4$ and 3-aminooxypropyl-1-azide. Four reactive groups on two different places in Tf bring much easier control of attachment compared to 59 amino groups.

Various types of molecules or particles can be modified with azide- or alkyne-moiety and subsequently react without significant limitations in CuAAC. [49,50] Copper(I) ions are generated in the reaction of $CuSO_4$ and ligand THPTA. Copper(I) ions are kept reduced by sodium ascorbate; oxygen terminates the reaction. The excess of THPTA and the presence of aminoguanidin suppress a biomolecule cleavage or the oxidation of aminoacids in the structure of a protein. Aminoguanidin is used regularly in all reactions to maintain equal conditions. The concentration ratio 1:5 (Cu/THPTA) was used in reactions of Tf with ND to protect Tf. The reaction rate is reduced by this excess of ligand; ratio 1:2 was used in reactions without Tf. The possibility of Tf-N_3 to react in CuAAC was verified by the reaction of Tf-N_3 with Fl-alkyne. The reaction yield was not quantified; the product was evaluated by SDS-PAGE. Tf-Fl stain on a photography taken under UV-lamp (Fig. 20B, p. 47) is a proof of the successful reaction between Tf-N_3 and Fl-alkyne. A molecular weight of approximately 75 kDa for all samples (Tf, Tf-N_3 and Tf-Fl) (Fig. 20A, p. 47) excludes a significant change in the size of modified Tf (dimer formation or cleavage, for

example). Conformation or activity change is, however, not observable by SDS-PAGE. Prepared Tf-N_3 can react in CuAAC with alkyne-modified ND.

Tf-N_3 was labeled by A_{488} before reaction with alkyne-modified ND. Absorbance spectrum of prepared Tf-A was analyzed (Fig. 21, p. 48); approximately two molecules of A_{488} are bound to Tf-N_3. A_{488}-5-sulfodichlorophenyl ester can react theoretically with 59 amino groups in the structure of Tf-N_3, however, no all primary amines are accessible on the Tf surface. Two A_{488} molecules bound to Tf is sufficient for observing Tf-A under confocal microscope.

Modified protein Tf-A was two times freeze-dryed from a buffer after purification steps. Weight after freeze-drying is thus the sum of the protein weight and the buffer weight. Mass fraction (the ratio of the protein weight to the total weight) has to be known for further reactions. The mass fraction of Tf-A was determined by three different methods – labeling protocol using absorption spectrum, AAA and the Bradford assay as 0.11, 0.10 and 0.09, respectively. All three results correspond well. AAA was considered as the most relevant method; the mass fraction 0.10 was used for the recalculation of all previous and next concentrations. Purchased Tf is according to both AAA and the Bradford assay not pure; the mass fraction was calculated as 0.74 and 0.65, respectively.

SDS-PAGE did not show any significant change in the size of modified Tf, but could not excluded conformation change or, the most important, activity change. This activity was tested using competitive binding assay of Tf and Tf-A. Tf and Tf-A concentration ratios for experiment were designed according to the linear equation for ratio I_{max}/I (paragraph 5.1.3). Only a slight decrease in binding activity to TfR was observed for Tf-A in comparison to Tf. The binding affinity of unmodified Tf is for both K562 and HT-29 cells approximately twice higher than binding affinity of Tf-A. The Tf-A binding activity remains in the same order of magnitude. Tf-A is therefore considered as well useful for targeting experiments.

6.1.2 Preparation of C_1ND-Tf particles for the targeting of cancer cells

Pretreated ND-COOH (irradiated with high-energy particle beam, annealed, oxidized to remove sp^2 carbons and reduce the heterogenity of the surface) form stable colloidal solutions in H_2O. A covalent surface architecture on ND-COOH particles was build from

silica and PEG layer, as it was implied in the paragraph 2.2.7.1. The possibility to introduce a reactive amino group to cross-linked silica layer allows high yield further modifications, by the alkyne-modified PEG chain, in this particular case. PEG chain is used as a spacer between the ND surface and Tf in order to reduce steric constraints and retain the Tf ability to react with TfR. Colloidal stability of C_1ND and C_1ND-Tf particles in the environment with higher ionic strength (PBS) was demonstrated by DLS (Fig. 23, p. 50). This colloidal stability is substantially improved by the PEG layer. DLS is a valuable method to determine significant differences between the particles size (at least few tens of nanometers) or differences between precipitated and stable colloids. However, the average diameter determined from DLS is dependent on various parameters such as particle concentration or surface charge. The accurate absolute size diameter is thus not a quantity achievable from DLS. The average diameter size from DLS is approximately 190 nm for C_1ND-Tf particles. The size distribution of C_1ND-Tf is not symmetric and the occurrence of higher diameters is significant.

Fluorescent dyes are bound to the surface of ND for confocal microscopy. NDs labeled by dyes are also required for flow cytometry. Low brightness of NDs is considered as their major drawback. The fluorescence from dyes was thus used in all targeting experiments instead of poorly detectable ND fluorescence. The confocal experiment with ND visualisation in the cells was also performed.

Non-adherent cells K562 express at a high rate TfR on the cell surface and are often used for targeting experiments with Tf. [36,45] The fluorescence of A_{488} was observed inside the cells after incubation with Tf-A (Fig. 24,1B, p. 51); the ability of modified Tf (Tf-A) to target cancer cells and to internalize was verified. No fluorescence was observed in the cells incubated with free Tf before adding Tf-A. Tf and presumably Tf-A are internalized by the same uptake mechanism. Blocking ND uptake mechanism by Tf confirms ND internalization by the same way (a receptor-mediated endocytosis through clathrin-coated pits). C_1ND particles were modified with Tf-A to create C_1ND-Tf particles which should be capable of targeting TfR on K562 cells. C_1ND-Fl particles were used as a negative control. The difference between the shown pictures of the cells incubated with these two conjugates is significant (Fig. 24, p. 51). C_1ND-Fl particles are present on cell membrane contrary to C_1ND-Tf particles that are inside the cell. C_1ND-Fl particles do not

internalize to the cells, but seem to have certain affinity to K562 cells. The quantitative comparison of the two conjugates is, however, problematic since the amount of a dye present on the ND surface is different. C_1ND particles were labeled directly by fluorescein and indirectly by A_{488} on Tf. Fluorescein as smaller molecule compared to Tf-A is able to access the surface more easily and the labeling reaction is expected to be more efficient.

C_1ND-Tf particles have an asymmetric size distribution with occurrence of higher diameters according to DLS measurement and ND aggregates can be seen under confocal microscope. Furthermore, the particles after experiment precipitated; decreased stability of C_1ND-Tf at RT was probably the reason. K562 non-adherent cells are not very suitable for confocal microscopy because cells are flattened by microscope slide and small artifacts or vesicles are formed on the cell membrane (Fig. 24, p. 51). HT-29 adherent cells are more suitable and were used in the next experiment. Confocal microscopy cannot provide statistical results under used setup. Flow cytometry is more convenient method employed in the further experiment. The cells were incubated by ND particles in the final concentration 1 mg/ml. This concentration is, however, rather theoretical. A significant amount of C_1ND-Tf was captured within purification procedure on the centrifugal filter tubes with no recovery. Purification in centrifugal tubes was not applied in the next experiment.

6.1.3 Preparation of C_1ND-A-Tf particles for the targeting of cancer cells

Consequently, a similar experiment was performed. Tf-A and C_1ND-A-Tf were used for the targeting of the cancer cells with consideration to previous experiments.

C_1ND particles were for the second targeting experiment labeled directly by A_{488} to avoid discrepancy between the fluorescence of two types of particles. Tf-A was subsequently bound to the C_1ND-A particles. The average size of C_1ND-A-Tf particles is approximately 190 nm, similarly to C_1ND-Tf (Fig. 25, p. 51). The size distribution is symmetric in this case; the modifications of particles increased the size as expected but they retained the particle quality according to DLS. One C_1ND-A-Tf particle contains approximately two Tf molecules on the surface according to calculation (the paragraph 5.1.5.1). The calculations of molecule quantities on the surface are, however, inaccurate; the weight of one ND particle is a rough approximation due to polydisperse NDs with irregular shape. CuAAC is

considered an efficient reaction for various types of molecules; Tf molecule is a protein and a large molecule. Moreover, every Tf has maximally four azide groups in its structure and right orientation of Tf is crucial to access to the proximity of the ND surface and to react. Two Tf molecules on the ND surface should be sufficient for the targeting experiment, although the effect of avidity (combined strength of more bonds) cannot be applied.

Targeting experiments with NDs in the cells were performed in medium in this case (Fig. 26, p. 53). Medium, where the cells have grown, was replaced by serum-free H-MEMd medium for the incubation time. Serum-free medium was employed to eliminate the presence of other proteins. Proteins have affinity to NDs, they adhere on them and can mask Tf on the surface that makes targeting difficult or impossible. Many cells in serum-free medium including the negative controls, however, did not survive 6 and 24 hour incubation since serum-free medium does not allow long incubation. It was difficult to find living cells after long incubation times under confocal microscope; these incubation times did not allow evaluation by confocal microscopy.

Flow cytometry was used, the gating using side and forward scatter excludes death cells. The fluorescence ratio of C_1ND-A to C_1ND-A-Tf (calculated from fluorescence spectra measurement as 2.17) was included to evaluate the flow cytometry results (Tab. 15, p. 52). Fluorescence intensity of C_1ND-A particles was divided by 2.17 to enable comparing of the particles with equal fluorescence. The difference in the fluorescence of these two particles is caused probably by washing procedures after the reaction with Tf. During washing procedures, the adhered A_{488} is washed away and, moreover, a small part of ND is lost. C_1ND-A-Tf particles have higher affinity for K562 cells after incubation time of 1, 3, 6 and 24 hours than C_1ND-A particles, according to flow cytometry. The difference is up to 34% for 3 hour incubation. The affinity of C_1ND-A-Tf is lower than C_1ND-A in the majority of HT-29 incubation times. HT-29 as adherent cells do not seems to be suitable for flow cytometry measurement, contrary to confocal microscopy. The determined cell fluorescence intensity from flow cytometry does not reflect the location of A_{488}. Particles can be placed either on the cell membrane or inside the cell. Location of particles can be observed under confocal microscope. No strict regularity was seen under the confocal microscope; both C_1ND-A-Tf and C_1ND-A particles could be found on the cell membrane

or inside the cells (Fig. 26, p. 53). C_1ND-A particles placed on the cell membrane and C_1ND-A-Tf localized in the cells were observed for only limited number of cells.

The result of the cancer cells targeting by Tf is not very convincing. It is either the problem of the targeting system (Tf-TfR) or the properties of particles. According to previous research [35,37,52,53,62], the Tf-TfR system should be able to target the nanoparticles in principle, even though the way of Tf conjugation to the surface of ND was different. The possible reason for the insufficient effectiveness of Tf-TfR targeting system can be a low amount of Tf on the ND surface (there are only two of them per a nanoparticle). To address this issue, another targeting system (GCP II inhibitor - GCP II) and different particles (C_2ND) were used.

6.2 PREPARATION OF ND CONJUGATE WITH GCP II – INHIBITOR

Targeting system GCP II inhibitor – GCP II has three important advantages over Tf-TfR system. i) Various methods can be employed for evaluating the ND conjugate with GCP II-inhibitor; reaction ability and activity of conjugate can be confirmed besides the success of conjugation. ii) U373 cancer cells can be used in targeting experiments. The cells are very convenient for the study, because GCP II expression of U373 cells can be blocked by compound doxycycline. The same cells which do not express GCP II (negative cells) are a convenient negative control in the targeting experiments (more convenient negative control in comparison to non-targeting particles). iii) GCP II expression is more specific than TfR expression. TfR is express in almost all cells whereas GCP II is expressed predominantly on prostate cancer cells and in neovasculature in many types of solid tumors.

6.2.1 Preparation and evaluation of C_2ND1-I particles

6.2.1.1 Preparation of particles

ND-COOH particles were coated with the thin layer of silica (< 1 nm) and polymer HPMA. Newly prepared C_2ND1 particles were thanks to HPMA layer also stable in the environment with higher ionic strength (PBS) (Fig. 27, p. 54). The average size diameter of C_2ND1 particles was approximately 120 nm; particles keep the irregular shape of ND-COOH. Particles modified with GCP II-inhibitor and fluorescein (C_2ND1-I and C_2ND1-Fl) have the same size characteristics as C_2ND1. The CuAAC reaction conditions for the

preparation of C_2ND1-Fl and C_2ND1-I were the same. It was calculated that there are 250 fluorescein molecules present on one ND particle so it can be assumed that approximately 250 molecules of GCP II-inhibitor are present on one ND particle. This number is a rough estimate since Fl-alkyne is a twice smaller molecule than the modified inhibitor (Fig. 17, p. 38) and its charge is different.

C_2ND1 and C_2ND1-I particles were simultaneously labeled (Fig. 19, p. 46). Two different concentrations of A_{488} were used. Less labeled particles were created initially for confocal microscopy. A_{488} fluorescence interferes with low ND fluorescence less for a lower amount of A_{488} on the particle. Nevertheless, observing the result using ND fluorescence was due to cell auto-fluorescence a demanding task, therefore, NDs with higher amount of A_{488} were used for confocal microscopy experiment. C_2ND1-I particles contain less azide groups than C_2ND1 particles; inhibitors occupy part of azide groups, so the amount of A_{488} bound to the ND surface calculated from the absorption spectra is in agreement.

6.2.1.2 SPR study of C_2ND1-I and inhibition assay of C_2ND1-I-A1

To evaluate reaction ability and activity of ND conjugate with GCP II-inhibitor, SPR study and inhibition assay was performed. The ability of ND to bind to GCP II was evaluated by SPR measurement. GCP II was immobilized on the thin gold sensor placed in the SPR instrument through a streptavidin-biotin interaction. This connection ensures GCP II orientation on the gold sensor similar to the GCP II position on the plasma membrane. A suitable ligand interacts with immobilized molecule, adsorbs to metal surface and causes a change in the local refractive index. Delocalized oscillating electrons (surface plasmons) are present on the metal sensor surface. Linear polarized light can interact at certain conditions (appropriate angle and wavelength) with these electrons and resonate. Resonation changes the intensity of reflected light. This change is dependent on the refractive index at short distance (approximately 300 nm) from gold sensor. [85,86] C_2ND1-I particles changed according to high signal the local refractive index, thus interacted with GCP II (Fig. 31, p. 57). There is no possibility to discover by SPR measurement how ND particles bind the GCP II. C_2ND1 particles do not bind the GCP II layer; the connection of C_2ND1-I to GCP II has to be specific, though. No C_2ND1-I binding on the gold sensor without GCP II layer further confirms the specifity of the connection.

Inhibition assay allows to find out how GCP II and GCP II-inhibitor are bound. The ability of an inhibitor to inhibit the reaction means that C_2ND1-I-A1 is bound to active site of the enzyme (GCP II). The used inhibitor is an urea-based inhibitor modified on PEG chain with alkyne moiety enabling the reaction with ND (Fig. 17, p. 38). The modification of the inhibitor with long PEG chain (PEG_{12}) is crucial to enable the inhibitor to be flexible and to bind to active site inside the enzyme without ND particle interfering. Folate hydrolase activity of GCP II is used for the cleavage of the substrate PteGlu2 to produce PteGlu. Full inhibition (no reaction conversion) for the highest inhibitor concentration brought an expected result (Fig. 34, p. 59). The reaction conversion (v_i/v_0) grows with the decrease of C_2ND1-I-A1 (inhibitor) concentration reaching an average of 0.92 for concentrations lower than 0.5 pM. Interestingly, the factor v_i/v_0 does not reach value 1 even for the lowest particle concentrations ($5 \cdot 10^{-14}$ pM, data not shown). It means that conversion of the reaction in presence of particles is lower than conversion of the reaction without particles. One can suggest that even at low concentrations of nanoparticles an adsorption of PteGlu or another interfering process occurs. Product PteGlu adhered to the particles more than substrate PteGlu2 probably because of less negative charges in the molecule (negative charges dominate on the surface of C_2ND1-I-A1). In order to estimate a possible adsorption of PteGlu or PteGlu2 to nanoparticles, experiment with particles without inhibitor (C_2ND1-A1) was performed. Although the reaction conversion should not be lowered by C_2ND1-A1 particles since it does not contain the inhibitor, the value v_i/v_0 is lowered to 0.56. The decrease is caused by the fact that PteGlu (and also PteGlu2) in a large extent adhered to C_2ND1-A1 particles in the concentration of 5 nM. The difference between C_2ND1-I-A1 and C_2ND1-A1 particles is, however, significant. Indeed, the inhibitory activity of C_2ND1-I-A1 particles was confirmed.

6.2.1.3 Targeting of U373 cancer cells by C_2ND1-I-A2

NDs with or without GCP II inhibitor were capable to be internalized in both GCP II positive and negative cells equally, i.e. a specific targeting effect was not observed (Fig. 36, p. 61). ND particles were adhered after 1 hour incubation on the cell membrane in all cases. This result is very similar to the targeting experiments with Tf. C_1ND-A-Tf and C_1ND-A were also adhered on the cell membrane. This fact indicates that adhesion forces are significant and prevail over the potential targeting effect. Once the particles were

adhered to the cell membrane, they internalized spontaneously as it was discussed in the paragraph 2.3.1. ND particles with no affinity to the cell membrane were needed, therefore C_2ND1 particles optimization was performed in the purpose of a higher polymer density on the surface.

6.2.2 Preparation and evaluation of C_2ND4-I particles

6.2.2.1 Polymerization optimization

Radical polymerization of HPMA initiated at higher temperature by 2,2'-Azobis(2-methylpropionitrile) was used for preparing of C_2ND particles. The reaction is performed by a so called "grafting from" method, what means sequential growth of the polymer directly from the surface. Because ND can act as a crosslinker, the reaction has to be performed with high excess of HPMA polymer compared to ND to keep a distance between ND particles. The mobility of ND is reduced at lower temperature and in more viscous solvents. On one hand, HPMA monomers can, being smaller molecules, move in the solution faster to create polymers, on the other hand, polymers mobility and possibility to combine two active chain ends is reduced. The viscosity of solvent postpones the termination and prolongs the reaction time. Reactions were performed in ethanol or DMSO in higher concentrations. Temperature during the reaction was decreased. Only 1.5% of HPMA was substituted by AzpAAm for polymerization. Higher amount of the azidopropyl chains is assumed to create hydrophobic domains enabling proteins or cells to adhere. C_2ND2, C_2ND3 and C_2ND4 particles were prepared.

Newly prepared particles (Fig. 19, p. 46) were mixed with HSA in order to evaluate the possibility of protein adhesion to the surface of the ND particles. Almost 60% of HSA from the reaction was absorbed on the surface of ND-COOH particles (Fig. 29, p. 55). The surface of ND-COOH particles is not protein-resistant. The difference among C_2ND2, C_2ND3 and C_2ND4 is in the range of observational error and therefore undetectable. The surface of these particles, however, seems to be almost protein resistant. The Bradford assay is not a sufficiently sensitive method to distinguish the modification of prepared particles. Indeed, the stability study revealed large differences between particles (Fig. 30, p. 56). C_2ND2 particles were prepared under almost the same conditions as C_2ND1 particles used for already performed experiments (ethanol in the same concentration, 70 °C). The difference was in the substitution of HPMA with only 1.5% AzpAAm. C_2ND2

particles were unstable in 0.5M NaCl. DMSO in higher monomer concentrations, lower temperature (60 °C) and substitution of HPMA with 1.5% AzpAAm were used for C_2ND3 particles preparation. C_2ND3 particles were more stable in 0.5M NaCl, however, the diameter increased in the course of time. DMSO in the highest monomer concentrations, lowest temperature (55 °C) and substitution of HPMA with 1.5% AzpAAm were polymerization conditions which created stable C_2ND4 particles even in 1M NaCl after 24 hours. C_2ND4 particles had the most proper characteristics, according to our assumption. Thicker polymer layer on C_2ND4 particles suggests also higher average size diameter (approximately 140 nm) than for C_2ND2 (approximately 100 nm) and C_2ND3 (approximately 90 nm) particles. C_2ND4 particles were used for further reactions. Although C_2ND4 were polymerized with only 1.5% AzpAAm, approximately 360 molecules of A_{488}-alkyne was bound to surface C_2ND4-A1 (contrary to 250 molecules of fluorescein on C_2ND1-Fl particles). It can be assumed that approximately 360 molecules of GCP II-inhibitor are present on one C_2ND4-I particle.

6.2.2.2 SPR study and inhibition assay of C_2ND4-I

The ability of ND to bind to GCP II was evaluated again by SPR measurement. C_2ND4-I particles behaved in the same manner as C_2ND1-I particles and interacted with GCP II. The specifity of connection was confirmed by zero binding of C_2ND4 particles and C_2ND4-I particles on the gold sensor without GCP II layer (Fig. 32, p. 58). The response seems to be concentration dependent; 500nM C_2ND4-I particles show twice higher signal than 250nM C_2ND4-I particles. SPR measurement of C_2ND4-I particles in different concentrations (3; 9; 27; 83 nM) was fitted by kinetic model one-to-one (Fig. 33, p. 58). This model supposes only one type of interaction (the most probable is interaction of one ND particle per one immobilized GCP II if only one type is involved). The conception of one ND particle bond to one immobilized GCP II using one inhibitor is possible. The area of ND surface is large and approximately 360 molecules of inhibitor can be theoretically spread about 5 nm from each other. This assumption, however, does not correspond with the extremely low dissociation constant of the C_2ND4-I from GCP II on gold sensor. The connection of GCP II and C_2ND4-I is extremely strong. This strength is usually mediated by more bonds between ligand and layer, so called avidity. One hypothetical explanation reaching a compromise between our results is that NDs are bound by only one inhibitor to the GCP II

layer, some particles dissociate upon PBS addition, but are immediately re-bound by another inhibitor to another GCP II. SPR signal remains constant during this change of ND location. The program for fitting curves was unable to fit the constant curve of dissociation precisely; K_{off} was determined with a high error. An analyte is transported to the surface by convection (flow rate) and diffusion. Correction for diffusion was used to fit the curves for minimizing mass transport effects. This effect occurs when the binding rate of analyte to the ligand is faster than diffusion of analyte to the surface. [85,86] High density of GCP II (ligand) is present on the gold sensor and C_2ND4-I particles (analyte) have high affinity to GCP II therefore the rate of binding is high. NDs are large particles with low diffusion ability. Moreover, flow rate was set as only 20 µl/min.

The ability of an inhibitor to inhibit the reaction and bound to the active site of GCP II was confirmed by inhibition assay once again. The concentration range was optimally selected, full inhibition for the highest inhibitor concentration and no inhibition for the lowest particle concentration was achieved (Fig. 35, p. 60). No substrate or product adhered to the particles surface (C_2ND4-I or C_2ND4) even in the highest concentration. This is in contrast to previous results and therefore another confirmation that polymer procedure optimization was successful and newly prepared particle have the more convenient surface. C_2ND4 particles (with no inhibitor) do not reduce reaction conversion in any concentration. K_D, a dissociation constant of the complex, was calculated from kinetic fitting of SPR measurement as 160 pM. The lower the value of K_D is the stronger is the interaction between ligand and analyte. K_D can be replaced by K_I if analyte and ligand are an inhibitor and enzyme. K_I was calculated as 18.8 pM using inhibition assay data. The discrepancy between these values is an expected result due to a difference between used methods. Inhibition assay is performed in solution, which means that both GCP II and C_2ND4-I particles are accessible from all directions. Side-by-side immobilized GCP II are accessible with limitations. The connection of GCP II to C_2ND4-I particle is facilitated in solution, thus lower K_I value from inhibition assay is expected.

6.2.2.3 Targeting of U373 cancer cells by C_2ND4-A2-I

The more suitable surface of ND particle due to the higher density or length of polymer chains was created within polymerization optimization. This surface should have ensured the decrease of the particles adhesion to the cells. Both NDs, with or without GCP II-

inhibitor (C_2ND4-A2-I and C_2ND4-A2 particles), were able to internalized to cancer cells with and without GCP II expression, suggesting the lack of selectivity (Fig. 37, p. 61). Targeting was not successful despite of the fact that newly prepared particles have improved surface properties than previously used particles according to other measurements (DLS, Bradford assay). Apart from confocal microscopy, flow cytometry was used as a quantitative method. No significant distinction among two different particles in two different cells was observed (Tab. 16, p. 62). Small difference in the fluorescence intensity can be observed between C_2ND4-A2-I and C_2ND4-A2 particles. C_2ND4-A2-I particles appear to adhere less on the cell surface. It can be explained by higher abundance of negative charges on the particles with inhibitor and thus lower affinity to the cell membrane. The experiments clearly revealed that much more convenient particles with no affinity to the cell membrane are required and that a thicker polymer layer has to be created on the ND surface in order to achieve selective targeting. To coat spherical ND particles could be a suitable approach since non-spherical particles can be the reason why other effects than targeting dominate.

6.3 ND-VISUALISATION

The fluorescence from dyes was used in all targeting experiments instead of poorly detectable ND fluorescence. Low brightness of NDs is considered as their major drawback. Cell auto-fluorescence, fluorescence from media and the type of confocal microscope (its configuration and sensitivity) are some of the features crucial for ND fluorescence detection. The fluorescence intensity is expected to be significantly increased in nearby future, therefore this handicap should be overcome. The possibility of ND visualization under certain conditions was, however, confirmed (Fig. 38, p. 62). This experiment indicates that LNCaP cells have lower auto-fluorescence than U373 cells. This experiment, moreover, confirms the non-stability and aggregation of ND-COOH particles in PBS. The aggregates of ND-COOH particles cannot enter the cells due to their large size and are located mostly on the cell membrane. This aggregates are detected more easily (voltage on detector is lower) than colloidally stable C_1ND particles. ND-COOH particles do not aggregate within medium pre-incubation period. Serum contains proteins which adhere to the particles surface and decelerate and postpone ND-COOH precipitation. Particles are internalized to the cell prior to slower precipitation.

7. CONCLUSION

ND particles coated either by PEG or HPMA polymer were prepared. Particles enable further modifications using azide-alkyne cycloaddition. Two active biomolecules were successfully attached to the ND surface by azide-alkyne cycloaddition – Tf and a GCP II-inhibitor.

Tf was modified before conjugation to the surface. It was shown that this modification do not significantly change the structure and Tf ability to react with TfR. Targeting of the cancer cells with the conjugate of ND and Tf was not sufficiently selective. The possible reason for the insufficient effectiveness of Tf-TfR targeting system can be a low number of Tf molecules on the ND surface.

The activity of GCP II-inhibitor on the ND surface and the affinity to GCP II was confirmed. Targeting by the ND conjugate with GCP II-inhibitor was not selective as well as for Tf. The effect of targeting molecule is minimalized probably due to strong non-specific adhesion of particles to the cell membrane.

Future research requires spherical particles containing higher density of polymer on the surface, because targeting experiment with both particles did not show specificity against receptor-expressing cells.

NDs are known to have low fluorescence brightness that is why fluorescent dyes were used in all previous experiments. However, we succeded to define the conditions for observing ND fluorescence it the cells.

8. REFERENCES

[1] H. Sahoo, *Rsc Adv.* **2012**, *2*, 7017–7029.

[2] U. Resch-Genger, M. Grabolle, S. Cavaliere-Jaricot, R. Nitschke, T. Nann, *Nat. Methods* **2008**, *5*, 763–775.

[3] J. Zhang, R. E. Campbell, A. Y. Ting, R. Y. Tsien, *Nat. Rev. Mol. Cell Biol.* **2002**, *3*, 906–918.

[4] W. J. Parak, T. Pellegrino, C. Plank, *Nanotechnology* **2005**, *16*, R9–R25.

[5] X. Shi, Y. Tu, X. Liu, E. S. Yeung, H. Gai, *Phys. Chem. Chem. Phys.* **2013**, *15*, 3130–3132.

[6] T. Gensch, M. Böhmer, P. F. Aramendía, *J. Phys. Chem. A* **2005**, *109*, 6652–6658.

[7] O. Faklaris, V. Joshi, T. Irinopoulou, P. Tauc, M. Sennour, H. Girard, C. Gesset, J. C. Arnault, A. Thorel, J. P. Boudou, *Acs Nano* **2009**, *3*, 3955–3962.

[8] J. I. Chao, E. Perevedentseva, P. H. Chung, K. K. Liu, C. Y. Cheng, C. C. Chang, C. L. Cheng, *Biophys. J.* **2007**, *93*, 2199–2208.

[9] T. Nguyen, H. C. Chang, V. W. K. Wu, *Diam. Relat. Mater.* **2007**, *16*, 872–876.

[10] K. B. Holt, *Philos. Trans. R. Soc. Math. Phys. Eng. Sci.* **2007**, *365*, 2845–2861.

[11] V. Vaijayanthimala, H. C. Chang, *Nanomed.* **2009**, *4*, 47–55.

[12] C. C. Fu, H. Y. Lee, K. Chen, T. S. Lim, H. Y. Wu, P. K. Lin, P. K. Wei, P. H. Tsao, H. C. Chang, W. Fann, *Proc. Natl. Acad. Sci.* **2007**, *104*, 727–732.

[13] Y. R. Chang, H. Y. Lee, K. Chen, C. C. Chang, D. S. Tsai, C. C. Fu, T. S. Lim, Y. K. Tzeng, C. Y. Fang, C. C. Han, *Nat. Nanotechnol.* **2008**, *3*, 284–288.

[14] J. Havlik, V. Petrakova, I. Rehor, V. Petrak, M. Gulka, J. Stursa, J. Kucka, J. Ralis, T. Rendler, S.-Y. Lee, R. Reuter, J. Wrachtrup, M. Ledvina, M. Nesladek, P. Cigler, *Nanoscale* **2013**, *5*, 3208–3211.

[15] S.-J. Yu, M.-W. Kang, H.-C. Chang, K.-M. Chen, Y.-C. Yu, *J. Am. Chem. Soc.* **2005**, *127*, 17604–17605.

[16] V. Petrakova, A. Taylor, I. Kratochvilova, F. Fendrych, J. Vacik, J. Kucka, J. Stursa, P. Cigler, M. Ledvina, A. Fiserova, *Adv. Funct. Mater.* **2012**.

[17] V. N. Mochalin, O. Shenderova, D. Ho, Y. Gogotsi, *Nat. Nanotechnol.* **2011**.

[18] A. M. Schrand, S. A. C. Hens, O. A. Shenderova, *Crit. Rev. Solid State Mater. Sci.* **2009**, *34*, 18–74.

[19] X. Li, L. Wang, Y. Fan, Q. Feng, F. Cui, *J. Nanomater.* **2012**, *2012*, 1–19.

[20] A. M. Schrand, H. Huang, C. Carlson, J. J. Schlager, E. Osawa, S. M. Hussain, L. Dai, *J. Phys. Chem. B* **2007**, *111*, 2–7.

[21] Y. Zhu, J. Li, W. Li, Y. Zhang, X. Yang, N. Chen, Y. Sun, Y. Zhao, C. Fan, Q. Huang, *Theranostics* **2012**, *2*, 302.

[22] K. K. Liu, C. L. Cheng, C. C. Chang, J. I. Chao, *Nanotechnology* **2007**, *18*, 325102.

[23] Y. Xing, W. Xiong, L. Zhu, E. Ō sawa, S. Hussin, L. Dai, *Acs Nano* **2011**, *5*, 2376.

[24] O. Faklaris, D. Garrot, V. Joshi, F. Druon, J. P. Boudou, T. Sauvage, P. Georges, P. A. Curmi, F. Treussart, *Small* **2008**, *4*, 2236–2239.

[25] L. C. L. Huang, H. C. Chang, *Langmuir* **2004**, *20*, 5879–5884.

[26] Y. Li, X. Zhou, *Diam. Relat. Mater.* **2010**, *19*, 1163–1167.

[27] L. Wei, W. Zhang, H. Lu, P. Yang, *Talanta* **2010**, *80*, 1298–1304.

[28] U. T. Bornscheuer, *Angew. Chem. Int. Ed.* **2003**, *42*, 3336–3337.

[29] L. Cao, *Curr. Opin. Chem. Biol.* **2005**, *9*, 217–226.

[30] W. S. Yeap, Y. Y. Tan, K. P. Loh, *Anal. Chem.* **2008**, *80*, 4659–4665.

[31] A. A. Vertegel, R. W. Siegel, J. S. Dordick, *Langmuir* **2004**, *20*, 6800–6807.

[32] A. Prokop, J. M. Davidson, *J. Pharm. Sci.* **2008**, *97*, 3518–3590.

[33] Y. Y. Hui, C. L. Cheng, H. C. Chang, *J. Phys. Appl. Phys.* **2010**, *43*, 374021.

[34] D. Peer, J. M. Karp, S. Hong, O. C. Farokhzad, R. Margalit, R. Langer, *Nat. Nanotechnol.* **2007**, *2*, 751–760.

[35] H. Li, H. Sun, Z. M. Qian, *Trends Pharmacol. Sci.* **2002**, *23*, 206–209.

[36] T. R. Daniels, E. Bernabeu, J. A. Rodríguez, S. Patel, M. Kozman, D. A. Chiappetta, E. Holler, J. Y. Ljubimova, G. Helguera, M. L. Penichet, *Biochim. Biophys. Acta Bba-Gen. Subj.* **2012**, *1820*, 291–317.

[37] T. R. Daniels, T. Delgado, G. Helguera, M. L. Penichet, *Clin. Immunol.* **2006**, *121*, 159–176.

[38] H. Huang, E. Pierstorff, E. Osawa, D. Ho, *Nano Lett.* **2007**, *7*, 3305–3314.

[39] E. K. Chow, X.-Q. Zhang, M. Chen, R. Lam, E. Robinson, H. Huang, D. Schaffer, E. Osawa, A. Goga, D. Ho, *Sci. Transl. Med.* **2011**, *3*, 73ra21.

[40] C. Graf, D. L. J. Vossen, A. Imhof, A. van Blaaderen, *Langmuir* **2003**, *19*, 6693–6700.

[41] N. R. Jana, C. Earhart, J. Y. Ying, *Chem. Mater.* **2007**, *19*, 5074–5082.

[42] Z. Zhang, A. E. Berns, S. Willbold, J. Buitenhuis, *J. Colloid Interface Sci.* **2007**, *310*, 446–455.

[43] I. Rehor, J. Slegerova, J. Kucka, V. Proks, V. Petrakova, M-P. Adam, F. Treussart, S. Turner, S. Bals, M. Ledvina, A.M. Wen, F. Steinmetz, P. Sacha, P. Cigler, submitted

[44] B. D. Chithrani, W. C. W. Chan, *Nano Lett.* **2007**, *7*, 1542–1550.

[45] H. Iinuma, K. Maruyama, K. Okinaga, K. Sasaki, T. Sekine, O. Ishida, N. Ogiwara, K. Johkura, Y. Yonemura, *Int. J. Cancer* **2002**, *99*, 130–137.

[46] L. Zhang, F. X. Gu, J. M. Chan, A. Z. Wang, R. S. Langer, O. C. Farokhzad, *Clin. Pharmacol. Ther.* **2008**, *83*, 761–769.

[47] L. Yi, H. Sun, Y.-W. Wu, G. Triola, H. Waldmann, R. S. Goody, *Angew. Chem. Int. Ed.* **2010**, *49*, 9417–9421.

[48] D. Banerjee, A. P. Liu, N. R. Voss, S. L. Schmid, M. G. Finn, *Chem. Bio. Chem* **2010**, *11*, 1273–1279.

[49] S. I. Presolski, V. P. Hong, M. G. Finn, *Curr. Protoc. Chem. Biol.* **2011**, *3*, 153-162.

[50] V. Hong, S. Presolski, C. Ma, M. G. Finn, *Angew. Chem. Int. Ed.* **2009**, *48*, 9879–9883.

[51] T. Meinhardt, D. Lang, H. Dill, A. Krueger, *Adv. Funct. Mater.* **2011**, *21*, 494–500.

[52] Z. M. Qian, H. Li, H. Sun, K. Ho, *Pharmacol. Rev.* **2002**, *54*, 561–587.

[53] H. Li, Z. M. Qian, *Med. Res. Rev.* **2002**, *22*, 225–250.

[54] T. R. Daniels, T. Delgado, J. A. Rodriguez, G. Helguera, M. L. Penichet, *Clin. Immunol.* **2006**, *121*, 144–158.

[55] "UniProt," can be found under http://www.uniprot.org/

[56] C. M. Lawrence, S. Ray, M. Babyonyshev, R. Galluser, D. W. Borhani, S. C. Harrison, *Science* **1999**, *286*, 779–782.

[57] B. E. Eckenroth, A. N. Steere, N. D. Chasteen, S. J. Everse, A. B. Mason, *Proc. Natl. Acad. Sci.* **2011**, *108*, 13089–13094.

[58] P. Ponka, *Kidney Int.* **1999**, *55*, S2–S11.

[59] P. Ponka, C. N. Lok, *Int. J. Biochem. Cell Biol.* **1999**, *31*, 1111–1137.

[60] P. Aisen, *Int. J. Biochem. Cell Biol.* **2004**, *36*, 2137–2143.

[61] Y. Cheng, O. Zak, P. Aisen, S. C. Harrison, T. Walz, *Cell* **2004**, *116*, 565–576.

[62] O. Ishida, K. Maruyama, H. Tanahashi, M. Iwatsuru, K. Sasaki, M. Eriguchi, H. Yanagie, *Pharm. Res.* **2001**, *18*, 1042–1048.

[63] M.-F. Weng, B.-J. Chang, S.-Y. Chiang, N.-S. Wang, H. Niu, *Diam. Relat. Mater.* **2012**, *22*, 96–104.

[64] M. F. Weng, S. Y. Chiang, N. S. Wang, H. Niu, *Diam. Relat. Mater.* **2009**, *18*, 587–591.

[65] J. R. Mesters, C. Barinka, W. Li, T. Tsukamoto, P. Majer, B. S. Slusher, J. Konvalinka, R. Hilgenfeld, *Embo J.* **2006**, *25*, 1375–1384.

[66] K. Hlouchova, C. Barinka, J. Konvalinka: Glutamate Carboxypeptidase II as a Therapeutic Target in Proteinases Drug Targets (ed: B. Dunn) RSC Publishing, Cambridge, UK, **2011**, 62-95.

[67] C. Barinka, J. Starkova, J. Konvalinka, J. Lubkowski, *Acta Crystallograph. Sect. F Struct. Biol. Cryst. Commun.* **2007**, *63*, 150–153.

[68] T. Tsukamoto, K. M. Wozniak, B. S. Slusher, *Drug Discov. Today* **2007**, *12*, 767–776.

[69] S. Jayaprakash, X. Wang, W. D. Heston, A. P. Kozikowski, *Chem. Med. Chem* **2006**, *1*, 299–302.

[70] P. Majer, P. F. Jackson, G. Delahanty, B. S. Grella, Y. S. Ko, W. Li, Q. Liu, K. M. Maclin, J. Polakova, K. A. Shaffer, *J. Med. Chem.* **2003**, *46*, 1989–1996.

[71] J. Zhou, J. H. Neale, M. G. Pomper, A. P. Kozikowski, *Nat. Rev. Drug Discov.* **2005**, *4*, 1015–1026.

[72] P. F. Jackson, D. C. Cole, B. S. Slusher, S. L. Stetz, L. E. Ross, B. A. Donzanti, D. A. Trainor, *J. Med. Chem.* **1996**, *39*, 619–622.

[73] Z. Cai, S. Lin, P. G. Rhodes, *Eur. J. Pharmacol.* **2002**, *437*, 139–145.

[74] B. S. Slusher, J. J. Vornov, A. G. Thomas, P. D. Hurn, I. Harukuni, A. Bhardwaj, R. J. Traystman, M. B. Robinson, P. Britton, X.-C. M. Lu, F. C. Tortella, K.M. Wozniak, M. Yudkoff, B. M. Potter, P. F. Jackson, *Nat. Med.* **1999**, *5*, 1396–1402.

[75] S.-R. Chen, K. M. Wozniak, B. S. Slusher, H.-L. Pan, *J. Pharmacol. Exp. Ther.* **2002**, *300*, 662–667.

[76] A. J. Williams, X. M. Lu, B. Slusher, F. C. Tortella, *J. Pharmacol. Exp. Ther.* **2001**, *299*, 48–57.

[77] H. Tang, M. Brown, Y. Ye, G. Huang, Y. Zhang, Y. Wang, H. Zhai, X. Chen, T. Y. Shen, M. Tenniswood, *Biochem. Biophys. Res. Commun.* **2003**, *307*, 8–14.

[78] V. Sanna, G. Pintus, A. M. Roggio, S. Punzoni, A. M. Posadino, A. Arca, S. Marceddu, P. Bandiera, S. Uzzau, M. Sechi, *J. Med. Chem.* **2011**, *54*, 1321.

[79] S. S. Chandran, S. R. Banerjee, R. C. Mease, M. G. Pomper, S. R. Denmeade, *Cancer Biol. Ther.* **2008**, *7*, 974–982.

[80] S. Dhar, F. X. Gu, R. Langer, O. C. Farokhzad, S. J. Lippard, *Proc. Natl. Acad. Sci.* **2008**, *105*, 17356–17361.

[81] S. Dhar, N. Kolishetti, S. J. Lippard, O. C. Farokhzad, *Proc. Natl. Acad. Sci.* **2011**, *108*, 1850–1855.

[82] D. J. Javier, N. Nitin, M. Levy, A. Ellington, R. Richards-Kortum, *Bioconjug. Chem.* **2008**, *19*, 1309–1312.

[83] B. B. Kasten, T. Liu, J. R. Nedrow-Byers, P. D. Benny, C. E. Berkman, *Bioorg. Med. Chem. Lett.* **2013**, *23*, 565–568.

[84] N. J. Hrib, J. G. Jurcak, F. P. Huger, C. L. Errico, R. W. Dunn, *J. Med. Chem.* **1991**, *34*, 1068–1072.

[85] P. Pattnaik, *Appl. Biochem. Biotechnol.* **2005**, *126*, 79–92.

[86] P. A. Van Der Merwe: Surface Plasmon Resonance in Protein-Ligand Interactions: hydrodynamics and calorimetry (ed: S. Harding, P.Z. Chowdry) Oxf. Univ. Press, New York, USA, **2001**, 137–170.

Svoluji k zapůjčení této práce pro studijní účely a prosím, aby byla řádně vedena evidence vypůjčovatelů.

Jméno a příjmení	Adresa	Číslo OP	Datum vypůjčení	Poznámka